SHEAR BEHAVIOR OF STEEL PLATES WITH REINFORCED OPENINGS

By

Bo Chen, B. ENG.

A Thesis Submitted to the School of Graduate Studies in Partial

Fulfillment of the Requirements for the Degree of

Master of Applied Science

McMaster University

2009

MASTER OF APPLIED SCIENCE (2009)
(Civil Engineering)

McMaster University
Hamilton, Ontario, Canada

TITLE: Shear Behavior of Steel Plates with Reinforced Openings

AUTHOR: Bo Chen, B. Eng. (McMaster University)

SUPERVISOR: Dr. K. S. Sivakumaran

NUMBER OF PAGES: xxiii, 208

ABSTRACT

Steel structures are commonly used all over the world. Structural cold-formed steel sections can be used as the primary building members, as well as the secondary members with other structural materials. They can be used as joists, truss members, and studs; they can also be used as frame systems, floor systems and wall systems, etc.

It is common to see openings in these plated structures for all kinds of reasons. For example, openings are needed for ancillary systems such as water pipes, plumbing, electric wiring, etc. In cold-formed steel members, openings are often introduced in the web of a joist. The existence of large openings can change the stress distribution around the opening regions, thus changing the buckling and strength characteristics of web panels. The extent to which the openings can affect the plated structures depends on the size, shape, locations and number of the openings in the web. In this study, parametric studies were performed on a total of 42 simply supported plates with centrally located square openings utilizing the finite element modeling. The parameters of interest are the size of the opening (d_c/h), the slenderness ratio of the plate (h/t) and the aspect ratio of the plate (a/h). It was observed from the study that, a centrally located square opening can

significantly reduce the ultimate shear strength of the plate. The opening size is the primary parameter influencing a plate's ultimate shear strength. The ultimate shear strength of a plate decreases approximately linearly as the size of the opening increases. The ultimate shear strength also decreases as the slenderness of the plate increases and tends to increase as the aspect ratio increases. The aspect ratio is found to be the least significant parameter in the sense of affecting the ultimate shear strength of plates with square openings. This study also compared the ultimate shear strength obtained from finite element modeling with that calculated from the AISI (2007) method. It was shown that the AISI (2007) tends to underestimate the ultimate shear strength of thick to moderate thick plates with square openings, but overestimate the ultimate shear strength of thin plates with square openings. A new equation for estimating the shear reduction factor (q_s) is proposed based on the finite element analysis undertaken to better estimate the ultimate shear strength of plates with centralized square openings.

To compensate for the reduction in strength of steel members due to large openings, reinforcements may be used in practice. In this research, simply supported steel plates with an aspect ratio of 3 (a/h=3) and having a 60% reinforced square opening (d_c / h =0.6) under pure shear loads were analyzed through the finite element modeling. Four slenderness ratios (h/t), namely h/t=50, 100, 150 and 200 were considered. Three reinforcement schemes, namely the flat-reinforcement, the lip-reinforcement and the angle-reinforcement, are applied on the plates to evaluate the effectiveness of these three reinforcement schemes. It was observed from the research that all three reinforcement schemes were capable of restoring the shear strength of plates with square openings. However, the flat-reinforcement is found to be the most efficient way of the three reinforcement schemes considered.

ACKNOWLEDGMENTS

The author would love to express her sincere appreciation to her supervisor, Dr. K.S. Sivakumaran, for his aborative and precious academic guidance and financial support during the whole study period. Especially, the author has learned how to approach a particular problem systematically and resolve it step-by-step. The author has learned a lot from Dr. K.S. Sivakumaran, not only in the academic area but also the precious working attitude.

The author would like to thank the Department of McMaster Civil Engineering for their financial assistance.

The author would also like to extend her thanks to her affectionate parents. It is their endless love, support and encouragement that gives the author more confidence and motivity.

TABLE OF CONTENTS

LIST OF TABLES

LIST OF FIGURES

LIST OF SYMBOLS

A	Area of the plate= $h \cdot a$
$A_{opening}$	Area of the opening= $d_c b_c$
A_w	Area of web element = $h \cdot t$
a	Length of plate
b_c	Length of web hole
b_{eff}	Effective width
d_c	Depth of web hole
E	Modulus of elasticity (Young's modulus)
F_{pr}	Proportional limit
F_v	Nominal shear stress
F_y	Yielding stress of material
f	Stress distribution
h	Width of plate
h_r	Total width of the reinforcement plate
k	Buckling coefficient for plates under compression
$k_v^{opening}$	Shear-buckling coefficient for plates with openings
k_v^{solid}	Shear-buckling coefficient for solid plates

P_n	Nominal axial resistance of the compressed plate
t	Thickness of plate
t_r	Thickness of the reinforcement plate
V_n	Nominal shear strength of plates
w	Imperfection distribution
w_0	Value of the maximum imperfection point
ν	Poisson's ratio
λ	Slenderness factor defined by Equation 3.9
ρ	Reduction factor defined by Equation 3.8
σ_{cr}	Critical buckling stress of plate under compression
$\tau_{cr}^{opening}$	Critical buckling stress for plates with openings
τ_{cr}^{solid}	Critical buckling stress for solid plates
τ_{pr}	Proportional limit of plates under shear loads
τ_y	Shear yield stress
ϕ	Buckling model number

Chapter 1

INTRODUCTION

1.1 Steel and cold-formed steel

Steel is utilized as a structural material in many structures including buildings and many other types of construction. Steel has high a strength/weight ratio, has high ductility, and is environmentally friendly. Compared with some other common structural materials, for example wood and concrete, steel is isotropic and its stress-strain relationship is somewhat consistent and predictable. Because of its unique material properties and economical benefits, steel structures are now rapidly spreading all over the world. Figures 1.1(a), (b) and (c) show some of the well-known steel structures in the world, namely the Sky Dome in Canada, the Birds Nest in China and the Nagoya Domes in Japan, respectively.

There are essentially two types of structural steel products: hot-rolled steel and cold-formed steel. Hot-rolled steel sections are formed to shape at high temperature, and are rolled into sections while still hot. On the other hand, cold-formed steel sections are formed to shape from thin steel sheets at ambient temperature. They are formed either by bending or rolling cold flat sheets of steel into shapes which will support more loads than the flat sheets themselves. In the cold-forming process, the material at the corners of sections also becomes stronger due to strain hardening effect. Two types of cold-formed steel products, namely sections and panels, can be normally found in the market. Some commonly used cold-formed steel sections are C-sections, Z-sections, I beam, box sections and others. Figure 1.2 shows some of the cold-formed steel sections found in the market place. Cold-formed steel sections are more often used as the primary or secondary load carrying structural members, while cold-formed steel panels are usually used for wall panels, floor decks, roof decks and so on. Cold-formed steel sections are usually thinner than hot-rolled steel sections. The depths of cold-formed steel members range from 50 to 300mm (2 to 12 inches) and the thicknesses range from 0.90 to 6.4mm (0.035 to about 0.25 inches). Generally, elements (flanges and webs) of the cold-formed steel members have higher width to thickness ratios. Overall, cold-formed steel members are also lighter in weight, easier to carry and install, and thus more economical to mass-produce. In addition, the manufacturing and construction technologies for cold-formed steel members have been improved recently. Cold-formed steel can now be well corrosion protected, and form a wide variety of different shapes.

As the demand for higher strength, lighter weight, and more versatile structural materials increases, cold-formed steel structures are utilized more and more often in the frontier of construction. Cold-formed steel was first used as a structural material in the 1850's, and is now used very often not only in commercial buildings, but also in many residential buildings. Today, cold-formed steel sections are commonly used as site-assembled frames and panels for walls, roofs with high insulation performance, storage racking systems in warehouses, etc (Shanmugam, 1997). Using cold-formed steel in buildings is increasing rapidly in popularity. Figure 1.3 shows a two-storey commercial building framed entirely with load-bearing cold-formed steel members. Notice that cold-formed steel shear panels are extensively used in this building. In Figure 1.4, cold-formed steel members are used in the roof system construction.

Instability problems, such as lateral buckling and column buckling, are the major concerns in the design of hot-rolled steel structures. However, cold-formed sections subjecting to compressive, bending, shearing, or bearing loads are even more likely susceptible to local buckling in each individual plate member, since they have higher width/thickness ratios (usually ranging from 50 to 300). Thus, local buckling, distortional buckling and shear buckling are the common failure modes for cold-formed steel members.

1.2 Openings on Steel Sections

Structural cold-formed steel sections can be used as the primary building members, as well as the secondary structural members with other structural materials. They can be used as joists, truss members, and studs; they can be also used as frame systems, floor systems and wall systems, etc. It is common to see openings in these plated members for all kinds of reasons. For example, openings are needed for ancillary systems such as water pipes, plumbing, electric wiring, etc. In cold-formed steel sections, openings are often introduced in the web of a beam or a column. They can be formed either during the roll forming phase or cut out during the construction phase. The C-section cold-formed steel members are typically produced with a standard web hole at the middle of the web. Two of the most common opening types in practice are either a circular or a rectangular opening. Figures 1.5 and 1.6 show some applications of cold-formed steel webs with centrally located openings. It can be seen that the size of the openings is relatively large (more than 50% of the web area). The existence of such large openings can greatly change the geometry of the structure and degrade the integrity of the section. The presence of such openings can also change the stress distribution of the membrane stress at the opening regions, thus changing the buckling and the strength characteristics of the web panel, causing performance change to the overall members. The extent to which the openings can affect the behavior of a steel member depends on the size, the shape, the locations and the number of openings in the web. It is suggested that, for hot-rolled steel sections, the effect of openings on a steel section shall be considered if it reduces the flange or web area by more than 15% (CSA S16-01, 2004). For cold-formed steel sections, the effect of openings on the web panel shall be considered if the depth of the web hole is more than 14mm (AISI 2007). In practice, the openings can be more than 60% of the web area. Such holes can lead to significant reduction in the strength of the web. Moreover, the effect of openings on steel sections also depends on the way the loads are applied (e.g. compression, tension, shear etc).

As the loading condition differs, the impact of openings on structures differs. It was found by Shan et al. (1996) that web openings on compact webs could decrease the plastic moment capacity of a member by as much as 40%, but have little effect on slender webs since for slender webs, the flanges carry most of the bending moment. Shan's (1996) findings again reveal that cold-formed steel structures, which are made mainly from thin plated elements, are very versatile, since openings can be made on such structures without much reduction of their flexural strength.

To compensate for the reduction in strength of steel members due to large openings, reinforcements may be used. Reinforcements may be positioned near the openings to regain the strength. With proper reinforcements, the section can recover or even increase from its original strength. However, using additional opening reinforcements is sometimes an expensive and difficult operation. Therefore, more investigation is required to ensure the efficiency of the reinforcement.

1.3 Objectives and Scopes

The structural behavior of steel members with all different kinds of web openings has been investigated for many years. For example, the effect of web openings in column members was first investigated by Miller and Peköz (1994). However, very limited experimental and theoretical data were found on the behavior of plates with openings subjected to shear loading, especially for thin cold-formed steel plates. Furthermore, most of the studies from previous literature relating to openings in shear web elements have been concentrated on elastic buckling behavior, with a few on the post-buckling behavior. Thus, it is necessary to establish the effects of openings on steel sections in more detail. Once the behavior of web panels with openings is established, a cost effective reinforcement should be made on the web panels to compensate for the reduction of strength and stiffness caused by the openings. Some experimental and numerical studies have been conducted to establish reinforcement schemes for cold-formed steel webs. Pannock (2001), Ng, et al. (2005) and Acharya (2009) studied reinforcement schemes for cold-formed steel webs with large openings in the flexural zones of webs. Acharya el al. (2007) carried out experimental studies on the strength of cold-formed steel members with large openings in high shear zones. So far, there is no numerical study on reinforced steel plates with square openings in shear zones. Thus, the overall objective of this research is to numerically (Finite Element Method) investigate the shear behavior of plates with square openings and the shear behavior of such plates with shear reinforcements for the openings. The scopes of the research are listed as the following:

- Establishment of the behavior of solid plates subjected to uniaxial load to verify the commercial finite element analysis program ADINA8.5.
- Establishment of the behavior of solid plates subjected to shear load.
- Establishment of the effects of square openings on the behavior of plates subjected to shear load.
- Establishment and evaluation of reinforcement schemes for plates with square openings subjected to shear load.

1.4 Organization of Thesis

In this thesis, Chapter 2 reviews some of the past research related to and useful for later investigations. A commercial finite element analysis program ADINA8.5 is also introduced briefly. In Chapter 3, the finite element program ADINA8.5 is verified by performing a verification study on a simply supported thin square plate subjected to uniaxial edge compression. In Chapter 4, the behavior of solid plates with different plate dimensions is investigated by finite element modeling to better understand the behavior of web plates under pure edge shear loads. This can further verify the finite element analysis program. In Chapter 5, square openings with different dimensions are introduced to solid plates. The plates are again analyzed by the finite element models. The post-buckling behavior and the ultimate shear strength of such plates are studied. In Chapter 6, reinforcements are applied to plates with square openings. The effects of the reinforcements on the ultimate shear strength of plates with square openings subjected to pure shear loads are examined. A preferred reinforcing scheme will be proposed. Lastly, Chapter 7 is the conclusion, which sums up all the findings observed through this research.

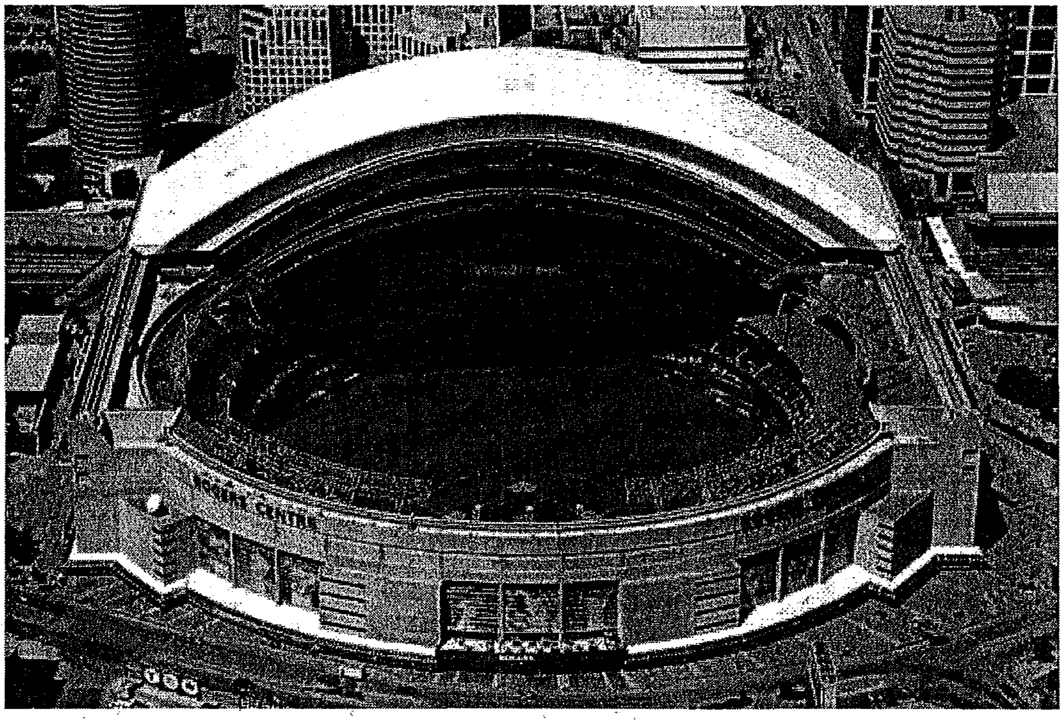

(a)

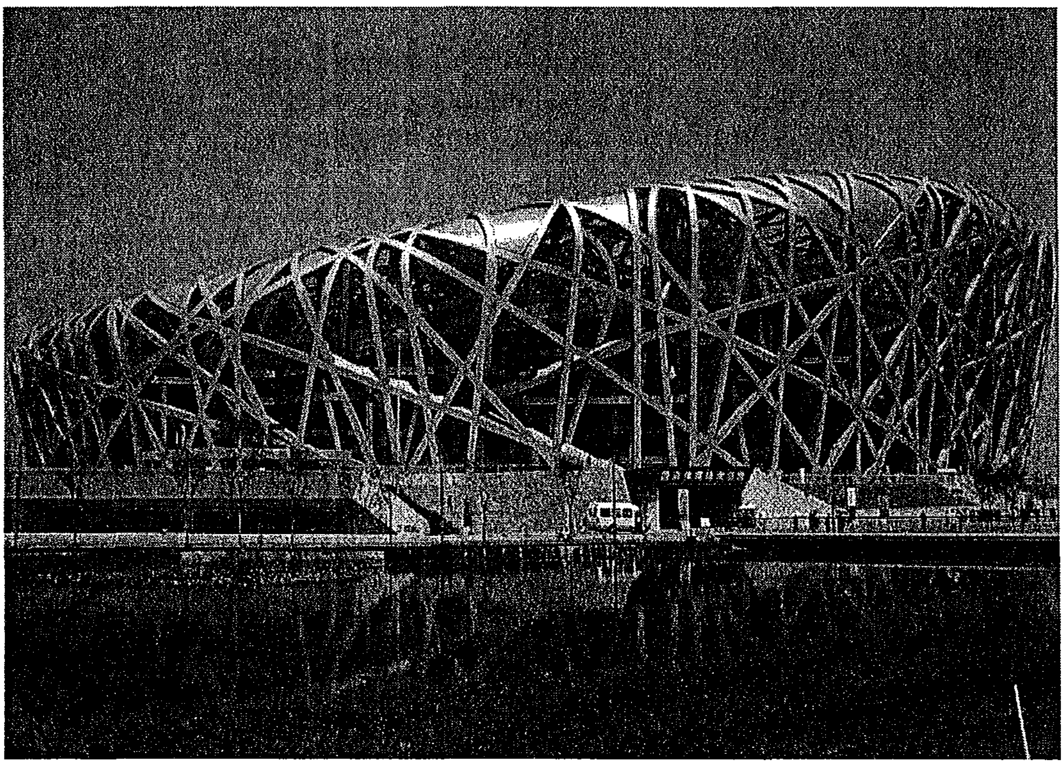

(b)

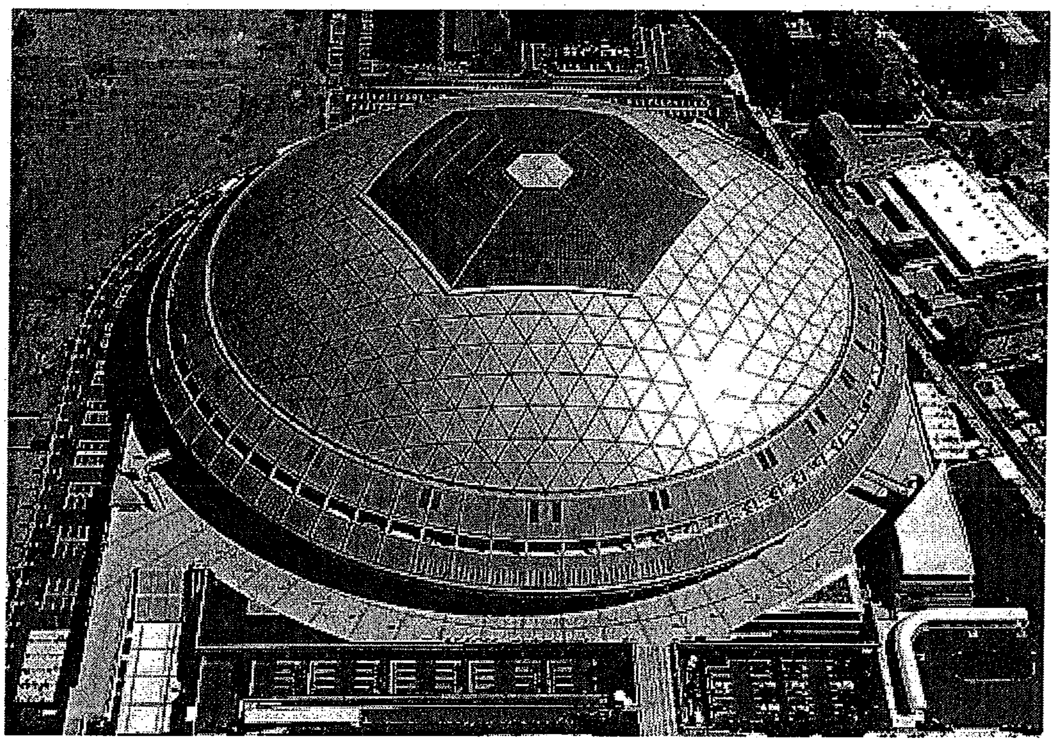

(c)

Figure 1.1 (a) Sky Dome in Canada (http://torontoist.com)
(b) Birds Nest in China (http://blog.monty.de)
(c) Nagoya Dome in Japan (http://hi.baidu.com)

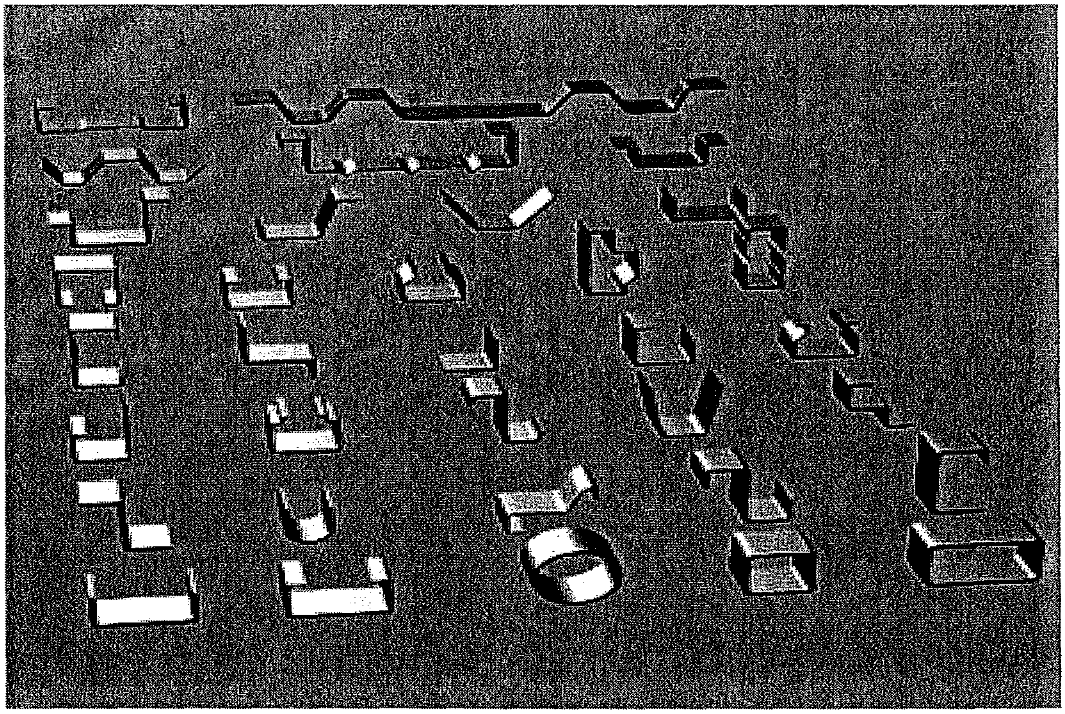

Figure 1.2 Cold-Formed Steel Sections (http://www.metals-b2b.com)

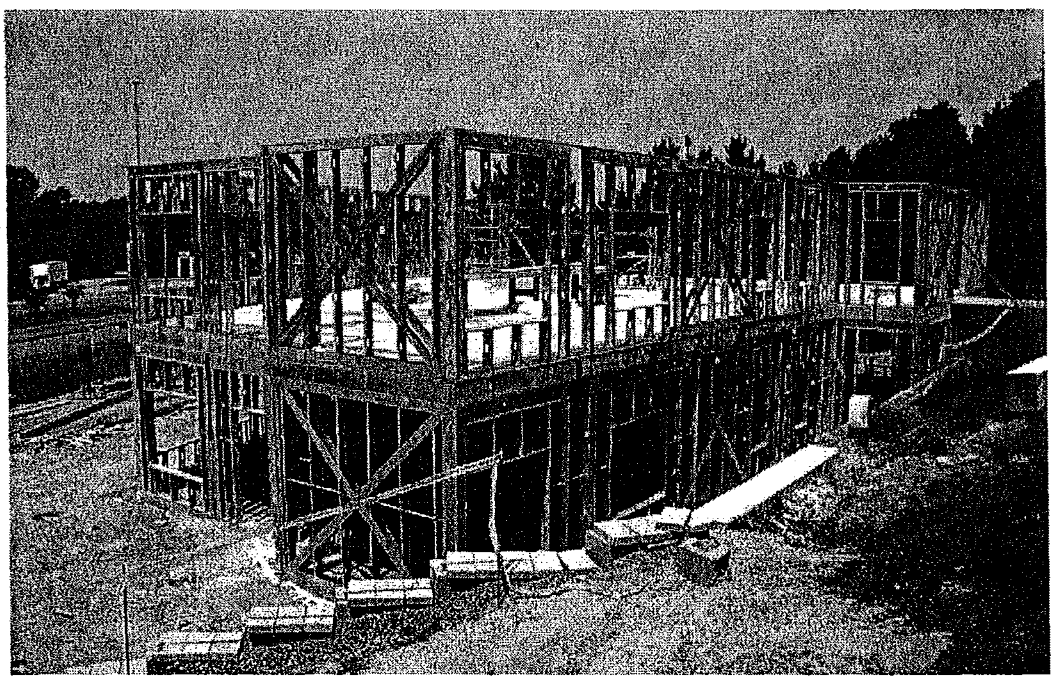

Figure 1.3 Two Story Commercial Building Framed Entirely with Load Bearing Cold-Formed Steel Members (http://www.k2engineeringinc.com)

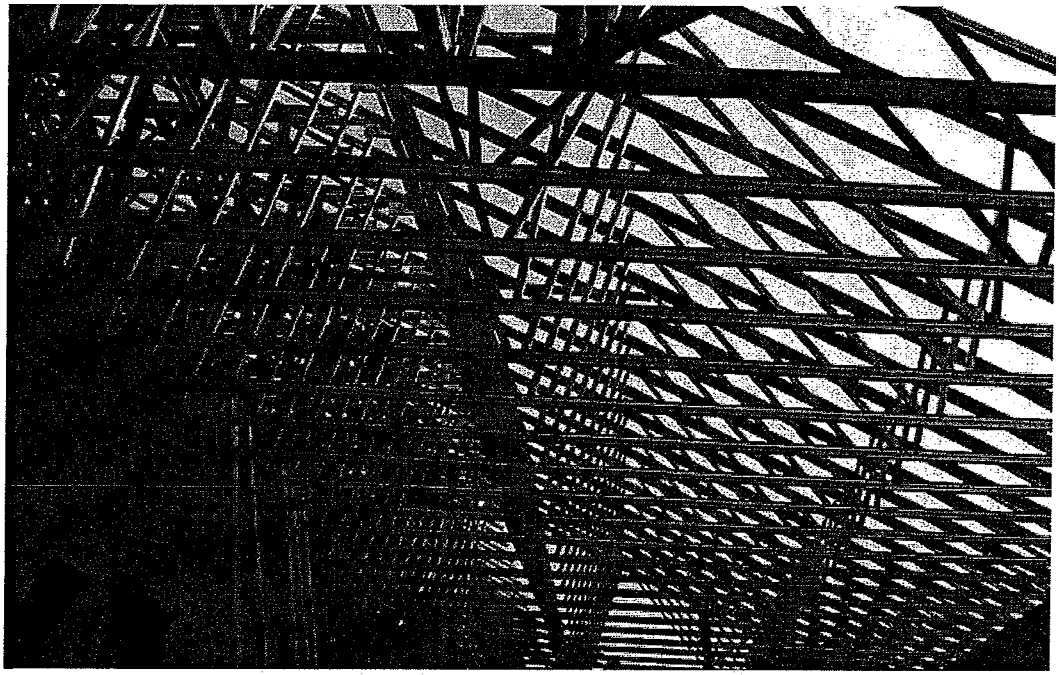

Figure 1.4 Cold-Formed Steel Sections Used as Roof System
(http://www.marinoware.com)

Figure 1.5 Cold-Formed Steel Webs with Circular Web Openings
(http://oikos.com)

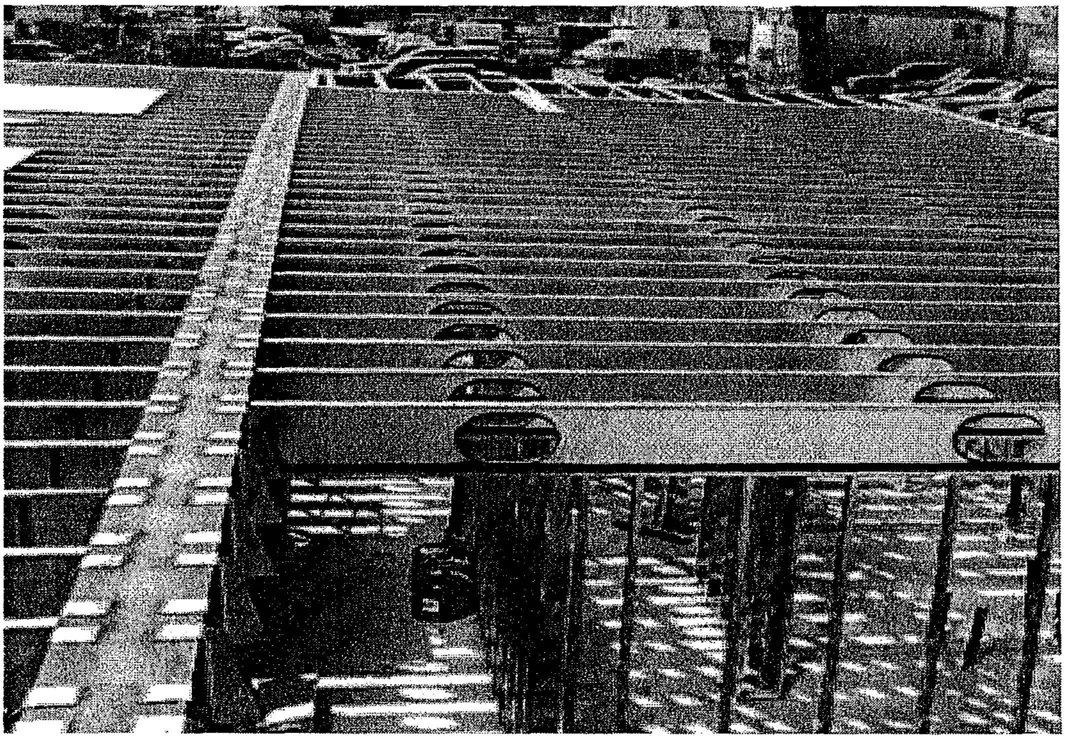

Figure 1.6 Openings on the Webs of a Floor Joist System (http://www.lgst.com)

Chapter 2

LITERATURE REVIEW AND INTRODUCTION TO THE FINITE ELEMENT ANALYSIS SOFTWARE-ADINA

2.1 Introduction

The primary role of the web plate in a steel section is to keep a relative distance between the top and the bottom flanges to provide efficient moment resistance and to sustain shear loads. A cold-formed steel section tends to have a thin web and thin flanges. The web tends to be deep, resulting in a slender web. Thus, the stability problem is the main issue for a cold-formed steel web plate. However, web buckling due to shear is essentially a local buckling phenomenon. Elastic shear buckling does not mean failure of the plate which may occur at several times the buckling load. Therefore, it is of interest to study the strength of cold-formed steel web panels including their post-buckling strength.

2.2 Stress-Strain Curve for Steel

Generally speaking, steel material can either behave as sharp yielding or gradual yielding. Mild-carbon hot-rolled steel usually has a sharp-yielding stress-strain relationship while cold-formed steel shows a gradual-yielding stress-strain relationship. Figures 2.1(a) and (b) show typical stress-strain relationships for materials that are sharp yielding and are gradual yielding, respectively. In these figures, 'F_y' is the yield stress; 'E' is the modulus of elasticity, which is defined as the slope of the initial straight portion of the stress-strain curve. ' F_{pr} ' is the proportional limit, which is defined as the stress up to which point where the slope of the stress-strain curve equals the modulus of elasticity (E). For materials that are sharp-yielding, the yield stress is defined as the stress where the yield plateau occurs. The slope of the stress-strain curve for sharp-yielding material equals to the modulus of elasticity (E) up to the yield point. For materials that are gradual-yielding, the yield point is not well defined in the stress-strain curve, thus the 0.2% offset method is usually used to define the yield stress of such material. The slope of the stress-strain curve gradual-yielding material equals to the modulus of elasticity only up to the proportional limit. After reaching the proportional limit, the slope of the stress-strain curve gradually decreases. The proportional limit is usually not lower than 70% of the yield stress. The AISI (2007) uses the gradual-yielding stress-strain curve for cold-formed steel, with the proportional limit equals to 80% of the yield stress.

2.3 Idealization of Web Boundary for Analysis

In plate structures, such as plate girders and steel shear walls, web transverse stiffeners are normally used to increase the buckling and the post-buckling strength of webs. As a result, steel sections are divided into panels by the transverse stiffeners. If the spacing and stiffness of these stiffeners are optimally designed, that is if they have low torsional stiffness and sufficient flexural stiffness, it can be assumed that they form nodal lines. Each panel can thus be considered to behave in a simply supported condition (Lee et al., 1998). Moreover, the other two edges of web panels are elastically restrained by the flanges. The real boundary condition at the edges of a web panel is something between simply supported and clamped. However, for a academic study, different researchers usually assume their own boundary conditions for the edges of the web panel. For example, Basler and Thurlimann (1959) had assumed that the web panels are simply supported. Chern and Ostapenko (1969) obtained the elastic buckling strength by assuming that the plate panels behave like a clamped support. Sharp and Clark (1971) assumed that the boundary condition lies halfway between the simply supported and clamped conditions (Lee et al., 1998). Lee et al. (1996) performed a finite element analysis on the shear buckling strength of over 300 web panels with different boundary restrains. Lee et al. (1996, 1998) concluded that the realistic boundary condition for a plate girder web panel is closer to the clamped support condition. The AISI (2007) specification has conservatively assumed the boundary conditions of web panels to be simply supported. For the sake of simplicity and also to be conservative, the current research will follow the AISI (2007)'s assumption by assuming the boundary condition of the web panel to be simply supported.

2.4 Shear Buckling of Solid Plates

Timoshenko and Gere (1961) proposed the differential equations for local buckling of rectangular plates. Stein (1947) produced a well known diagram of evaluating the shear buckling coefficient (k_v^{solid}) of flat plates, where 'k_v^{solid}'is a function of the plate aspect ratio and boundary conditions. Similar results for clamped plates were presented by Budiansky and Connor (1948). Lee et al. (1996) studied the shear buckling coefficient (k_v^{solid}) of plate girder web panels based on a finite element analysis.

In general, the simple equation, proposed by Timoshenko and Gere (1961), of calculating the elastic critical buckling of a flat solid plate subjected to pure shear is well accepted and utilized worldwide. The equation is the following:

$$\tau_{cr}^{solid} = k_v^{solid} \frac{\pi^2 E}{12(1-\nu^2)(h/t)^2} \tag{2.1}$$

For plates with all edges simply supported:

$$k_v^{solid} = 5.34 + \frac{4}{(a/h)^2}, \quad a/h \geq 1 \tag{2.2.a}$$

For plates with all edges clamped:

$$k_v^{solid} = 8.98 + \frac{5.6}{(a/h)^2}, \quad a/h \geq 1 \tag{2.2.b}$$

where 'τ_{cr}^{solid}' is the critical buckling stress for solid plates, 'k_v^{solid}' is the non-dimensional shear buckling coefficient, which depends on the type of applied load, aspect ratio and boundary conditions of the plate. 'E' and 'ν' are Young's modulus and Poisson's ratio, respectively while 'a' is the larger dimension of a plate's side, with 'h' being the smaller dimension. This will make sure that 'a/h' is always greater than 1.

2.5 Shear Buckling of Plates with Openings

Uenoya and Redwood (1977) studied the critical shear stresses of simply supported and clamped plates with different sizes of circular holes. It was found that the buckling stress of plates subjected to pure shear force decreases continuously with increasing size of the holes (Roberts et al., 1984).

The equation of elastic critical buckling of a flat plate with openings subjected to pure shear can be expressed in a similar form as for the solid plate (Narayanan and Der-Avanessian, 1984)):

$$\tau_{cr}^{opening} = k_v^{opening} \frac{\pi^2 E}{12(1-\nu^2)(h/t)^2} \tag{2.3}$$

where '$\tau_{cr}^{opening}$' is the critical buckling stress for plates with openings, '$k_v^{opening}$' is the non-dimensional shear-buckling coefficient modified according to the effects of the openings, 'h' is the width of the plate and 't' is the thickness of the plate, respectively. 'E' and 'ν' are Young's modulus and Poisson's ratio, respectively. The expressions for '$k_v^{opening}$' were proposed by Narayanan and Der-Avanessian (1984) for centralized circular and rectangular openings as the following:

<u>For plates with circular openings</u>:

when $d_c/h \leq 0.5$ and $b_c/h \leq 0.5$

$$k_v^{opening} = k_v^{solid}\left(1-\alpha_c \frac{d_c}{\sqrt{h^2+d_c^2}}\right) \tag{2.4.1}$$

when $d_c/h > 0.5$ and $b_c/h > 0.5$

$$k_v^{opening} = k_v^{solid}\left(1-\frac{d_c}{h}\right) \tag{2.4.2}$$

where 'd_c' is the diameter of the circular opening. $\alpha_c = 1.8$ for simply supported edges and 1.5 for clamped edges.

For plates with rectangular openings:

when $d_c/h \leq 0.5$ and $b_c/h \leq 0.5$

$$k_v^{opening} = k_v^{solid}\left(1 - \alpha_r \frac{A_{opening}}{A}\right) \tag{2.5.1}$$

when $d_c/h > 0.5$ and $b_c/h > 0.5$

$$k_v^{opening} = k_v^{solid}\left(1 - \frac{d_c}{h}\right), \text{ or } k_v^{opening} = k_v^{solid}\left(1 - \frac{b_c}{h}\right), \text{ whichever governs.} \tag{2.5.2}$$

where 'd_c' is the width of the rectangular opening and 'b_c' is the length of the opening, respectively. $A_{opening}$ = area of the opening= $d_c b_c$ and A= area of the plate= h·a. Meanwhile, α_r = 1.5 for simply supported edges and 1.25 for clamped edges.

2.6 Post-Buckling Strength of Plate Elements and the Tension Field Theory

Unlike one-dimensional structural members such as columns, two-dimensional elements such as plated elements, when subjected to in-plane loading, do not collapse immediately after reaching the buckling load. Depending upon geometry and boundary conditions, web plates are capable of carrying additional loads in excess of the buckling loads and remain stable in the buckled form. This additional load capacity is considered as the post-buckling strength. The post-buckling strength is the reserve capacity caused by the development of membrane stresses which are in turn caused by stretching of the mid-plane of the plates and stress redistribution within the plate. The stretching of the mid-plane results in a tension field within the plate as the plate deforms.

Diagonal tension field theory was first proposed for thin plates under shear loading by Wagner (1931) who found that a diagonal tension field formed during the buckling of a plate girder. He stated that after shear-buckling was achieved, the web panel acts more like a truss system, in which the diagonal tension field acts like a tension element anchored to the stiffeners. The ultimate shear capacity of a plate girder is assumed to consist of two contributions, which are the shear capacity of the web due to beam action and the shear resistance resulting from the formation of the diagonal tension field of the web after shear buckling occurs.

The magnitude of the post-buckling strength largely depends on the anchoring of the tension field, which depends on the bounding elements of the plate panel. In theory, the post-buckling strength reaches its maximum value when the perimeter of the plate is extremely stiff. For a plate girder, the bounding elements are the flanges and the transverse stiffeners.

Even though the post-buckling behavior was discovered as early as 1886 by Wilson, elastic buckling was used as a design basis for shear webs of plate girders almost exclusively until the 1960s. This was mostly because the equations for calculating the elastic shear buckling strength of web plates are relatively simple and had been well known for years, whereas a simple and comprehensive procedure to calculate the post-buckling strength of plated elements had not yet been developed. Studies on the post-buckling behavior of shear web plates for civil engineering purposes were initiated by Basler and Thurlimann (1959). Basler (1961) first developed the analytical method of calculating the post-buckling strength of plates under shear loads. The American Institute of Steel Construction (AISC, 1963) first adopted post-buckling strength into its specifications based on Basler's theories. Porter et al. (1975) further studied the post-buckling behavior of plate girders subjected to shear loads. Porter et al. (1975) proposed the Cardiff method to calculate the post-buckling strength of plate girders based on the tension field theory.

Lee et al. (1996), Lee et al. (1998) and Olaru et al. (2004) studied the shear strength, including the post-buckling strength, of plate girders based on a finite element analysis. Later, Alinia and Dastfan (2006) studied the shear strength, including the post-buckling strength, of shear walls, again based on finite element analysis.

2.7 Strength of Webs with Openings

The first paper on the strength of thin webs with web openings was written by Höglund (1971). In Höglund's research, thin plate girders, with slenderness ratios of 200 to 300, with circular and rectangular holes were statically loaded. Höglund (1971) concluded, based on experimental observations, that the girders with holes located in high shear zones failed at significantly lower loads than those located in high moment zones. This observation had indicated the relative importance of shear failure criteria in the design of web plates with openings.

Shan et al. (1996) later found that the existence of web openings can greatly decrease the shear strength of a cold-formed steel web plate. Davis and Yu (1973) studied the effect of openings on cold-formed steel back-to-back channel sections with specific dimensions. They proposed an expression for the shear reduction factor, which accounts for the reduction in shear strength of web panels caused by existence of web openings, for web panels containing centrally located circular holes. They again concluded that a circular web opening would reduce the shear strength of the web plates.

Experimental and theoretical studies on the buckling and collapse behavior of square shear webs having circular holes were also carried out by Rockey et al. (1967), Coughlan (1970), Rockey (1980), and Sabir and Chow (1983). The finite element method was first employed by Rockey et al. (1967) to examine the buckling of a square plate having a centrally located circular hole when subjected to edge shear loading. The relationship between the buckling load and the ratio of the opening diameter to the plate width was obtained for web plates that are either simply supported or clamped on four sides. Similar studies on webs containing square holes were reported by Shanmugam and Narayanan (1982). A systematic study of plate girders made with thin webs has been carried out experimentally and theoretically by Narayanan and Rockey (1981). They proposed a theoretical method of computing the ultimate shear capacity of flat plates containing centrally located circular or rectangular openings. Narayanan and Rockey (1981) concluded that the ultimate capacity of girders dropped linearly with an increase in the diameter of the opening. Narayanan and Chow (1985) further studied the shear buckling strength and shear ultimate strength of plates with eccentrically located square and circular holes. Some recent research on the shear capacity of steel plate girders with web openings was carried out by Pellegrino et al. (2008) and then by Hagen et al. (2009) using finite element modeling. Pellegrino et al. (2008) studied the post-buckling behavior of plates with single openings subjected to shear loads while Hagen et al. (2009) carried out a series of finite element modeling to study the ultimate shear capacity of steel girders with multi-web openings.

2.8 Strength of Webs with Reinforced Openings

The strength of hot-rolled steel webs with reinforced openings has been studied by Segner (1964), Congdon (1968), Copper et al. (1972), Wang et al. (1975), Larson et al. (1976), Redwood and Lupien (1978), Redwood and Shrivastava (1980), Narayanan and Der-Avanessian (1984, 1985), etc. In terms of cold-formed steel webs, Pennock (2001) carried out experimental studies on cold-formed steel joists with reinforced and unreinforced web openings subjected to bending and the combined effect of bending and shear. Ng (2004) carried out experimental studies on the flexural resistance of cold-formed steel webs with reinforced openings. Most recently, Acharya (2009) performed both an experimental study and undertook a finite element analysis on reinforcement schemes for cold-formed steel joists having large web openings in flexural zones.

Very little research can be found for shear reinforcements on cold-formed steel webs. Acharya (2009) performed experimental study on reinforcement schemes for cold-formed steel joists having large web openings in high shear zones. More details about research on shear reinforcements are presented in Section 6.2.

2.9 The Finite Element Analysis Software – ADINA

This research has exclusively used the finite element method for analysis. The commercial finite element analysis computer program ADINA8.5 was used. This section provides only some relevant theoretical background and solution techniques for the finite element method.

2.9.1 Introduction of ADINA Program

ADINA (Automatic Dynamic Incremental Nonlinear Analysis) is a multi-purpose commercial finite element analysis computer program. It can be used in structural, fluid and thermal analysis. The complete ADINA package includes the pre-processor ADINA-IN, the structural analysis module ADINA Structure, the heat transfer analysis module ADINA-T, the fluid flow analysis module ADINA-F, the post-processor ADINA-PLOT, etc. The structural analysis module ADINA Structure was used in the current research.

2.9.2 Method of Analysis

ADINA structure is used for displacement and stress analysis. It consists of a wide variety of analysis options such as linear and non-linear static analysis, linear and non-linear dynamic analysis, the eigenvalue problem, and frequency domain analysis, etc. The eigenvalue problem consists of the linearized-buckling analysis and the frequency analysis for which the solution is obtained by solving the corresponding generalized eigenvalue problem. In the current research, the linearized buckling analysis was use to determine the critical buckling load for both plates under compression and shear loading. Moreover, since the steel plate under consideration undergoes large displacements and also exhibits material non-linearity, the nonlinear static analysis was used to determine the ultimate strength for both the plate under compression and shear. The analysis method for each model is explained in more detail in the following chapters.

2.9.3 Shell Elements

ADINA provides a large element library which consists of different classes of elements to conform to various requirements for geometry modeling. Specifically, ADINA provides 11 different classes of elements, namely, the truss and cable elements, two-dimensional solid elements, three-dimensional solid elements, beam elements, iso-beam elements and axisymmetric shell elements, plate/shell elements, shell elements, pipe elements, general and spring/damper/mass elements, displacement-based fluid elements and lastly the potential-based fluid elements. Since the model under consideration of this research is a plate having large displacements, and is expected to experience both in-plane and out-of-plane displacements, shell elements were used. The shell element is a 4-node to 32-node (degenerate) isoparametric element that can be employed to model thick and thin general shell structures. It is formulated treating the shell as a three dimensional continuum with the assumptions used in the Timoshenko beam theory and the Mindlin/Reissner plate theory. The ADINA

2008 modeling guide suggests that the 4-node element is usually the most effective element for analysis of general shell structures, since it does not lock and has a high predictive capacity.

Shell elements can be used with different material models such as the elastic-isotropic, elastic-orthotropic, plastic-bilinear, plastic-multilinear, plastic-orthotropic, thermo-isotropic, thermo-orthotropic, thermo-plastic, creep, plastic-creep, multilinear-plastic-creep, creep-variable, plastic-creep-variable, multilinear-plastic-creep-variable and viscoelastic. In this research, the plastic-multilinear material model is used to represent the material property for cold-formed steel. Shell elements can also be used with a small displacement/small strain, large displacement/small strain, large displacement/large strain formulation. Problems involved in this research are large displacement/small strain problems. Furthermore, either 5 or 6 degrees of freedom can be assigned at a mid-surface node for a shell element. This research allows 6 degrees of freedom for the mid-surface node of plates.

Numerical integration is used to evaluate the element matrices. Gauss numerical integration is used inplanely in the shell element. Either Gauss or Newton-Cotes numerical integration can be used through the shell thickness. Usually, 2-point Gauss or 3-point Newton-Cotes integration is appropriate for an elastic material, but a higher integration order may be more effective for an elastic-plastic material model.

In the current study, as suggested above, the quadrilateral four-node shell elements for the non-linear analysis, which are capable to represent both plate and curved surface, were used. Each node of the shell element has six degrees of freedoms, namely three displacements and three rotations. This four-node element is capable to simulate both the membrane behavior and the flexural behavior of plates. The default 2 by 2 integration point arrangement for the 4-node element is used in the r-s element mid-plane. In the 't' direction (through-thickness of the shell element), the Newton-Cotes rule for integration points is preferred rather than the default Gauss quadrature rule because, instead of having integration points only within the thickness of plates, the Newton-Cotes rule also has the integration points lying at both the top and bottom surfaces. This allows one to capture the gradually yielding response of the plate starting from the boundaries. Further more, ADINA's default integration point number for Newton-Cotes rule is 3. In order to improve the accuracy of the model, an integration of 7 through the thickness is used for the later analysis. Figure 2.2 shows a 4-node shell element with a 2 by 2 integration point in the r and s directions. Figure 2.3 shows both the Gauss quadrature integration points and the Newton-Cotes integration points through the plate thickness (t-direction).

The large displacement/small strain formulation was used in this study because the buckling behavior of a plate involves large out-of-plane displacement, and the steel is considered as relatively incompressible material; thus, the strains are assumed to be small (ADINA, 2008).

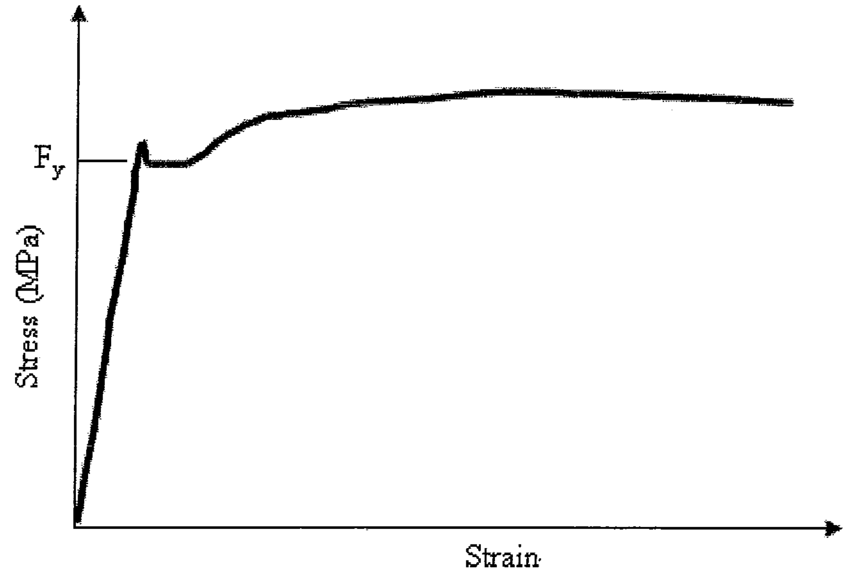

(a)

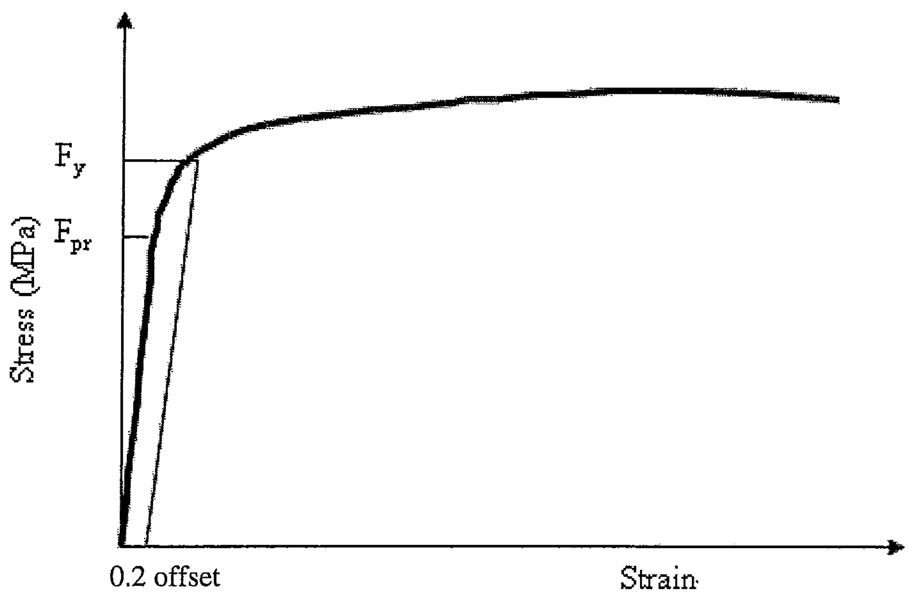

(b)

Figure 2.1 Stress-Strain Curves for Steel (a) Sharp-Yielding (b)Gradual Yielding

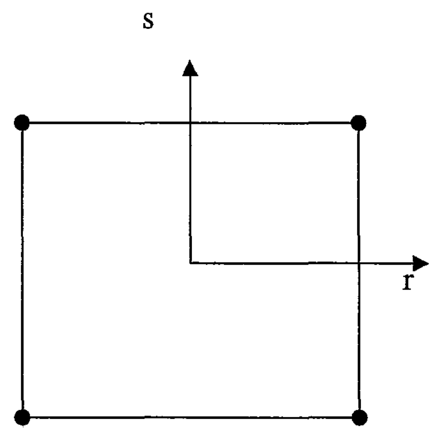

Figure 2.2 4-nodes Shell Element with Nodal Points at Middle Surface (ADINA, 2008)

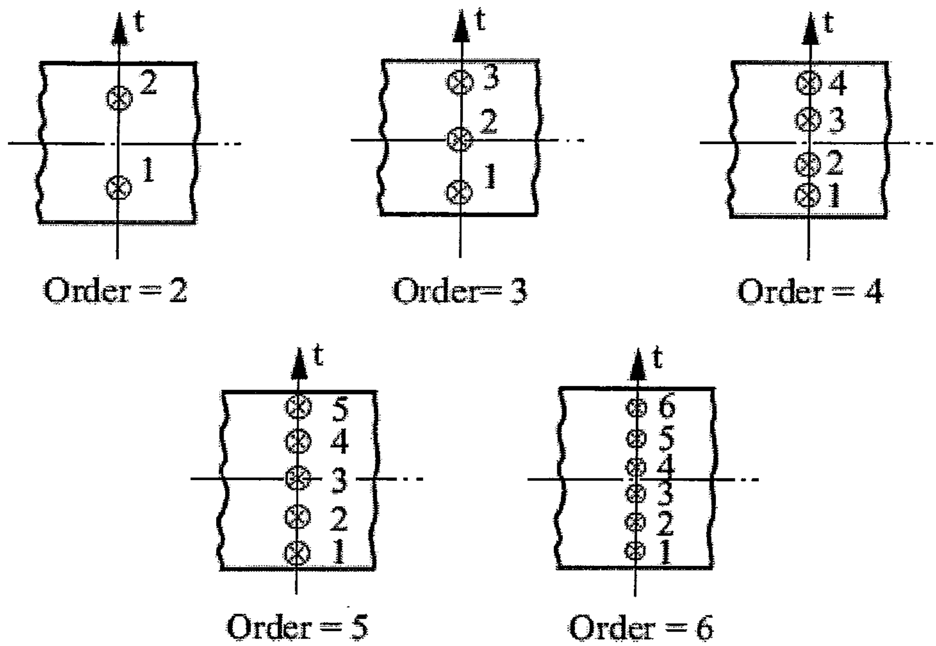

(a) Gauss Quadrature Numerical Integration Points through Thickness

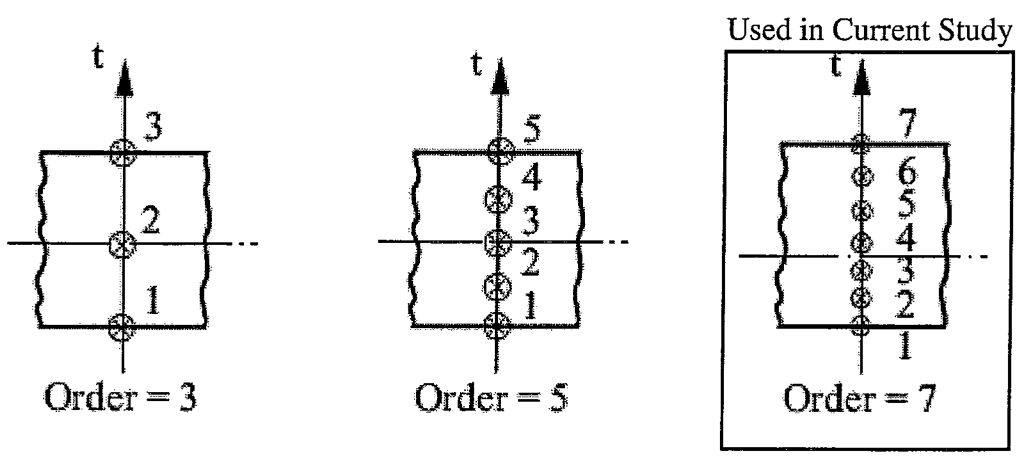

(b) Newton-Cotes Numerical Integration Points through Thickness

Figure 2.3(a) Gauss Quadrature Numerical Integration Points through Thickness (ADINA, 2008)

(b) Newton-Cotes Numerical Integration Points through Thickness ADINA, 2008)

Chapter 3

BEHAVIOR OF SQUARE PLATES UNDER UNIAXIAL COMPESSION

3.1 Introduction

In this chapter, a simply supported steel plate under uniaxial compressive loads will be analyzed using the commercial finite element software package ADINA8.5. Nonlinear types of behavior, including buckling, post-buckling and the ultimate strength of plates will be investigated. The purpose of this chapter is to compare the results obtained from the finite element study with those obtained from previous literature, thus to verify the accuracy and efficiency of the proposed finite element model.

The first part of this chapter presents the theoretical equations of calculating the critical buckling stress, the limiting width to thickness ratio (h/t) for yielding before buckling and the ultimate compressive strength of a simply supported plate under uniaxial compression. In the second part, a finite element model suitable of modeling a simply supported plate under uni-axial compression is proposed. In the third part, a convergence study is carried out to determine the appropriate finite element mesh density for the verification study. Lastly, the verification study is performed on a steel plate subjected to uni-axial compression using ADINA8.5. The critical buckling strengths and the ultimate compressive strengths obtained from the finite element modeling will be compared with those obtained from the literature described in Section 3.2. Since the purpose of this chapter is to verify the proposed finite element model and the finite element analysis program (ADINA8.5), for simplicity, the proposed models can be assumed be to flat with minimal imperfections to invoke the buckling behavior. The effect of residual stresses will also be ignored. All results and observations are presented in the following sections. It was shown that the proposed finite element model is able to predict the behavior of a simply supported plate under uniaxial compression consistently and accurately within reasonable errors.

3.2 Background Information of Plates Subjected to Uniaxial Compression

Figure 3.1 shows a plate subjected to in-plane compression. When a plate is subjected to opposite in-plane edge compressions in its mid-plane, as the edge compressions increase, the loaded edges shorten uniformly. However, when the compression reaches a certain critical value, the plate will undergo out-of-plane deflections, and become unstable at that load level. When edge loads reach this critical level, the energy of an edge compressed perfectly flat plate is equal to the energy stored in the same plate when it is in a slightly bent condition. This critical value of the edge compression is called the critical buckling load of the plate. As shown in Figure 3.1, if a rectangular plate with length 'a', width 'h' and thickness 't' is compressed by equal and opposite uni-axal in-plane loads along the width 'h', the theoretical critical buckling stress of such a plate can be formulated as the following (Timeshenko and Gere, 1961):

$$\sigma_{cr} = k\frac{\pi^2 E}{12(1-\nu^2)(h/t)^2} \tag{3.1}$$

Where 'σ_{cr}' is the critical buckling stress, 'k' is known as the plate-buckling coefficient, which depends on the type of applied stress, the 'a/h' ratio and the boundary conditions of the plate. 'E' and 'ν' are the Young's modulus and the Poisson's ratio, respectively. For a simply supported plate under opposite edge compression, k=$\frac{1}{\phi^2}+\phi^2+2$, where '$\phi$' is the buckling model number. Therefore, for a simply supported square plate under opposite edge compression, the buckling coefficient (k) for the first mode of buckling (ϕ=1) has the value of 4. From Equation 3.1, it can be seen that for a plate with given material properties, specific loading and boundary conditions, the critical buckling stress strongly depends on slenderness ratio (h/t) of the plate. As h/t decreases, 'σ_{cr}' can be as high as the yield stress (F_y), or even higher. The critical buckling stress 'σ_{cr}' is called the elastic buckling stress provided that the plate buckles within its elastic range, that is when 'σ_{cr}' is less than the yield stress of the plate 'F_y'. The limiting h/t value occurs when σ_{cr} is equal to F_y. Thus, when substituting F_y into Equation 3.1, the limiting h/t ratio is:

$$\frac{h}{t} = \sqrt{k\frac{\pi^2 E}{12(1-\nu^2)F_y}} \tag{3.2}$$

Therefore, when the 'h/t' ratio is below the limit value given by Equation 3.2, a plate will yield first before it buckles. Since cold-formed steel plates are generally very thin (that means they have high 'h/t' values), they are usually subjected to elastic buckling behavior. However, unlike columns, plates exhibit post-buckling strength after they reach their elastic buckling load. The post-buckling strength allows a plate to carry higher loads than the critical buckling load σ_{cr}, and remain stable in the buckled form. The post-buckling strength is caused by stretching of the mid-plane of plates and stress redistribution. Therefore, the ultimate strength of a plate is usually larger than its critical buckling strength. The North American Specification (AISI, 2007) provides equations to calculate the ultimate compressive strength of plated elements with different boundaries and loading conditions based on the 'effective width concept'. For plate elements with uniformly compressed loading condition, the average ultimate compressive strength can be found as follows:

$$\sigma_{average} = P_n / A \tag{3.3}$$

$$P_n = F_n \cdot A_{eff} \tag{3.4}$$

$$A_{eff} = b_{eff} \cdot t \tag{3.5}$$

where 'P_n' is the nominal axial resistance of the compressed member and 'A' is the area of the loaded edges. 'F_n' and 'b_{eff}' are defined as below:

AISI (2007)-B2.1 Effective Width of Uniformly Compressed Stiffened Elements

(Note: some symbols have been changed in order to be consistent with the symbols used in this research)

The effective width, b_{eff}, shall be determined from the following equations:

$b_{eff} = h$ When $\lambda \leq 0.673$, (3.6)

$b_{eff} = \rho \cdot h$ When $\lambda > 0.673$ (3.7)

where

h= Flat width of plate element

b_{eff} = Effective design width of compression elements

ρ=Reduction factor

$= (1-0.22/\lambda)/\lambda \leq 1$ (3.8)

λ is a slenderness factor determined as follows:

$$\lambda = \sqrt{\frac{f}{F_{cr}}} \quad (3.9)$$

$$F_{cr} = k\frac{\pi^2 E}{12(1-v^2)(h/t)^2} \quad (3.10)$$

where

t= Thickness of the uniformly compressive stiffened elements

E=modulus of Elasticity (203000MPa)

v =Poisson's ratio of steel (0.3)

k= Plate buckling coefficient (k=4 for stiffened elements supported by a web on each longitudinal edge)

f=Calculated stress in an element = F_n (for axially compressive loaded members)

For concentrally loaded compression members, F_n is determined as follows if the member is not fully braced against lateral buckling:

AISI (2007)-C4 Concentrically Loaded Compression Members

(Note: some symbols have been changed in order to be consistent with the symbols used in this research)

This section applies to members in which the resultant of all loads acting on the member is an axial load passing through the centroid of the effective section calculated at the stress, P_n, defined in this section.

The nominal axial strength [compressive resistance], P_n, shall be calculated as follows:

For $\lambda_c \leq 1.5$ $$F_n = (0.658^{\lambda_c^2}) \cdot F_y \tag{3.11}$$

For $\lambda_c > 1.5$ $$F_n = \left(\frac{0.877}{\lambda_c^2}\right) \cdot F_y \tag{3.12}$$

Where

$$\lambda_c = \sqrt{\frac{F_y}{F_e}} \tag{3.13}$$

F_e = The least of the elastic flexural, torsional and torsional-flexural buckling stress determined according to Sections C4.1 through C4.4.

In the current study, since the plate is assumed to be fully braced against lateral torsional buckling, $F_n = F_y$.

3.3 Finite Element Model for Plates under Compressive Loads

In this section, a general finite element analysis model for analyzing the post-buckling behavior of a simply supported rectangular plate is proposed. Based on a study carried out by Pellegrino et al. (2008), the deformed shape and the buckling coefficient are not sensitive to the shape of the mesh element. Thus, quadrilateral four-node shell elements are used for this study. The four-node element is capable of representing both flat plate surface and curved shell surface. Each node of the shell element has six degrees of freedom, namely three displacements and three rotations. The details of shell elements were presented in Chapter 2. The idealized elastic-perfectly-plastic stress-strain relationship for steel is used for this verification study. The model ignores the effect from geometrical initial imperfections and the effects of residual stress for simplicity.

3.3.1 Loading and the Boundary Conditions

Figure 3.1 shows the dimensions and the loading conditions of plates needed to be studied. A simply supported rectangular plate, with length 'a', width 'h' and thickness 't', is subjected to equal and opposite uniaxial in-plane compressions acting along the width 'h' of the plate. The x-y plane is at the middle plane of the plate. The z-plane is perpendicular to the plate and is zero at the geometric center of the plate. The plate is geometrically symmetrical about the x-axis and the y-axis and is subjected to symmetrical loading conditions. The plate thus behaves symmetrically about both the x and y axes, and are expected to buckle in a symmetrical shape. In theory, only a quarter plate is necessary to be modeled. However, in order to be consistent with the later finite element models for plates under shear loads, a full plate will be analyzed in this verification study.

Figure 3.2 shows the loading details and the boundary conditions for the finite element model of such plates. In Figure 3.2, 'U_1', 'U_2' and 'U_3' are the displacements in the x, y and z directions, respectively, while 'θ_1', 'θ_2' and 'θ_3' are the rotations about the x, y, and z directions, respectively. 'L1', 'L2', 'L3' and 'L4' are the four edges of the plate. 'L5' and 'L6' are the symmetrical lines of the plate about x and y directions, respectively. 'L1', 'L2', 'L3' and 'L4' are fixed in the movement in the z-direction and the rotation about the z-direction. In addition, 'L1' and 'L3' are constrained so that all points along 'L1' or 'L3' have the same displacement in the x-direction. In other words, the two loaded edges ('L1' and

'L3') acting as two rigid edges. Moreover, the y-direction displacement and the x-direction rotation are fixed along 'L5'; the x-direction displacement and the y-direction rotation are fixed along 'L6'.

The compression applied on the edges of plates can either be a uniform incremental compressive stress or a uniform incremental compressive displacement. Since a uniform incremental compressive displacement is more analogous to the loading condition in a laboratory test, a uniform incremental compressive displacement strategy is used in this study. As indicated in Figure 3.2, concentrated loads are applied at the middle of the two loaded edges. Since the two loaded edges ('L1' and 'L3' in Figure 3.2) are constrained so that all points on the two loaded edges displace the same amount in the x-direction, a uniform incremental compressive displacement condition can be achieved in this finite element model.

3.3.2 Method of Analysis

The analysis under consideration is a non-linear static analysis. The non-linearity is caused by both the material property and the large displacement behavior of the plate. The essence of the nonlinear static analysis in a finite element model is to solve the equilibrium equation along both the loading and unloading paths. One way to achieve this in ADINA8.5 is to use the automatic step incrementation, which includes the automatic-time-stepping (ATS) method and the load-displacement-control (LDC) method. The ATS method is a load-controlled loading method. A prescribed load and time steps are required to be specified by the user. If no convergence can be obtained through the user-defined load steps, ADINA8.5 will automatically subdivide the time steps until the convergence is achieved. On the other hand, the LDC method, also called the "arc length" method, is a displacement controlled loading mechanism. It allows users to control the displacement of a control point, and track the nonlinear equilibrium path until collapse. Both these methods are capable of modeling the buckling and post-buckling behavior of plates. However, in this particular modeling, it was found that the LDC method takes more computational effort in the post-processing step when trying to collect data at each time step. Thus, the ATS will be adopted to carry out the finite element analysis for all models in this research. The time steps are specified so that there are at least 100 load steps during each loading process to insure sufficient data points can be obtained to obtain a reasonably accurate load-displacement diagram. The ADINA8.5's default 10-maximum-subdivision within each step is used.

3.3.3 Material Model

In order to process the analysis, a proper yielding criterion needs to be selected. Since cold-formed steel is a ductile and isotropic material, which will start to yield after it reaches a certain load level, the von Mises yield criterion is applicable in this case. The von Mises yield criterion suggests that yielding of a material occurs when its second deviatoric stress invariant reaches a critical value. Furthermore, this criterion can also be introduced in terms of the equivalent tensile stress, which allows one to predict yielding of a material under a multi-axial loading condition from the results of simple coupon tensile tests.

As mentioned before, the elastic-perfectly-plastic stress-strain relationship is used in this chapter for the purpose of verifying the finite element model and the computer program ADINA8.5. Figure 3.3 shows the elastic-perfectly-plastic stress-strain relationship used in this chapter.

3.3.4 Initial Geometric Imperfections

Initial geometric imperfections are the out-of-flatness of plated elements in its unloaded condition (Williams, 1979). Cold-formed steel members are susceptible to initial imperfections, which are inevitable routine by-products of plate rolling, fabrication, transportation, etc. Also, in a finite element model, the buckling response analysis cannot be made on a perfectly flat plate. It is necessary to impose some form of disturbance on a perfectly flat plate to evoke the buckling behavior. This disturbance can be either load or geometrical disturbance. In order to conform to the real situation, the geometrical disturbance, namely initial geometric imperfection, was imposed on the finite element models in this research. Moreover, Williams (1979) has shown that in most cases, the deflections and stresses of plate due to external load will be greatest if the form of the initial imperfection is similar to that of the critical buckling mode shape. Thus, the distribution of initial imperfection of a plate is assumed to be consistent with its predicted buckling shape. For a simply supported plate under uni-axial compression, the buckling shape consists of a half wave in the transverse direction and a series of half waves in the longitudinal direction. Therefore, a double sine function is used to represent the distribution of the geometric imperfection in a plated element:

$$w = w_0 \cdot \mathrm{Sin}(\pi \frac{x}{h}) \cdot \mathrm{Sin}(\pi \frac{y}{h}) \tag{3.11}$$

where 'w' is the imperfection distribution, 'w_0' is the value of the maximum imperfection point. 'a' is the length of the plate, and 'h' is the width of the plate. One should note that Equation 3.11 represents only the first fundamental buckling mode shape. Figure 3.4 schematically shows the geometrical imperfection distribution of a plate in both transverse and longitudinal directions for plates with a=2h.

The purpose of this chapter is to analyze a flat plate. In theory, there is no imperfection on such a plate. However, as mentioned before, in a finite element model, it is necessary to impose some form of disturbance on a perfectly flat plate to evoke the buckling behavior of the plate. Thus, a very small initial imperfection will be imposed on the model just to initiate the buckling behavior of the plate, and the shape of the imperfection will be the same as the fundamental elastic buckling mode shape expressed in Equation 3.11.

3.4 Convergence Study

The principle of a finite element method is to analyze a continuous object by discretizing it into pieces of inter-connected elements. The plate needs to be divided into a sufficient number of elements to allow for the development of an accurate buckling mode and displacement. Thus, as the number of elements increases, the results are closer to the real solution. However, a finely meshed finite element model requires more computational effort, especially when dealing with non-linear problems. In order to build an accurate and effective finite element model, a proper mesh density should be used. In this section, a convergence study is carried out to select a suitable mesh density for the future verification study. The critical buckling loads obtained in this section are obtained through the linearized-buckling analysis introduced in Chapter 2.9.2 and the ultimate strengths are obtained from the ADINA static analysis with the ATS method.

As shown in Figure 3.1, a four edged simply supported square plate with a=h=500mm is considered. The thickness of the plate is t=5mm. Thus, the width to thickness ratio (h/t) is calculated to be 100. The plate is under uniaxial compression along two opposite edges of the plate. As explained before, a full plate is analyzed in order to be consistent with the finite element models for plates subjected to shear loads in the later chapters. The plate is assumed to be elastic-perfectly-plastic with F_y =350MPa and ν =0.3. The effect of the residual stress is ignored. A small geometrical initial imperfection ($\frac{w_0}{h} = 0.001$) is imposed to initiate the buckling action of the plate. The analysis includes 5 identical models with only changing the mesh configurations. Model numbers 1 to 5 will have mesh configurations of 6x6, 10x10, 16x16, 20x20 and 30x30, respectively. Thus models 1 to 5 have an increasing number of total mesh elements. The buckling loads and the ultimate shear strengths of the models are presented in the Table 3.1. The percentage changes in the buckling load and the ultimate strength of each model will be compared.

In Table 3.1, the first column from the left indicates the mesh configurations for the 5 plate models. The second column indicates the total number of elements in each of the 5 plates. The third and the fifth columns list the buckling strength and the ultimate compressive strength of the 5 plates, respectively. The fourth column calculated the percent differences in the buckling strength between two adjacent mesh configurations. The sixth column shown the percent differences in the ultimate compressive strength between two adjacent plates. It is evident from Table 3.1 that as the mesh becomes finer (increasing total number of elements), the percentage differences in both the buckling loads and ultimate strengths between two adjacent plates become smaller. As suggested by Thangavadivel (2003), the percentage difference of around 5% for both the buckling and ultimate load is generally acceptable for analysis purpose. Therefore, from Table 3.1, it is shown that a mesh configuration of 10x10, 16x16, 20x20, and 30x30 are all qualified. However, since the later verification analysis will include plates with changing plate thicknesses, in order to be more conservative, the 20x20 mesh configuration with 400 elements in total was chosen for the following verification analysis problems.

3.5 Verification Study on Simply Supported Plate under Uniaxial Compression

The previous section has selected the desired mesh configuration for a square plate with a=h=500mm as 20x20. In this section, the selected mesh configuration will be used to analyze a series of plate models with different width to thickness (h/t) ratios. The results will then be compared with some theoretical values calculated in Section 3.2.

A simply supported square plate (a=h=500mm) is subjected to uniaxial compression along two opposite edges. Five identical plate models with varying thicknesses will be studied in this verification study. The h/t ratios of the five plates are 20, 50, 100, 150 and 200 respectively. The plate is assumed to be elastic-perfectly-plastic with F_y =350MPa, E=200000MPa and ν=0.3. A very small initial geometric imperfection with $\frac{w_0}{h} = 0.001$ is imposed in order to initiate the buckling action of the plate in the finite element model.

3.5.1 Comparison of Critical Buckling Load

The buckling loads are obtained from ADINA8.5 by performing linearized buckling analysis. In linearized buckling analysis, critical buckling stress is calculated by solving the corresponding generalized eigenvalue problem. Figure 3.5 shows that the square plate buckled in model one when subjected to uniaxial compression. The predicted critical buckling stress will then be compared with the critical buckling stress calculated using Equation 3.1. The comparison between the results obtained from the proposed finite element model and those obtained from Equation 3.1 are presented in Table 3.2. As shown in Table 3.2, the critical buckling stress obtained from the finite element model is in good agreement with the values calculated from Equation 3.1. The maximum percent difference between the critical stress obtained from the finite element method and Equation 3.1 is 2.28%, which is within an acceptable variation range. For h/t equals 20, the calculated critical buckling stress is actually higher than the yielding stress (F_y=350 MPa), which means that the plate will yield first before buckling takes place. One should also note that for h/t=20, the critical buckling load obtained from solving the eigenvalue problem is also higher that the ultimate strength of the plate. In reality, this means such a plate will not buckle until it reaches its ultimate compressive capacity.

3.5.2 General Behavior of Plates

Figure 3.6 to Figure 3.10 show the relationship between the applied average compressive stresses versus the out-of-plane deflection at the middle of the plate for plates with different slenderness ratios (h/t). The average compressive stresses are obtained by dividing the total load applied along each edge of the plate by the width (h) and the thickness (t) of the plate. It can be seen from these figures that for thick plates, for example plates with h/t=20 and 50, no post-buckling strength exists. As the plates become thinner, more post-buckling strength exists.

Figure 3.11 shows the contours of the z-displacement of plates at failure with h/t= 20, 50, 100, 150 and 200. Figure 3.12 shows the material plasticity condition of plates at failure with h/t= 20, 50, 100, 150 and 200, where the red zones indicate a plastic condition of material and the purple zones indicate an elastic condition of material. It can be seen that as the plate becomes thicker, more material in the plate becomes plastic. For example, when h/t=20, almost the whole plate becomes plastic, such a plate fails due to complete yielding.

3.5.3 Comparison of Ultimate Compressive Strength

Table 3.3 and Figures 3.13 show the comparison results between the ultimate strengths of plates obtained from the finite element method and those calculated following the AISI (2007) equations. It can be seen that the ultimate strengths obtained from finite element modeling are very similar to those obtained from the AISI (2007) method for relative thicker plates; but are slightly higher than those calculated from the AISI (2007) for thinner plates. The maximum difference between the results obtained from the two methods is about 14%, which occurs when h/t=200 (the thinnest plate). The AISI (2007) may have underestimated the post-buckling strength of plates. As stated in Chapter 2, post-buckling strength becomes more dominant as a plate becomes thinner. Thus, the ultimate compressive strength calculated from the AISI (2007) method may be underestimated more for thin plates. Moreover, specifications tend to stay on a more conservative side for safety considerations. Thus, it is expected that the finite element method will give a little higher ultimate compressive strength compared to the ultimate compressive strength obtained from the AISI (2007).

3.6 Conclusion

In conclusion, the finite element model developed in this section has well simulated the buckling and post-buckling behavior of a simply supported square plate under uniaxial loads along its two opposite edges. Through the verification study, it can be seen that the finite element model can predict the buckling load and the ultimate strength of the plate with reasonable accuracy.

Table 3.1 Buckling and Ultimate Strengths of Plates with Different Mesh Configurations

Mesh Configuration	Total Number of Elements	Buckling Load (MPa) σ_{cr} (MPa)	%Diff.	Ultimate Load (MPa) σ_{ul} (MPa)	%Diff.
6x6	36	75.38		165.80	
			2.56		5.20
10x10	100	73.98		157.60	
			1.04		2.60
16x16	256	73.50		153.61	
			0.38		1.33
20x20	400	73.22		151.60	
			0.18		0.53
30x30	900	73.09		150.80	

Table 3.2 Buckling Strengths of Plate Models with Different b/t Values

b/t	σ_{cr} (FEM) MPa	σ_{cr} (E3.1) MPa	%Diff.
20	1848.80	1807.60	2.28
50	289.46	289.22	0.08
100	73.22	72.31	1.26
150	32.24	32.14	0.31
200	18.14	18.08	0.33

Table 3.3 Ultimate Strength of Plate Models with Different b/t Values

b/t	σ_{ul} (FEM) MPa	σ_{ul} (AISI,2007) MPa	%Diff.
20	349.77	349.69	0.02
50	262.56	254.39	3.21
100	151.60	143.10	5.94
150	107.35	98.94	8.50
200	85.95	75.53	13.80

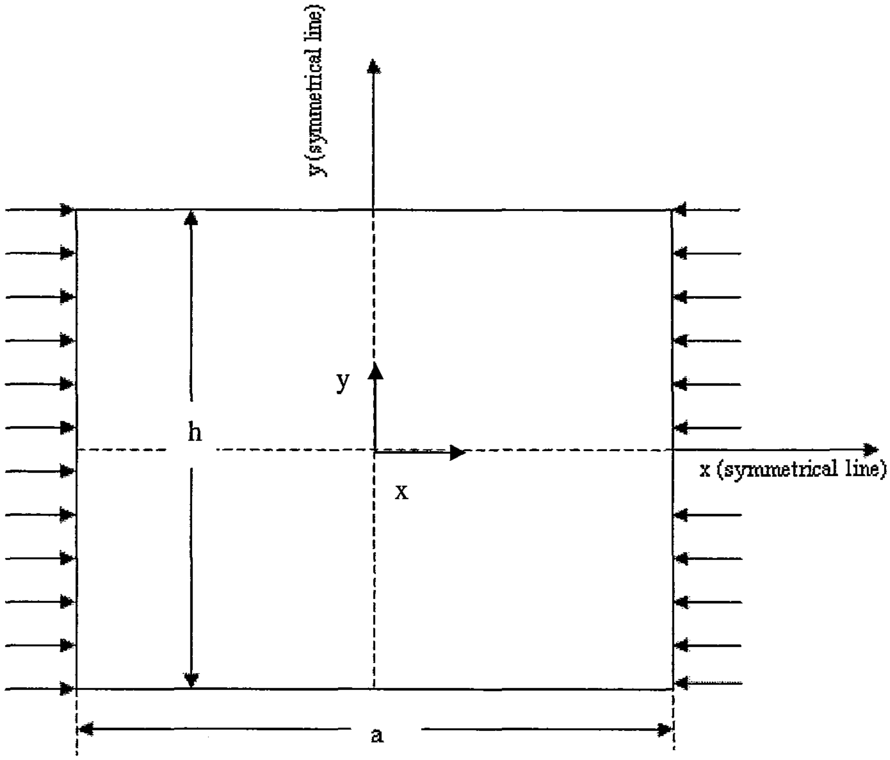

Figure 3.1 Simply Supported Plate Subjected to Uniaxial Compression

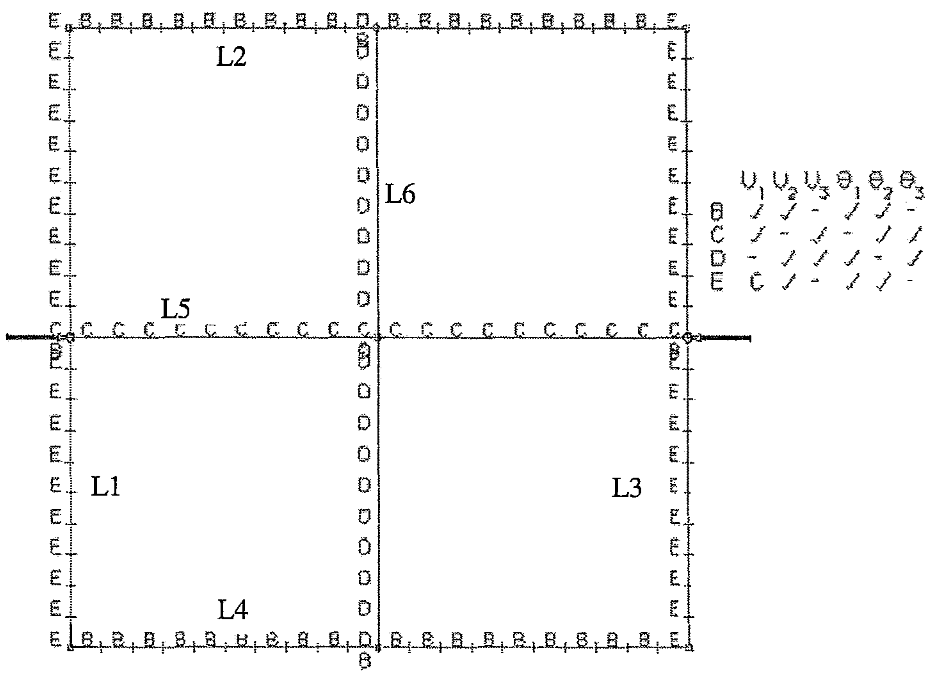

Figure 3.2 Loading and Boundary Conditions of the Finite Element Model for a Plate Subjected to Uniaxial Compression

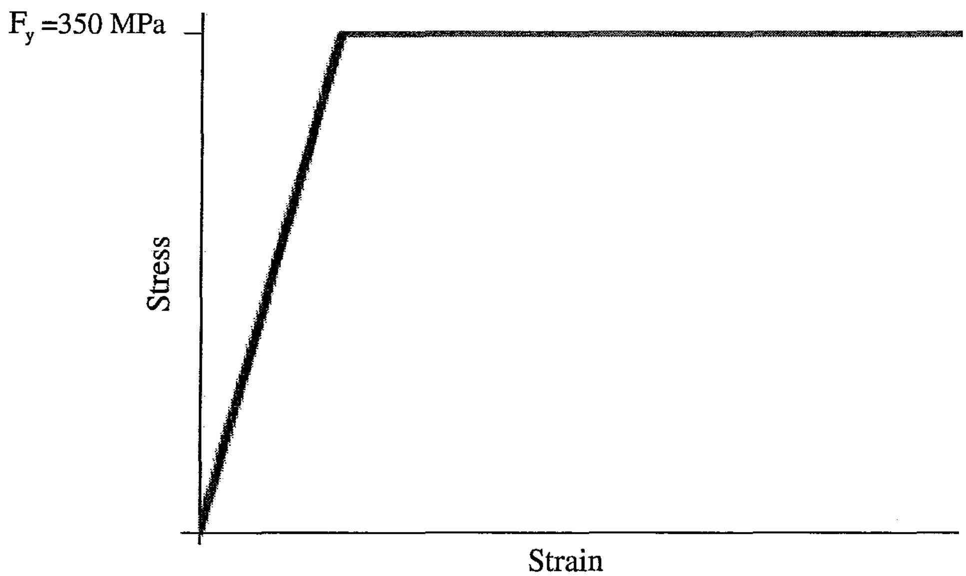

Figure 3.3 Elastic-Perfect-Plastic Stress-Strain Curve

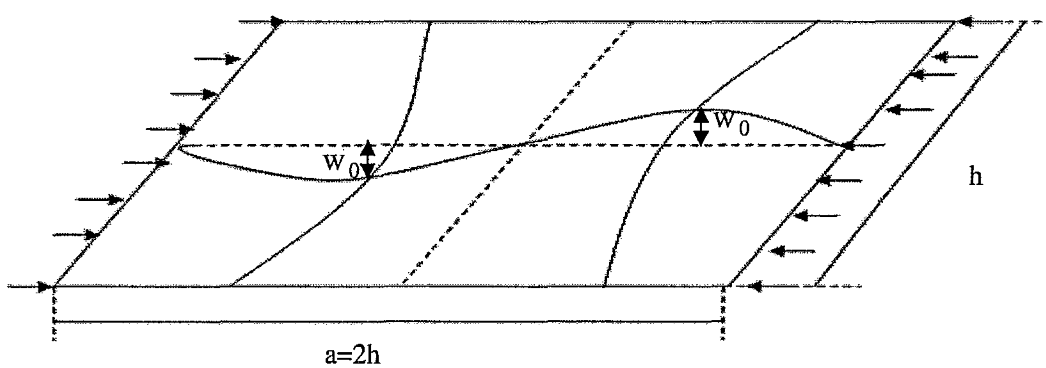

Figure 3.4 Geometrical Imperfection Distribution for Plates with a=2h.

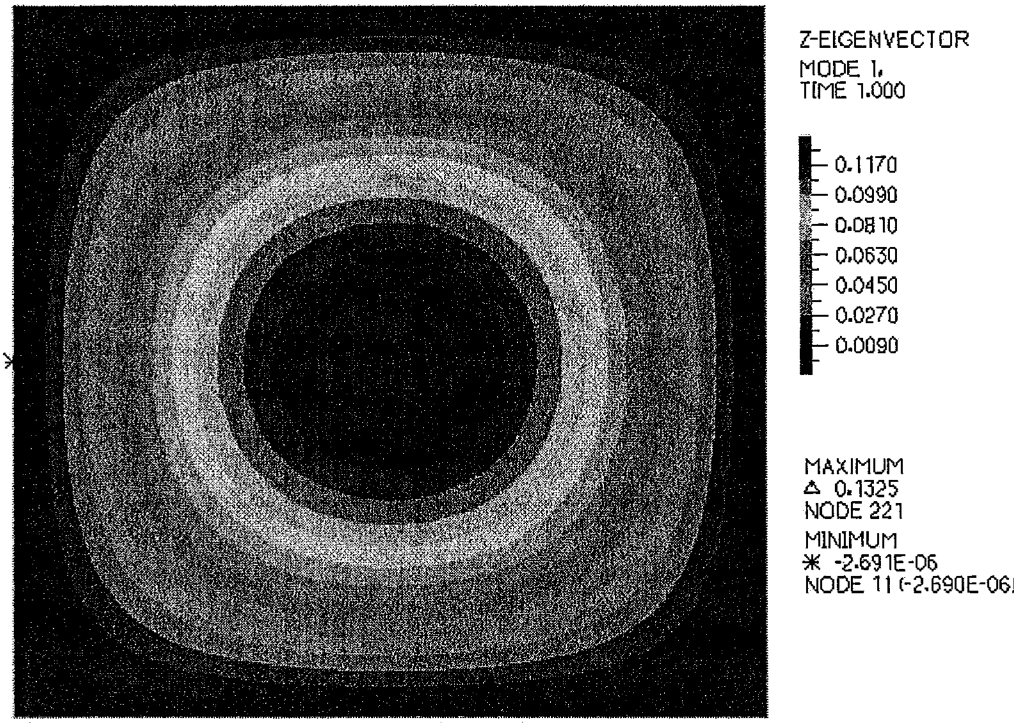

Figure 3.5 Buckled Shape of Simply Supported Square Plate under Uni-axial Edge Compression

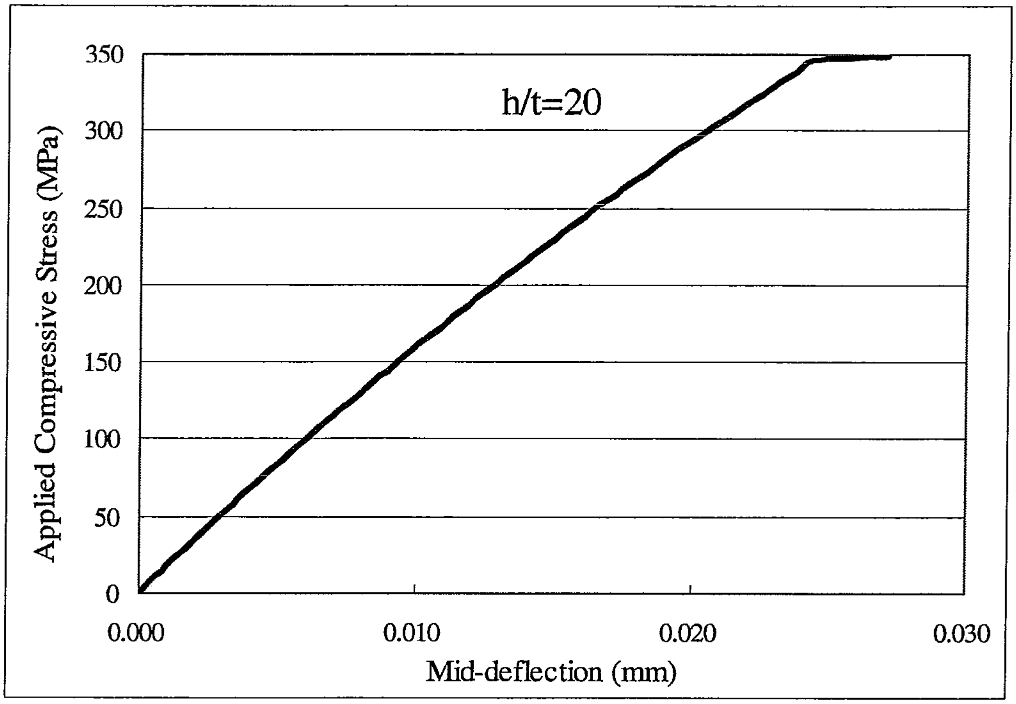

Figure 3.6 Applied Average Compressive Stress Versus Out of Plane Deflection at the Middle of the Plate (h/t=20)

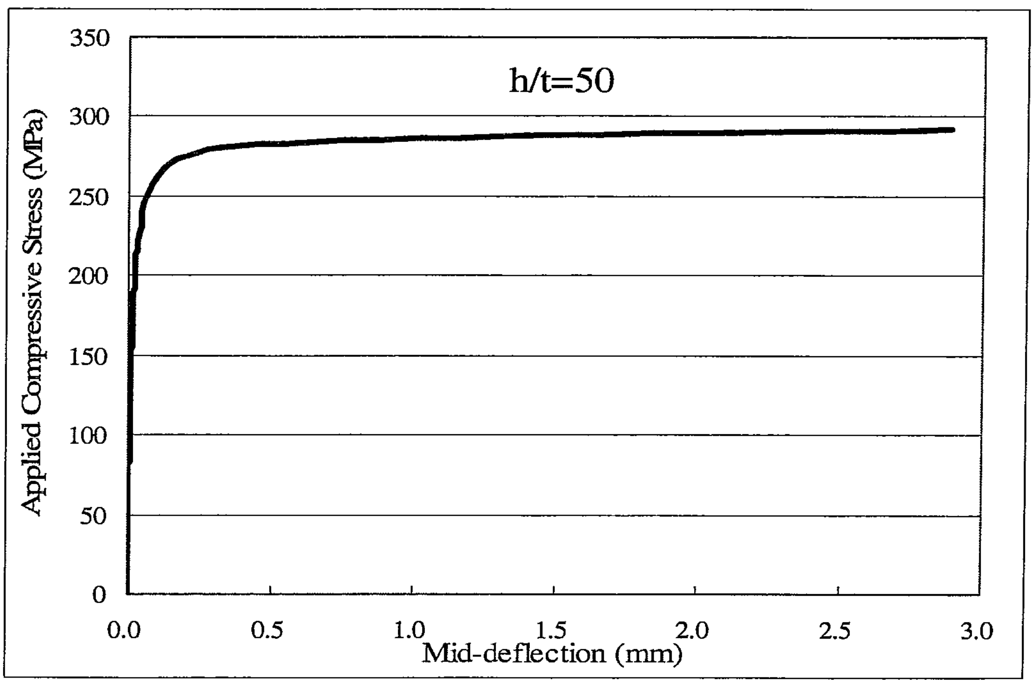

Figure 3.7 Applied Average Compressive Stress Versus Out of Plane Deflection at the Middle of the Plate (h/t=50)

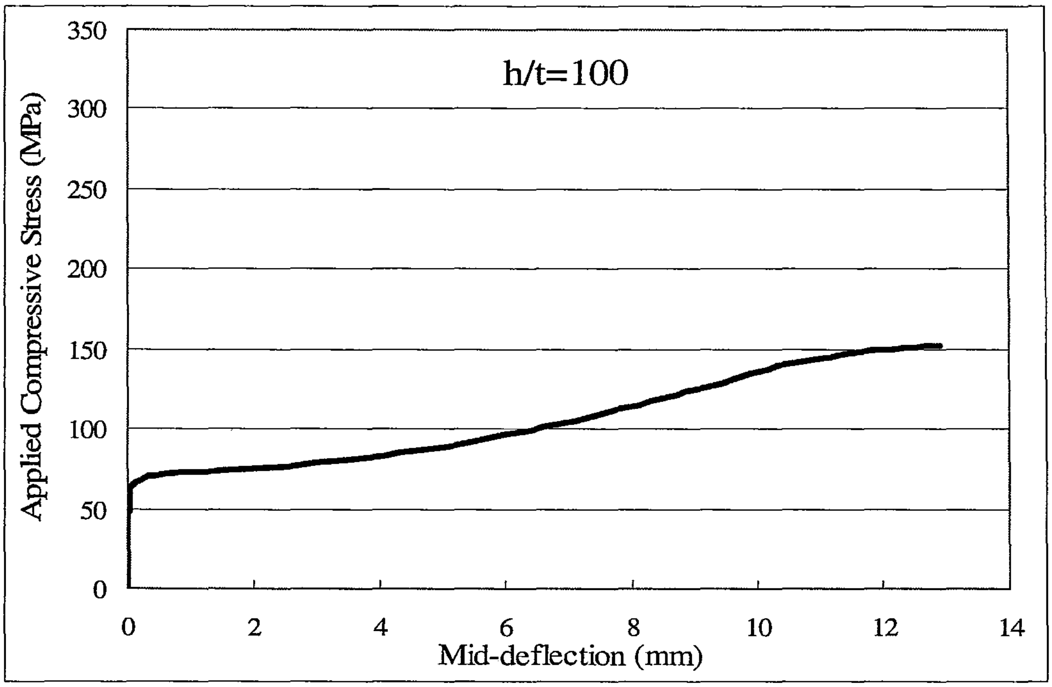

Figure 3.8 Applied Average Compressive Stress Versus Out of Plane Deflection at the Middle of the Plate (h/t=100)

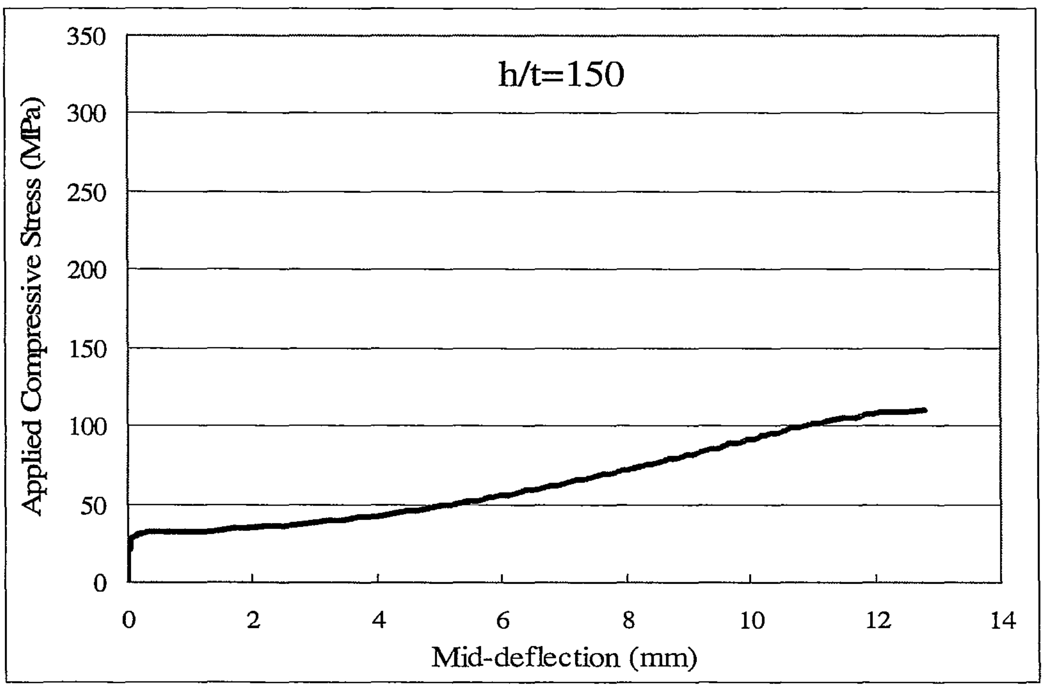

Figure 3.9 Applied Average Compressive Stress Versus Out of Plane Deflection at the Middle of the Plate (h/t=150)

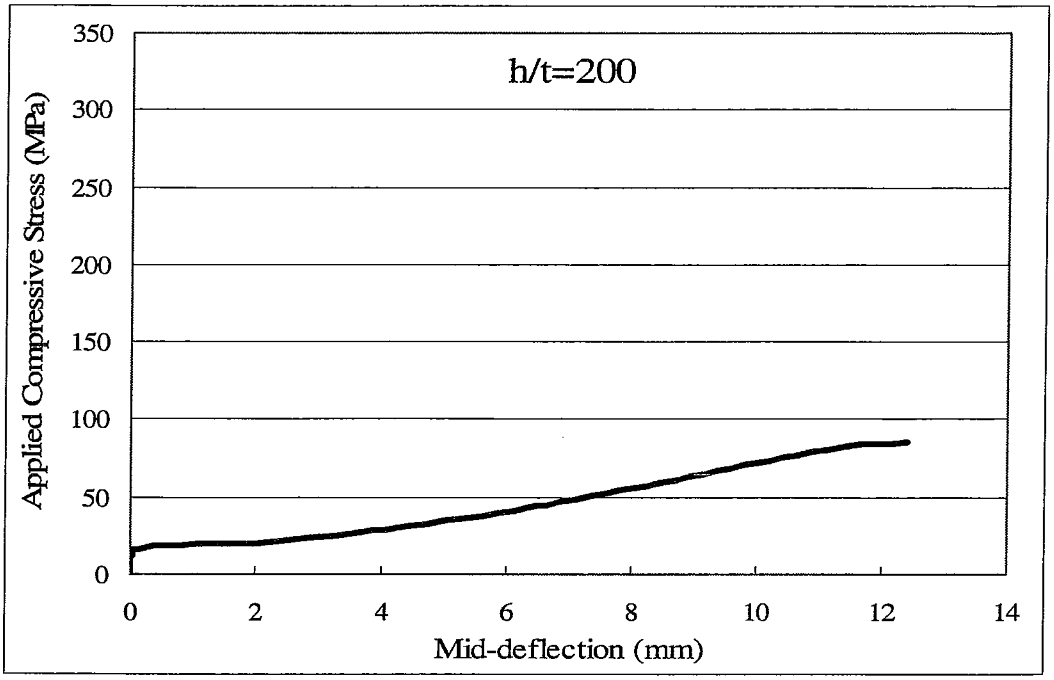

Figure 3.10 Applied Average Compressive Stress Versus Out of Plane Deflection at the Middle of the Plate (h/t=200)

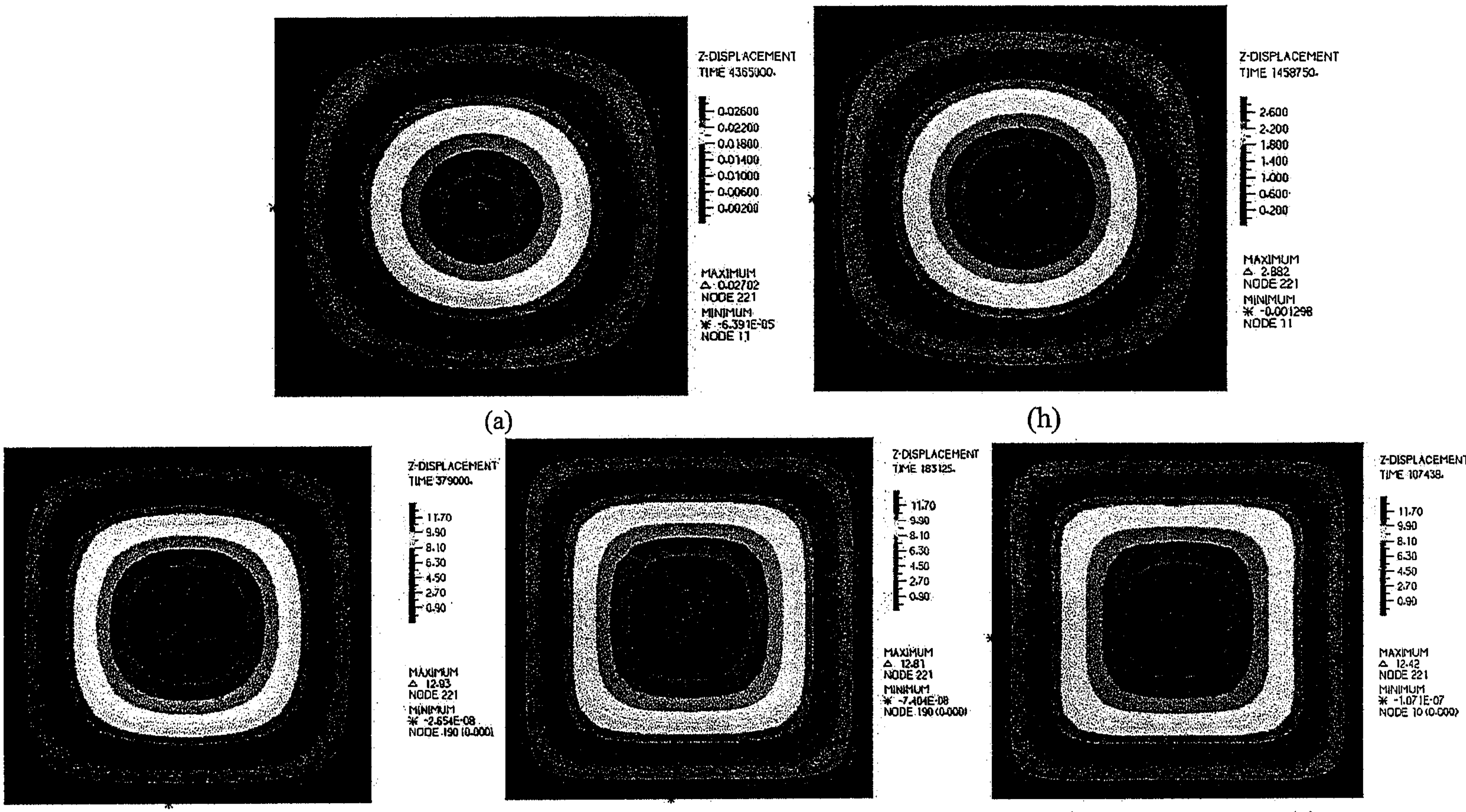

(a) (h)

(c) (d) (e)

Figure 3.11 Out-of-Plate Deflections of Plates at Failure as a Function of the Slenderness Ratio
(a) h/t=20 (b) h/t=50 (c) h/t=100 (d) h/t=150 (e) h/t=200

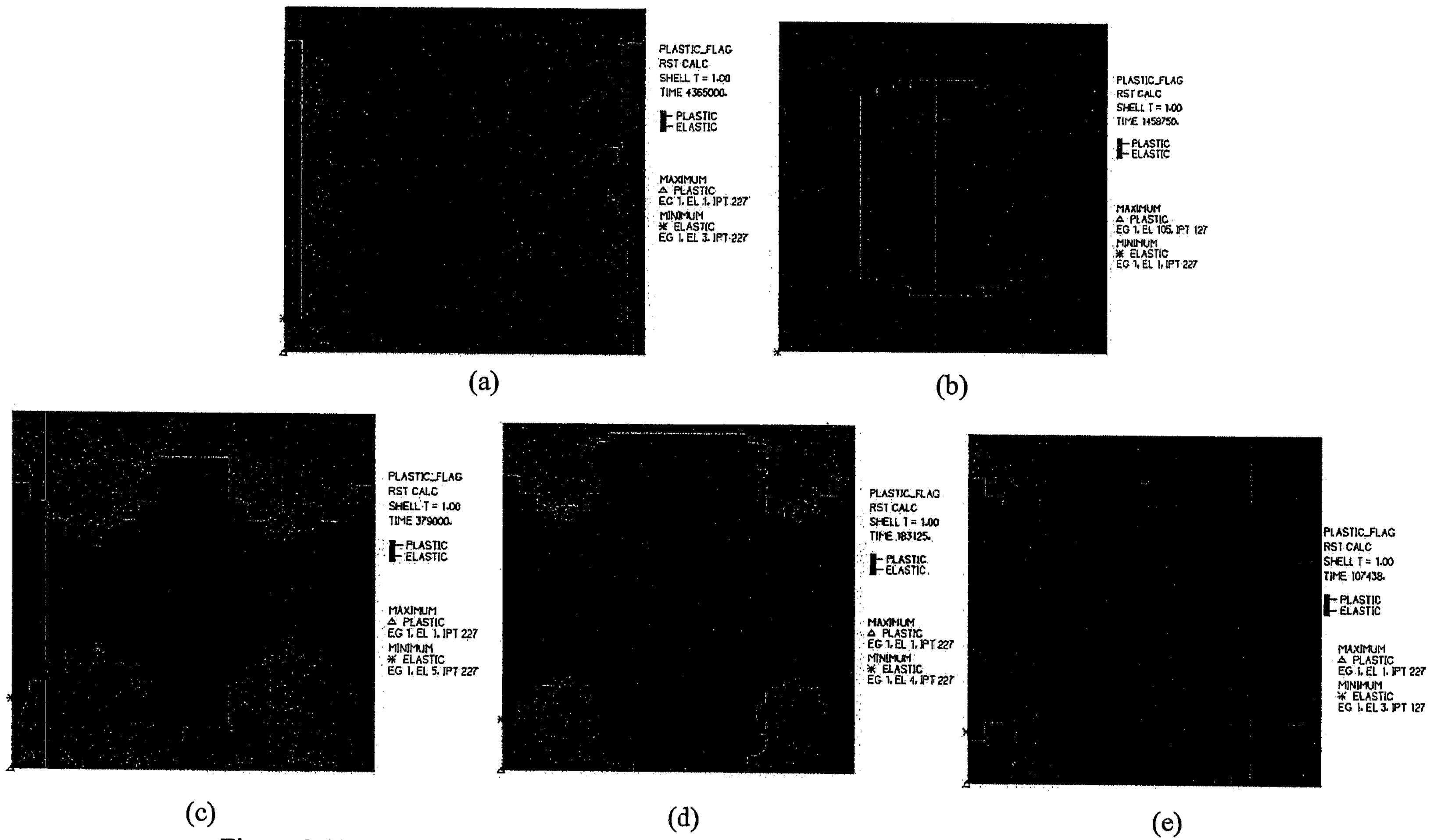

Figure 3.12 Material Failure Band Plot of Plates as a Function of the Slenderness Ratio
(a) h/t=20 (b) h/t=50 (c) h/t=100 (d) h/t=150 (e) h/t=200

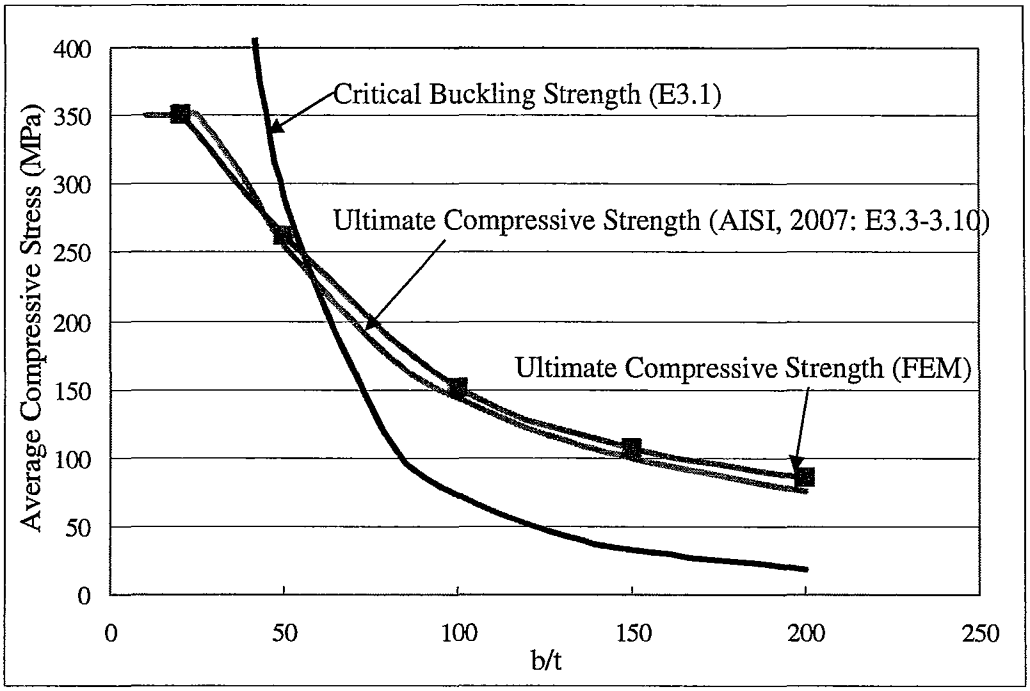

Figure 3.13 Ultimate Compressive Strengths of Plates Obtained From the Finite Element Method and the AISI (2007) Method

Chapter 4

SHEAR BEHAVIOR OF SOLID PLATES

4.1 Introduction

As introduced in Chapter 1, steel structural members may fail in shear, especially around the supporting area, where beams or girders are subjected to high shear force. This chapter will concentrate on the ultimate shear strength of solid plate webs having various dimensions.

In Chapter 4, simply supported steel plates under pure shear loads will be analyzed using the commercial finite element software package ADINA8.5. The nonlinear behavior, including buckling, post-buckling and the ultimate strength of the plate will be investigated through the use of finite element models. The purpose of this chapter is to study the ultimate shear strength of plates with various dimensions. The ultimate shear strengths obtained from the finite element analysis will be compared with those obtained from the current North American Specification for the Design of Cold-formed Steel Structural Members (AISI, 2007). The AISI (2007) code equations will then be proposed to be modified based on the finite element results.

The first part of this chapter presents the theoretical methods of calculating the shear critical buckling stress, the limiting width to thickness ratio (h/t) for yielding before buckling of plates subjected to pure shear loads and the ultimate shear strength of solid web plates. In the second part, a finite element model suitable for modeling a web plate subjected to shear loads is proposed. In the third part, a convergence study is carried out to decide how many mesh elements should be used for future analysis. In the fourth part, an imperfection sensitivity study is carried out to further study the effects of the initial geometrical imperfection on the ultimate shear capacity of plates. In the fifth part, parametric studies are performed on plates under shear loads using the proposed finite element models. The post-buckling behavior of such plates will be studied. The ultimate shear strengths obtained from the finite element analysis will be compared with those calculated from the AISI (2007) code method. The equations of calculating the shear capacity of plates under shear loads in the AISI (2007) will then be modified based on the results obtained from the finite element analysis. The detailed results and observations are presented in the following sections.

4.2 Background Information of Plates Subjected to Shear Loads

As indicated in Figure 4.1(a), when a plate is subjected to pure shear loads along the edges, at the initial loading stage, equal tensile and compressive principle stresses are developed prior to shear buckling occurs. As the applied shear loads increase, the compressive and tensile stresses within the plate increase equally until shear buckling load is reached. After shear buckling load is reached, plates cannot take any additional compressive load. As indicated in Figure 4.1(b), by stress redistribution within the plate, the additional shear loads are then resisted by the tensile membrane stress only. According to Porter et al.'s theory (1975), the edge elements of the plate serve as an anchor to the diagonal tension field. Therefore, the rigidity of edge members greatly influences the magnitude of the post-buckling strength of the plate. As indicated in Figure 4.1(c), if the edge elements are flexible, the edge member will bend inward, plate failure will be initiated by forming plastic hinges at the edge members. As indicated in Figure 4.1(d), if the edge elements are rigid, plate failure will be governed by frame action.

4.2.1 Shear Buckling Strength of Solid Plates

Similar to plates subjected to uni-axial compressions, plates under edge shear forces exhibit buckling behavior when the applied shear force reaches the shear buckling load. As shown in Figure 4.2, if a rectangular plate with length ‘a’, width ‘h’ and thickness ‘t’ is subjected to uniform shear loads, the critical shear buckling strength of such plate can be formulated as the following (Timoshenko and Gere , 1961):

$$\tau_{cr}^{solid} = k_v^{solid} \frac{\pi^2 E}{12(1-\nu^2)(h/t)^2} \tag{4.1.1}$$

For plates with all edges simply supported

$$k_v^{solid} = 5.34 + \frac{4}{(a/h)^2}, \quad a/h \geq 1 \tag{4.1.2}$$

where ‘E’ and ‘ν’ are Young’s modulus and Poisson’s ratio, respectively. ‘τ_{cr}^{solid}’ is the critical buckling stress of plates under shear loads. ‘k_v^{solid}’ is the non-dimensional shear-buckling coefficient, which depends on the aspect ratio and the boundary conditions of plates. Equation 4.1.2 is the approximate relationship between the shear-buckling coefficient ‘k_v^{solid}’ and the aspect ratio ‘a/h’ for simply supported plates subjected to shear loads. ‘a’ is the larger dimension of plate sides and ‘h' is the smaller. This will make sure that ‘a/h’ is always greater that 1. For example, for a simply supported square plate under uniform edge shear, the shear-buckling coefficient 'k_v^{solid}' has the value of 9.34. From Equation 4.1.1, it can be seen that for a plate with given material properties, specific loading and boundary conditions, the critical buckling load depends on the slenderness ratio (h/t) of the plate. As 'h/t' decreases, 'τ_{cr}^{solid}' can be as high as the shear yield stress (τ_y), or even higher. The limiting 'h/t' value is when 'τ_{cr}^{solid}' is equal to 'τ_y'. Thus, when substituting 'τ_y' into Equation 4.1.1, the limiting 'h/t' ratio is:

$$\frac{h}{t} = \sqrt{k_v^{solid} \frac{\pi^2 E}{12(1-\nu^2)\tau_y}} \tag{4.2}$$

Therefore, when the 'h/t' ratio is below the limiting value, the plate will yield first before it buckles. Substituting the material properties for cold-formed steel, that is ν=0.3 and $\tau_y = F_y / \sqrt{3}$ MPa, Equation 4.2 becomes:

$$\frac{h}{t} = \sqrt{k_v^{solid} \frac{\pi^2 E}{12(1-\nu^2)(F_y / \sqrt{3})}} \approx 1.25\sqrt{E k_v^{solid} / F_y} \tag{4.3}$$

Therefore, for a steel plate with material properties of ν=0.3, and which possess on a sharp-yielding stress-strain relationship, when the slenderness ratio (h/t) is greater than $1.25\sqrt{Ek_v^{solid}/F_y}$, the plate will buckle before it yields.

However, for cold-formed steel with a gradual-yielding stress-strain relationship discussed in Section 2.2, during the gradually yielding process, the slope of the stress-strain curve changes continuously, which means the modulus of elasticity (E) also changes continuously. The theoretical value of critical shear buckling stress thus should be reduced according to the reduction in modulus of elasticity (E).

4.2.2 Ultimate Shear Strength of Solid Plates

Cold-formed steel members are generally comprised of thin plate elements (high h/t value). These members are usually susceptible to local buckling of individual plate elements. However, the critical shear buckling strength does not necessarily mean failure of the plate. As discussed before, plate elements exhibit post-buckling strength after they reach the elastic buckling load. The ultimate shear strength of a thin plate is usually larger than its shear buckling strength. The North American Specification (AISI, 2007) provides procedures to estimate the ultimate shear capacity of solid web plates as given below:

AISI (2007)-C3.2.1 Shear Strength [Resistance] of Webs without Holes

(Note: some symbols haves been changed in order to be consistent with the symbols used in this research)

The nominal shear strength [resistance], V_n, shall be calculated as follows:

$$V_n = A_w F_v \tag{4.4.1}$$

(a) For h/t $\leq \sqrt{Ek_v^{solid}/F_y}$

$$F_v = 0.60 F_y \tag{4.4.2}$$

(b) For $\sqrt{Ek_v^{solid}/F_y} <$ h/t $\leq 1.51\sqrt{Ek_v^{solid}/F_y}$

$$F_v = \frac{0.60\sqrt{Ek_v^{solid} F_y}}{(h/t)} \tag{4.4.3}$$

(c) For h/t $> 1.51\sqrt{Ek_v^{solid}/F_y}$

$$F_v = \frac{\pi^2 E k_v^{solid}}{12(1-\nu^2)(h/t)^2} = 0.904E\,k_v^{solid}/(h/t)^2 \tag{4.4.4}$$

where

A_w = Area of web element = (h · t)

E= Modulus of elasticity of steel

F_v = Nominal shear stress

V_n = Nominal shear strength [resistance]

t= Web thickness

h= Depth of flat portion of web measured along plane of web

ν=Poisson's ratio = 0.3

k_v^{solid} = Shear buckling coefficient determined as follows:

1. For unreinforced webs, $k_v^{solid} = 5.34$

2. For webs with transverse stiffeners satisfying the requirements of Section C3.6:

   When $a/h \leq 1.0$

$$k_v^{solid} = 4.00 + \frac{5.34}{(a/h)^2} \tag{4.4.5}$$

   When $a/h > 1.0$

$$k_v^{solid} = 5.34 + \frac{4.00}{(a/h)^2} \tag{4.4.6}$$

where

a= Shear panel length of unreinforced web element

= Clear distance between transverse stiffeners of reinforced web elements

As seen from the above equations, the ultimate shear strength of a solid web plate is a function of the slenderness (h/t) and the aspect ratio (a/h) of the web plate. Figure 4.3 shows the shear strength of a plate as functions of the slenderness and the aspect ratio calculated according to the AISI (2007) method when the material properties are fixed.

Taking a close look at the AISI (2007) procedure of calculating the ultimate shear capacity of web plates presented above, it can been seen that, since the AISI (2007) adopted the gradual-yielding stress-strain curve for cold-formed steel, web plates can be divided into three cases, namely, (a) thick, (b) moderate thick and (c) thin. Plates falling into region (a) will fully yield before they reach the corresponding shear buckling stress. Such plates undergo material failure rather than suffering from an instability failure and are usually referred to as thick plates. Thus, the ultimate shear strength of web plates falling in case (a) is the material strength of plates, which is the shear yield strength of steel (τ_y). Using Von Mises yield criterion, $\tau_y = \frac{F_y}{\sqrt{3}}$ ≈ 0.577. The AISI (2007) uses $\tau_y \approx 0.60F_y$, which is higher than $\frac{F_y}{\sqrt{3}}$, to keep consistent with the reduction factor of safety normally used in for shear yielding in allowable stress design standards such as the AISC Specification. Region (c) is for plates having their critical shear buckling strength less than the proportional limit in shear ($0.8\tau_y$=$0.8^* F_y / \sqrt{3}$). Such plates undergo elastic buckling behavior. The AISI (2007) estimates the ultimate strength of such thin plates as its shear buckling strength, which is $F_v = \frac{\pi^2 E k_v^{solid}}{12(1-\nu^2)(h/t)^2} \approx$ $0.904 E k_v^{solid} / (h/t)^2$. For plates with h/t ratio falling in case (b), which is the transition zone between elastic buckling and yielding, plates undergo inelastic buckling. The AISI (2007) estimates the ultimate strength of such plates as the geometric mean of their shear buckling stress and 0.8 times the shear yield stress, which is,

$$F_v = \sqrt{\tau_{cr}\tau_{pr}} = \sqrt{\tau_{cr}(0.8\tau_y)} \tag{4.5}$$

where 'τ_{cr}' is the elastic shear buckling stress. 'τ_{pr}' is the proportional limit of shear, which is defined as $\tau_{pr}=0.8\,\tau_y$. Substituting 'τ_{cr}' and '$0.8\,\tau_y$' into Equation 4.5, one can obtain that $F_v = \dfrac{0.64\sqrt{Ek_v^{solid}F_y}}{(h/t)} \approx \dfrac{0.60\sqrt{Ek_v^{solid}F_y}}{(h/t)}$. It is obvious that the procedure provide in AISI (2007) did not incorporate the post-buckling behavior of web plates into its ultimate shear capacity. It is possible that the AISI (2007) may under estimate the shear strength of thin web plates.

4.3 Finite Element Model for Plates under Shear Loads

In this section, a general finite element model for analyzing the post-buckling behavior of a simply supported rectangular cold-formed steel plate subjected to pure shear loads is proposed. As explained in Section 3.3, the quadrilateral four-node shell elements are used in this model. The automatic-time-step (ATS) is used as the analysis method, and the linearized-buckling-analysis is used to obtain the critical buckling strength of plates in this chapter. As stated in Section 3.3.2, at least 100 load steps are used for each loading process to insure sufficient numbers of data point for the load-displacement diagram. The proposed finite element model uses an idealized stress-strain relationship for cold-formed steel proposed by Sivakumaran and Abdel-Rahman (1998). The model has included the effects of the geometrical initial imperfection, and has ignored the effects of the residual stress. The reason for neglecting the residual stress is stated in the following sections.

4.3.1 Loading and the Boundary Conditions

Figure 4.2 shows the dimensions and the loading conditions of plates need to be studied. It is a simply supported rectangular plate with length 'a', width 'h' and thickness 't'. The x-y plane is at the middle plane of the plate. The z-plane is perpendicular to the plate and is zero at the geometric center of the plate. The plate is subjected to pure shear loads along four edges.

The loading details and the boundary conditions for the proposed finite element model are shown in Figure 4.4. In this figure, 'U_1', 'U_2' and 'U_3' are the displacements in the 'x', 'y' and 'z' directions, respectively, while 'θ_1', 'θ_2' and 'θ_3' are the rotations about the 'x', 'y', and 'z' directions, respectively. 'L1', 'L2', 'L3' and 'L4' are the four edges of the plate. 'Point 1' and 'Point 2' are the lower left corner and the upper left corner of the plate, respectively. Unless otherwise specified, all nodes are fixed in the z-direction rotation (θ_3) to restrain the rigid body rotation about z-axis and are free in all the other degree of freedoms. In order to simulate a simply supported boundary condition, the four edges of the plate (L1, L2, L3 and L4) are fixed in z-direction translation only. In addition to the 'z' direction translation, point 1 is also fixed in the 'x' and 'y' translation to eliminate the rigid body movement of the plate in 'x' and 'y' directions; Point 2 is also fixed in x-translation to avoid the rigid body rotation of the plate about 'z' axis.

To simulate a pure shear loading state, uniformly distributed line loads are applied along the four edges of the plate. The shear loads are directly applied to the nodes as a system of conservative forces and are kept tangential to the edges of the plate during the deformation process.

4.3.2 Material Model

The von Mises yield criterion is adopted as the yielding criterion for steel as explained in Section 3.3.3. Sivakumaran and Abdel-Rahman (1998) has shown that, instead of a well-defined yield point, cold-formed steel possesses a gradual yielding behavior followed by a certain level of strain hardening. Within a cold-formed steel section, the yield strength and ultimate strength differs between the corner area and the flat area. Since this study focuses only on the flat plates, the stress-strain relationship for the flat area will be used for all models in this research. For analysis purpose, Sivakumaran and Abdel-Rahman (1998) proposed an idealized multi-linear stress-strain relationship for cold-formed steel material. Figure 4.5 shows this stress-strain relationship, where 'F_y' is the yield stress of steel, which depends on the steel grade selected in the analysis. In this research, the commonly used 350MPa yield strength is used as the value of 'F_y'.

To simulate the non-linear material stress-strain relationship discussed above, the ADINA8.5 isothermal plasticity material models were chosen for the analysis. More specifically, the plastic-multilinear model is used for all studies in this research. The plastic-multilinear model is an elastic-plasticity model based on incremental plasticity theory. It assumes the material to be elastic–plastic followed by strain hardening. The ADINA8.5's default isotropic hardening rule is used as the strain hardening rule for models in this research.

4.3.3 Initial Geometrical Imperfections

As discussed in Section 3.3.4, all structures are in reality imperfect. There are generally two types of imperfections in steel sections, namely global and local imperfection. To analyze the behavior of a web plate within a steel section, the local initial imperfection should be included. Moreover, in a numerical non-linear analysis, some forms of disturbances are necessarily to be applied on a perfectly flat plate to evoke the buckling behavior of the plate.

Geometrical imperfection is a function of plate width, thickness, forming process, installation etc. For this study, a double sine function proposed in Section 3.3.4 is again used to represent the distribution of the geometrical imperfection in a web plate.

Dawson and Walker (1972) have proposed an equation to express the relationship between the magnitude of the initial imperfection and the dimensions of the plate as the following:

$$w_0 / t = \gamma(F_y / \sigma_{cr}) \tag{4.6}$$

where 'w_0' is the maximum magnitude of the initial imperfection. 't' is the thickness of the plate. 'F_y' is the yield stress of the plate. 'σ_{cr}' is the compressive buckling strength of the plate. Based on curve fitting to experiment data, Dawson and Walker (1972) further showed that γ=0.2 is adequate for plates with simply supported boundary conditions. Substituting γ=0.2 into Equation 4.6 obtains the following equation:

$$w_0 / t = 0.2(F_y / \sigma_{cr}) \tag{4.7}$$

Schafer and Peköz (1998) have concluded some rules of thumb to predict the maximum local imperfection in a stiffened cold-formed steel element that apply for a thickness, t, of less than 3 mm. According to their suggestion, the maximum geometrical imperfection amplitude for the local buckling of cold-formed steel sections is presented as:

$$\frac{w_0}{t} = 0.145(\frac{h}{t})\sqrt{\frac{Fy}{E}} \qquad => \quad w_0 \approx 0.006h \qquad (4.8)$$

where 'h' is the width of the plate, 't' is the thickness of the plate, 'h/t' is the slenderness ratio of the plate, 'F_y' is the yield stress of the plate and 'E' is the elastic modulus of the plate.

Figure 4.6 shows the 'w_0/t' values as a function of the slenderness of plates obtained from Equation 4.7 and Equation 4.8, respectively. It can be seen that the magnitude of the initial imperfection increases as the slenderness of plates increase. The British Steel Design Code provides an upper limit for the value of the maximum imperfection point, w_0, following Equation 4.8. Equation 4.7 seems to have over-conservatively calculated the imperfection magnitude of plates. Thus, for analysis purposes, the present study used one-half of the imperfection magnitude value calculated from Equation 4.8.

As a summary, the present finite element model will use the double sine function (Equation 3.14) to predict the shape of the initial imperfection, and will use (1/2)*(Equation 4.8) to predict the maximum value of the imperfection, which is $w_0 \approx (0.5)(0.006h) = 0.003h$. Since all plates in this research have h=100mm, w_0=0.3mm was used for all models.

4.3.4 Residual Stress

Residual stresses are stresses that exist in steel sections as a result of the deformations during the cold-forming fabricating processes, and the thermal gradients that are induced in the welding process. The residual stresses in hot-rolled steel members are mainly caused by temperature gradients after hot rolling, flame cutting and welding processes. On the other hand, residual stresses in cold-formed steel members are mainly caused by bending of plated elements during the forming process. Rondal (1987) has shown that the flexural residual stress has negligible or no effect on the ultimate strength of cold-formed steel sections. Rodal (1992), Abdel-Rahman and Sivakumaran(1998) and Schafer and Peköz (1998) have experimentally and analytically studied the changing of the yield strength and the residual stresses in cold-formed steel sections due to cold-working. It was found from these researches that cold-formed steel sections have elevated yield strengths in the corner regions due to the cold-working process. The induced residual stresses and increase of yield strength tend to compensate each another. Also, due to complication and lack of systematic data, residual stresses are normally ignored in numerical analysis. As a result, the residual stresses are neglected in the current study, also.

4.4 Convergence Study

In order to ensure the accuracy of the analysis, convergence study should be performed on each model prior to further analysis. In this research, convergence studies will be performed on plates with different aspect ratios. For plates having the same aspect ratio, the convergence study will be carried out on the thinnest plate, since thin plates may experience more non-linearity because of the large deformation they undergo during the loading process. In this section, a sample convergence study will be carried out for shear plates with a/h=1 (square plate). Similar convergence studies will be carried out to choose suitable mesh configurations for the finite element models with different aspect ratios.

The dimensions of the plate model for this convergence study is shown in Figure 4.2, with a=h=100mm and t=0.4mm. Thus, the slenderness ratio (h/t) is 250. The loading details and the boundary conditions for the finite element model for this plate are shown in Figure 4.4. The plate is under uniform shear loading along four edges. The applied loads and the boundary conditions were described in Section 4.3.1. The plate is assumed to have a multi-linear material model as described in Section 4.3.2 with F_y=350MPa and ν=0.3. The initial imperfection is imposed as stated in Section 4.3.3, with the amplitude of the initial imperfection calculated as one-half of the value calculated from Equation 4.8, which is w_0 =(0.5)(0.6mm)=0.3mm. The effect of residual stresses was ignored as explained in Section 4.3.4.

The analysis includes 5 identical models with only changing the mesh configurations. Model number 1 to 5 will have mesh configuration of 10x10, 16x16, 20x20, 24x24 and 28x28, respectively. Thus models 1 to 5 have an increasing number of total mesh elements. The shear buckling loads and the ultimate shear strengths of the models are presented in the Table 4.1. The percentage changes in the buckling load and the ultimate strength of each model will be compared.

In Table 4.1, the mesh configurations for each plate model were listed in the first column from the left. The second column from the left indicates the total number of elements for each of the 5 plate models. The shear buckling strengths and the ultimate shear strengths for the 5 plate models are recorded in the third and the fifth columns, respectively. The fourth column calculated the percent differences in the shear buckling strength between plates with two adjacent mesh configurations. The sixth column calculated the percent differences in the ultimate shear strength between plates with two adjacent configurations. It can be seen from Table 4.1 that as the total number of elements increases, the percentage differences in both the buckling loads and ultimate strengths between two adjacent plates decrease. Again, as suggested by Thangavadivel (2003), a percentage difference of less than 5% for both the buckling and ultimate load is considered to be acceptable for analysis purpose. Thus, a mesh configuration of 20x20, and 24x24, 28x28 are all qualified. However, since the models for a/h=1 will include plates with different plate thicknesses, in order to be more conservative, a 24x24 mesh configuration with a total of 576 elements was used to model plates with a aspect ratio of 1.

Similar convergence studies were performed on plates with aspect ratios of 2, 3, 4 and 5. The selected mesh configurations for plate models with aspect ratios 1, 2, 3, 4 and 5 are listed in Table 4.2.

4.5 Geometrical Initial Imperfection Sensitivity Study

As stated before, the initial imperfection can affect the shear capacity of plates. This section will study the effect of the magnitude of the initial imperfection on the ultimate shear strength of plates.

The plates considered for the imperfection sensitivity study have the boundary and loading conditions as described in Section 4.3.1; and the material properties as described in Section 4.3.2 with F_y =350MPa and ν=0.3. The dimensions of the plates are a=300mm and h=100mm. A double sine function, as described in Section 4.3.3, is used to represent the distribution of the geometric imperfection. Residual stresses are ignored as explained in Section 4.3.4.

Three groups of plates with different slenderness ratios, namely h/t=50 (group a), h/t=75 (group b), h/t=200 (group c), were studied. The slenderness ratios were selected so that they include the thick plate ($h/t \le \sqrt{Ek_v^{solid}/F_y}$), moderate thick plate ($\sqrt{Ek_v^{solid}/F_y} < h/t \le 1.51\sqrt{Ek_v^{solid}/F_y}$) and thin plate ($h/t > 1.51\sqrt{Ek_v^{solid}/F_y}$). Within each group, there are five plates. Each plate has a different maximum initial imperfection (w_0). The five maximum initial imperfections are w_0/t =0.001, 0.010, 0.100, 0.500 and 1.000. The mesh configuration was selected according to Section 4.4, which is a 24x72 mesh configuration for plates with an aspect ratio of 3.

The ultimate strengths of plates with different maximum initial imperfection for each group are listed in the Table 4.3, where w_0/t is the maximum initial imperfection value imposed on plates. It can be seen that, for all three groups of plates, namely h/t=50, h/t=75 and h/t=200, as the magnitude of the initial imperfection increases, the ultimate shear strength of the plate decreases. The difference in the shear capacities between w_0/t =0.001 and w_0/t =1 for plates with h/t=50 is about 28.57%. The difference in the shear capacities between

w_0/t =0.001 and w_0/t =1 for plates with h/t=75 is about 45.96%. The difference in the shear capacities between w_0/t=0.001 and w_0/t=1 for plates with h/t=200 is about 1.49%. Thus, it can be concluded that up to w_0/t=1, the initial imperfection has the most severe effect on plates with h/t=75 (moderately thick plates); some effect on plates with h/t=50 (thick plates). The effect caused by the initial imperfection up to w_0/t=1 on plates with h/t=200 (thin plates) are very little (1.49% difference between w_0/t=1 and w_0/t=0.001), and may be ignored. Figures 4.7 to 4.9 show the average shear stress-strain curves for these three groups of plates, namely with h/t=50, 75 and 200. Where the average applied shear stresses are obtained from dividing the total applied shear line loads by the length of the plate edges; and the average shear strains are calculated as tangent of the rotated angle of plates at each load step. Figure 4.10 shows the ultimate shear strength versus the maximum initial imperfection (w_0)/plate thickness (t). It can be seen that, for all three groups of plates, the ultimate shear strength decreases approximately linearly with the increasing in the magnitude of the imperfection. Moreover, for plates with h/t=200 (thin plates), the line is almost horizontal. This indicates that the magnitude of the initial imperfection has very little effect on the ultimate shear capacity of thin plates. As discussed before, the ultimate strength of a plate is comprised by the pre-buckling strength and the post-buckling strength of that plate. Only the pre-buckling strength depends on the initial imperfection. As the plate becomes thinner, the post-buckling strength becomes dominant and the pre-buckling strength becomes insignificant. Thus, the effect of the initial imperfection fades out as the plate approaches infinitely thin.

4.6 Parametric Study on Plates Subjected to Shear Loads

In this section, 40 simply supported plate models with 5 different aspect ratios, ranging from 1 to 5, will be studied with the width of the plates being fixed as h=100mm. The five aspect ratio are a/h=1, a/h=2, a/h=3, a/h=4, a/h=5. For each aspect ratio group, 8 identical plate models with varying thickness will be studied. The AISI (2007) limits the h/t for an unreinforced flexural web panel to a maximum value of 200, thus the h/t ratios selected in this study starts from h/t=50, and increases at every 25 interval until h/t=200. However, one extra h/t value, namely h/t=250, was also studied to obtain a more complete view on how the ultimate shear strength of a plate changes as the h/t ratio changes.

The finite element model described in Section 4.3 was used for the parametric study. The loading details and the boundary conditions are shown in Figure 4.4. The plate is assumed to have a multi-linear material model with F_y=350MPa and ν=0.3. The mesh configurations to be used for plates with different aspect ratios were selected through the convergence study and are listed in Table 4.2. The initial imperfection is imposed as described in Section 4.3.3. Figure 4.11 shows the shapes of the initial imperfections for plates with different dimensions. The magnitude of the initial imperfection will be $w_0 = 0.3\text{mm}$ for all plates.

4.6.1 Results and Discussions

Figures 4.12 to 4.16 show the relationship between the average applied shear stress and the average shear strain for plates with aspect ratios from 1 to 5, respectively. It can be seen that, for plates having the same aspect ratios, the thinner the plate is, the lower the ultimate shear strength.

Tables 4.4 to 4.8 show all the results obtained from the finite element analysis, including the shear buckling strength and the ultimate shear strength, for plates with aspect ratios from 1 to 5, respectively. Each of the five tables has 8 columns. The first column from the left shows the 9 plates with various slenderness ratios. The second and third columns show the shear buckling strength obtained from the linearized-buckling analysis and from Equation 4.1.1, respectively. The fourth column compares the percentage difference between values in the second and the third columns. It can be seen that the percentage difference between the shear buckling strengths obtained from the linearized-buckling analysis and those obtained from Equation 4.1.1 are less than 2.0% for all plate models. The fifth column in Tables 4.4 to 4.8 records the ultimate shear strength of plates obtained from the finite element analysis. The sixth column calculates the post-buckling strength of plates, which is obtained by subtracting the elastic buckling strength from the ultimate shear strength of plates. It can be seen that for thin plates, significant post-buckling strengths exist. The seventh column calculates the post-buckling strength divided by the shear buckling strength of plates. The last column calculates contribution of the post-buckling strength to the ultimate shear strength by dividing the post-buckling strength by the ultimate shear strength of plates. It can be seen that as the h/t values increase, the τ_p / τ_{cr} values increase. This indicates that the contribution of the post-buckling strength to the ultimate strength of a plate increases as the h/t ratio increases.

Figure 4.17 shows the relationship between the ultimate shear strengths and the slenderness ratios (h/t) of plates having aspect ratios (a/h) from 1 to 5. It can be seen from Figure 4.17 that the ultimate shear strength of solid plates decreases at a decreasing rate as the h/t values increase. It can also be found from Figure 4.17 that the ultimate shear strength of solid plates decreases as the a/h ratios increase. Figure 4.18 shows the relationship between the ultimate shear strengths and the aspect ratio (a/h) of plates having different slenderness ratios (h/t). It can be seen that the ultimate shear strength of solid plates decreases at a decreasing rate as the a/h values increase. The data lines in Figure 4.18 flat out when a/h approaches to 5. In other words, as the aspect ratio becomes large, the effect of the 'a/h' value on the ultimate shear capacity of plates fades out. In practice, cold-formed steel members are normally used without intermediate stiffener, which means that the 'a/h' for the web panels tend to be very large (a/h>>5). Thus, for cold-formed steel members, the effect on the ultimate shear strength of web panels caused from the aspect ratio (a/h) can be normally neglected.

4.6.2 Comparison between Shear Capacities Obtained from the Finite Element Analysis and the AISI (2007) Method

Figures 4.19 to 4.23 show the ultimate shear strength of plates as a function of slenderness ratio obtained from both the finite element analysis and the AISI (2007) method for plates with a/h=1,2,3,4 and 5, respectively. Regions (a), (b) and (c) in Figures 4.19 to 4.23 correspond to the three cases of web panels defined in Equations 4.3.2, 4.3.3 and 4.3.4, respectively.

It can be seen that in regions (a) and (b), the ultimate shear capacities obtained from the finite element analysis are somewhat lower than those calculated following the AISI (2007) specification. For plates in region (a), as discussed in Section 4.2.2, when calculating the ultimate shear capacity of thick webs, the AISI (2007) uses $\tau_y = 0.60 F_y$ instead of $\tau_y = \frac{F_y}{\sqrt{3}} \approx 0.577$. Thus the nominal ultimate shear strength for plates in region (a) tends to be over-estimated using the AISI (2007) method. This, however, does not mean the AISI (2007) is under-conservative, since proper reduction factor of safety will be applied to compensate the over-estimation of the ultimate shear strength for plates in region (a).

For plates in region (b), the AISI (2007) calculates the nominal shear strength as shown in Equation 4.5, which is an approximate equation proposed by Basler (1961) based on experimental data fitting with possibly some errors and uncertainties exist. Moreover, when calculating the nominal shear strength in region (b), the AISI (2007) uses $0.8\,F_y$ as the proportional limit of shear, while the material model used in this study has a shear proportional limit of $0.75\,F_y$ as shown in Figure 4.5.

The major differences of the ultimate shear strengths between the finite element analysis results and the AISI (2007) results occur for case (c) plates (thin plates). The shear capacities obtained from finite element study for thin plates are higher than that calculated from the AISI (2007) equations. This is because that the AISI (2007) calculates the ultimate shear strength of plates based on either the shear yield stress or the shear-buckling strength of web plates. Any additional post-buckling strength that may exist after the web has buckled is neglected. However, appreciable amounts of post-buckling strengths can build up for thin plates. Thus the current AISI specification has over conservatively estimated the ultimate shear strength of thin shear webs. Modifications are needed to be made on Equation 4.4.4 in Section 4.2 to include the post-buckling strength of thin web plates. Take a close look on Equation 4.4.4, one can realize that the nominal shear stress calculated from this equation is the critical shear strength of the plate. Thus, in addition to the shear-buckling strength, the post-buckling strength observed in the finite element modeling could be added to Equation 4.4.4.

Figure 4.24 shows the relationship between the post-buckling strength normalized by the shear buckling strength and the slenderness ratios up to h/t=200 for plates with varying aspect ratios. It can be seen that the ratio of the post-buckling shear strength divided by the shear buckling strength increases approximately linearly as the h/t ratio increases. Thus the new proposed equation could use a linear equation to represent the relationship between the ratio of the post-buckling strength divided by the shear buckling strength of plates and their slenderness ratios (h/t). Figure 4.25 shows the relationship between the post-buckling strength normalized by the shear buckling strength and the aspect ratios up to a/h=5 for plates with varying slenderness ratios. It can be seen that when $a/h \leq 2$, the ratio of the post-buckling shear strength divided by the shear buckling strength increases for plates with a/h=1 to plates with a/h=2. However, the real function between the ration of the post-buckling shear strength divided by the shear buckling strength and the aspect ratio (a/h) is unknown for plates with $a/h \leq 2$ since only two data points (a/h=1 and a/h=2) are available. In this study, a linear relationship is assumed as a rough estimation of the relationship between the ratio of the post-buckling shear strength divided by the shear buckling strength and the aspect ration (a/h) for plates with $a/h \leq 2$. When a/h>2, the ratio of the post-buckling shear strength divided by the shear buckling strength decreases approximately linearly as the a/h ratio increases. As a result, one linear equation could be used in each a/h range to include the effects on the post-buckling strength of plates caused by changing of the aspect ratio. The modified equation is derived by curve fitting the finite element results as the following:

(c) For $h/t > 1.51\sqrt{Ek_v^{solid}/F_y}$

$$F_v = \tau_{cr} + \tau_p, \qquad \text{(4.4.4-modified)}$$

where

$$\tau_{cr} = \frac{\pi^2 E k_v^{solid}}{12(1-\nu^2)(h/t)^2}$$

$$\tau_p = [0.048(h/t - 1.51\sqrt{Ek_v^{solid}/F_y}) \cdot f(a/h)]\,\tau_{cr}$$

$$f(a/h) = 0.01*(a/h) + 0.2, \qquad \text{for } 1 \leq a/h \leq 2$$

$$= -0.02*(a/h) + 0.26, \qquad \text{for } a/h > 2$$

Figures 4.26 to 4.30 show the ultimate shear strength of plates as a function of their slenderness obtained from the finite element analysis and from the AISI (2007) method when Equation 4.4.4 is modified for plates with a/h=1,2,3,4 and 5, respectively. It can be seen that with Equation 4.4.4 being modified to include the post-buckling strength, the proposed AISI (2007) method is able to better estimate the ultimate shear strength of solid web plates.

4.7 Conclusion

This chapter studied the ultimate shear capacity of simply supported plates subjected to pure edge shear loading through a series of finite element modeling. The relationships between the shear capacity, the slenderness ratio and the aspect ratio of plates were studied. It was shown that the ultimate shear capacity of a plate decreases as the slenderness ratio (h/t) of the plate increases. The ultimate shear capacity also decreases, but to a lesser extent, as the aspect ratio (a/h) of the plate increases. By comparing the shear strength obtained from the finite element modeling with that obtained from the AISI (2007) equations, the results indicated that by ignoring the post-buckling strength of slender plates, the AISI (2007) has underestimated the shear strength of thin plates, since the post-buckling strength can be many times larger than the shear-buckling strength of thin plates. Thus the current AISI (2007) specification appears to have over conservatively estimated the ultimate shear strength of webs.

Table 4.1 Buckling and Ultimate Strength of Plate Models with Different Mesh Densities (a/h=1, h/t=250)

Mesh Configuration	Total Number of Elements	Buckling Load (MPa) τ_{cr} (MPa)	%Diff.	Ultimate Load(MPa) τ_{ul} (MPa)	%Diff.
10x10	100	29.80		78.99	
			5.11		11.08
16x16	256	28.35		71.11	
			1.43		3.00
20x20	400	27.95		69.04	
			0.68		1.66
24x24	576	27.76		67.91	
			0.36		1.04
28x28	784	27.66		67.21	

Table 4.2 Selected Mesh Densities for Different Aspect Ratios

a/h	Mesh Configuration
1.0	24x24
2.0	24x48
3.0	24x72
4.0	24x96
5.0	24x120

Table 4.3 Ultimate Shear Strengths of Plates with Different Maximum Initial Imperfection

τ_{ul} (MPa) / w_0/t	h/t=50	h/t=75	h/t=200
0.001	204.75	166.17	51.00
0.010	202.13	161.72	51.08
0.100	194.78	158.20	50.91
0.500	174.50	139.69	50.70
1.000	159.25	113.85	50.25

Table 4.4 Shear-Buckling Strength, Ultimate Strengths and the Post-Buckling Strength of Plates (a/h=1)

h/t	τ_{cr} - FEM (MPa)	τ_{cr} - Eq. 4.1.1 (MPa)	%Diff.	τ_{ul} (MPa)	τ_p (MPa)	τ_p/τ_{cr}	τ_p/τ_{ul}
50	688.00	685.46	0.37	201.58	-	-	-
75	308.68	304.65	1.32	173.78	-	-	-
100	173.20	171.36	1.07	144.79	-	-	-
125	110.93	109.67	1.14	121.48	10.55	0.10	0.09
150	77.16	76.16	1.31	104.03	26.87	0.35	0.26
175	56.65	55.96	1.24	91.21	34.56	0.61	0.38
200	43.38	42.84	1.26	81.50	38.12	0.88	0.47
250	27.76	27.42	1.25	67.85	40.09	1.44	0.59

Table 4.5 Shear-Buckling Strength, Ultimate Strengths and the Post-Buckling Strength of Plates (a/h=2)

h/t	τ_{cr} - FEM (MPa)	τ_{cr} - Eq.4.1.1 (MPa)	%Diff.	τ_{ul} (MPa)	τ_p (MPa)	τ_p/τ_{cr}	τ_p/τ_{ul}
50	473.01	465.29	1.66	195.60	-	-	-
75	209.99	206.79	1.55	156.41	-	-	-
100	114.78	113.14	1.45	121.40	6.62	0.06	0.05
125	75.32	74.45	1.17	97.89	22.57	0.30	0.23
150	52.53	51.75	1.51	82.10	29.57	0.56	0.36
175	38.62	37.98	1.68	70.89	32.27	0.84	0.46
200	29.61	29.08	1.82	62.50	32.89	1.11	0.53
250	18.97	18.61	1.93	50.68	31.71	1.67	0.63

Table 4.6 Shear-Buckling Strength, Ultimate Strengths and the Post-Buckling Strength of Plates (a/h=3)

h/t	τ_{cr} - FEM (MPa)	τ_{cr} - Eq.4.1.1 (MPa)	%Diff.	τ_{ul} (MPa)	τ_p (MPa)	τ_p/τ_{cr}	τ_p/τ_{ul}
50	430.25	424.52	1.35	191.55	-	-	-
75	192.00	188.67	1.76	149.98	-	-	-
100	108.10	106.13	1.86	113.12	5.02	0.05	0.04
125	69.25	67.92	1.95	89.72	20.47	0.30	0.23
150	48.10	47.17	1.99	74.46	26.36	0.55	0.35
175	35.35	34.65	2.02	63.82	28.47	0.81	0.45
200	27.08	26.53	2.06	55.96	28.88	1.07	0.52
250	17.33	16.98	2.04	45.00	27.67	1.60	0.61

Table 4.7 Shear-Buckling Strength, Ultimate Strengths and the Post-Buckling Strength of Plates (a/h=4)

h/t	τ_{cr} - FEM (MPa)	τ_{cr} - Eq.4.1.1 (MPa)	%Diff.	τ_{ul} (MPa)	τ_p (MPa)	τ_p/τ_{cr}	τ_p/τ_{ul}
50	414.40	410.25	1.01	189.78	-	-	-
75	184.92	182.33	1.42	147.05	-	-	-
100	104.10	102.56	1.50	109.67	5.57	0.05	0.05
125	66.69	65.64	1.60	86.11	19.42	0.29	0.23
150	46.32	45.58	1.62	70.99	24.67	0.53	0.35
175	34.04	33.49	1.64	60.53	26.49	0.78	0.44
200	26.06	25.64	1.64	52.81	26.75	1.03	0.51
250	16.69	16.41	1.68	41.64	24.96	1.50	0.60

Table 4.8 Shear-Buckling Strength, Ultimate Strengths and the Post-Buckling Strength of Plates (a/h=5)

h/t	τ_{cr} - FEM (MPa)	τ_{cr} - Eq.4.1.1 (MPa)	%Diff.	τ_{ul} (MPa)	τ_p (MPa)	τ_p / τ_{cr}	τ_p / τ_{ul}
50	407.45	403.64	0.94	189.03	-	-	-
75	181.80	179.40	1.34	145.75	-	-	-
100	102.40	100.91	1.48	107.90	5.50	0.05	0.05
125	65.56	64.58	1.52	84.50	18.94	0.29	0.22
150	45.54	44.85	1.54	69.34	23.80	0.52	0.34
175	33.48	32.95	1.60	58.32	24.84	0.74	0.43
200	25.62	25.23	1.56	49.80	24.18	0.94	0.49
250	16.41	16.15	1.61	36.89	20.49	1.25	0.56

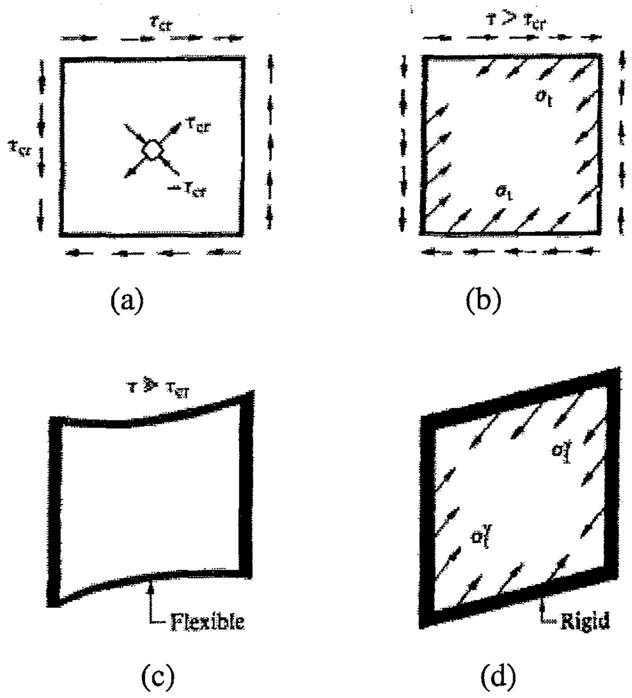

Figure 4.1 Failure Mechanism of Square Plate Subjected to Pure Edge Shear Loading (Narayanan, 1985)

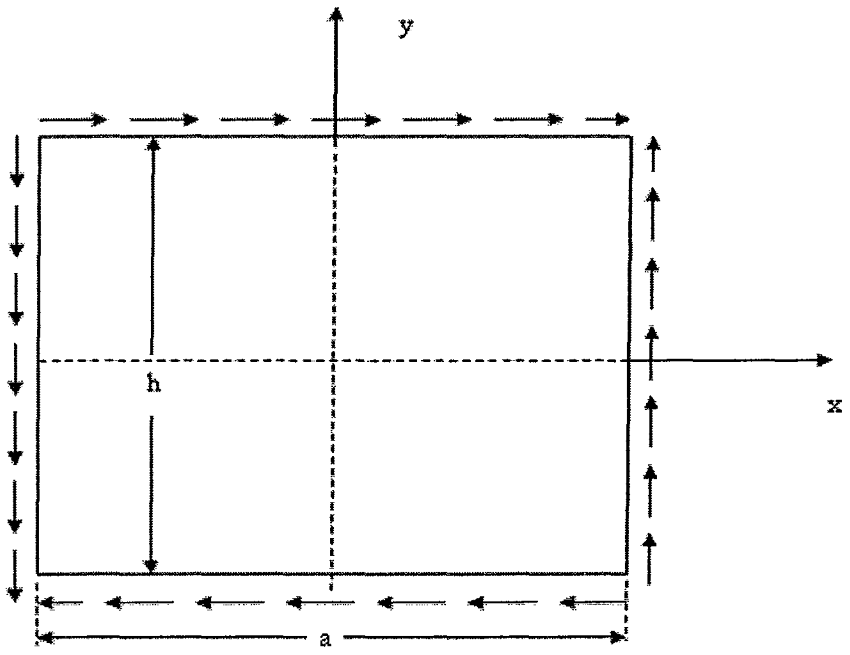

Figure 4.2 Simply Supported Plates Subjected to Uniform Edge Shear

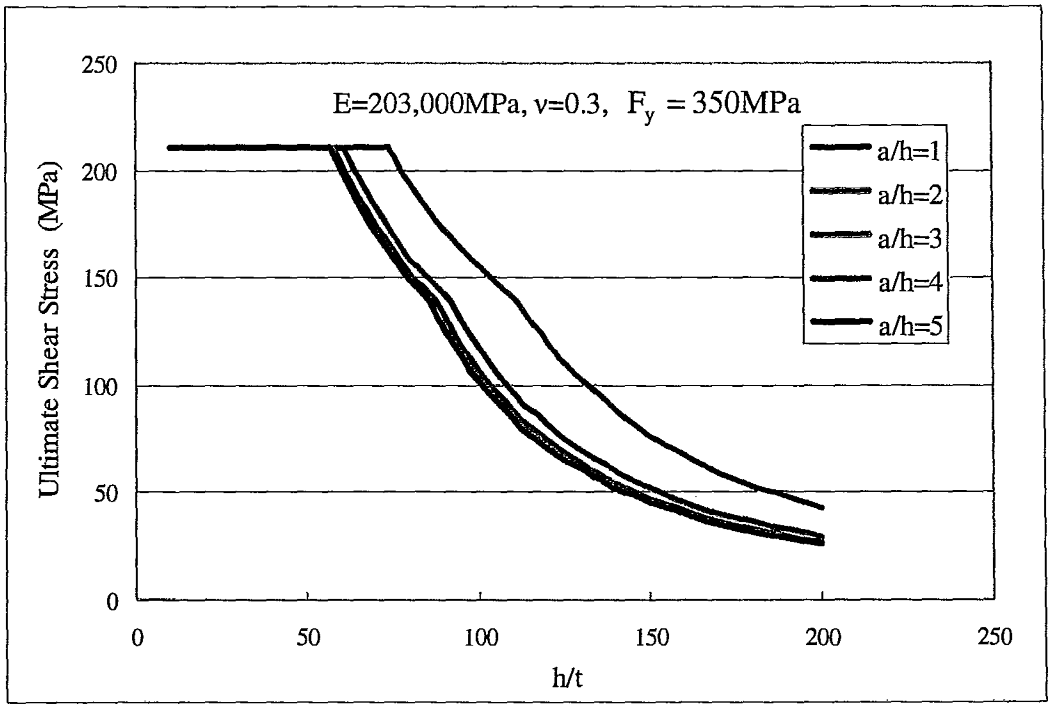

Figure 4.3 τ_{ul} Versus h/t Diagram obtained from the AISI 2007 Procedure for Shear Webs

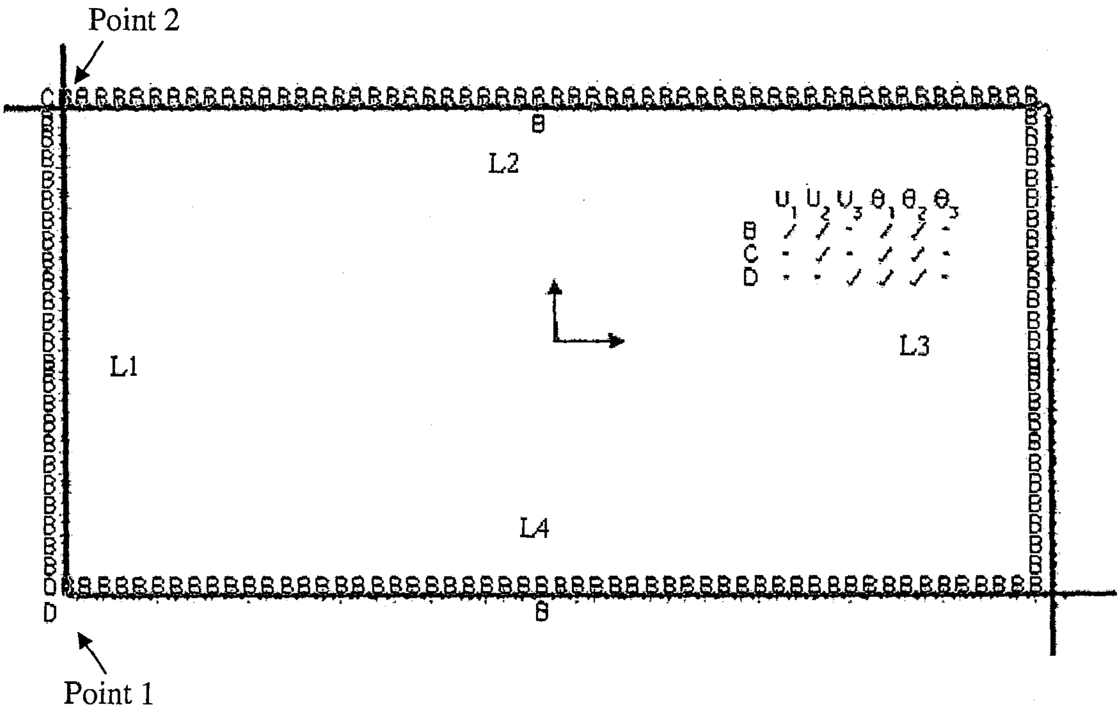

Figure 4.4 Loading and Boundary Conditions of the Finite Element Model for a Plate subjected to Shear Loads

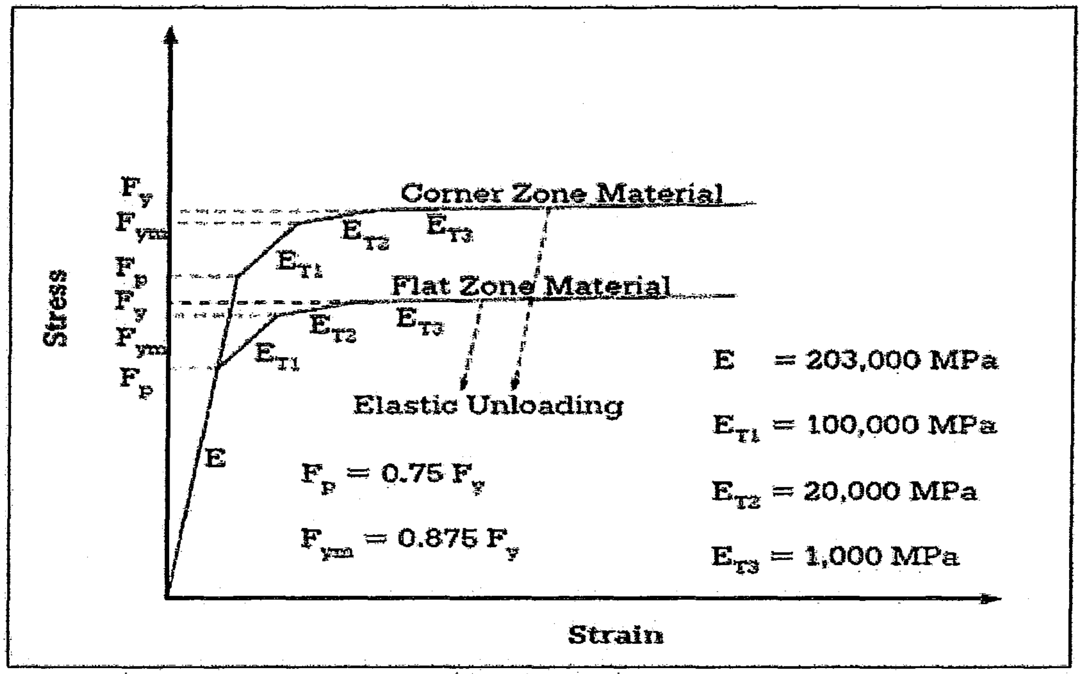

Figure 4.5 Experiment Based Stress-Strain Relationship for CFS (Abdel-Rahman and Sivakumaran, 1997)

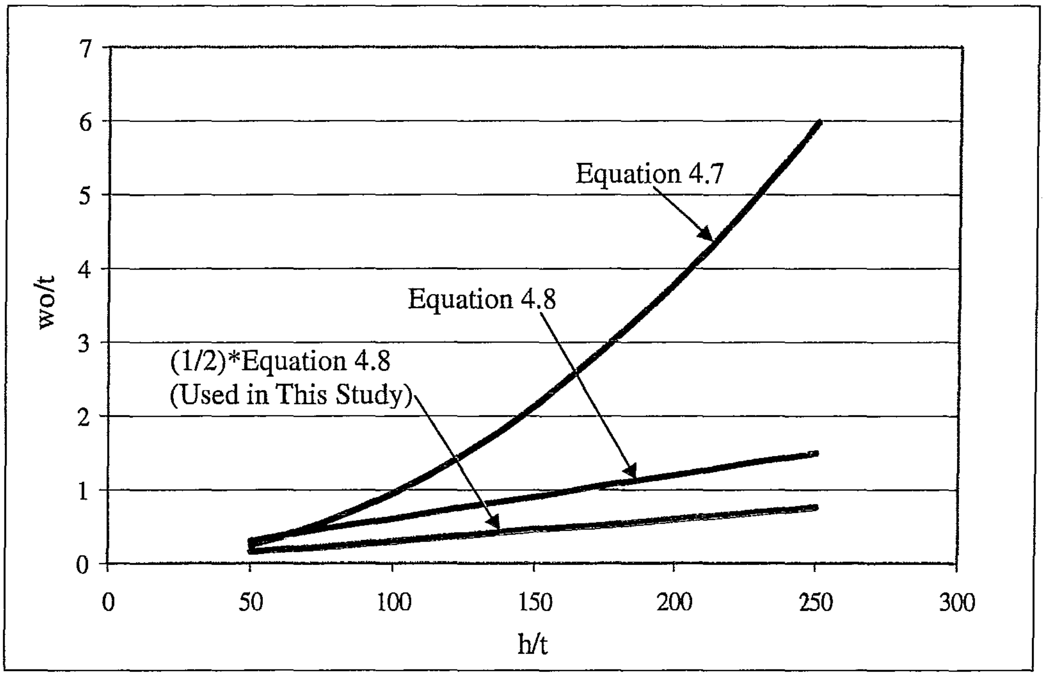

Figure 4.6 Magnitude of the Initial Imperfection/Plate Thickness Versus Slenderness Ratio of Plates

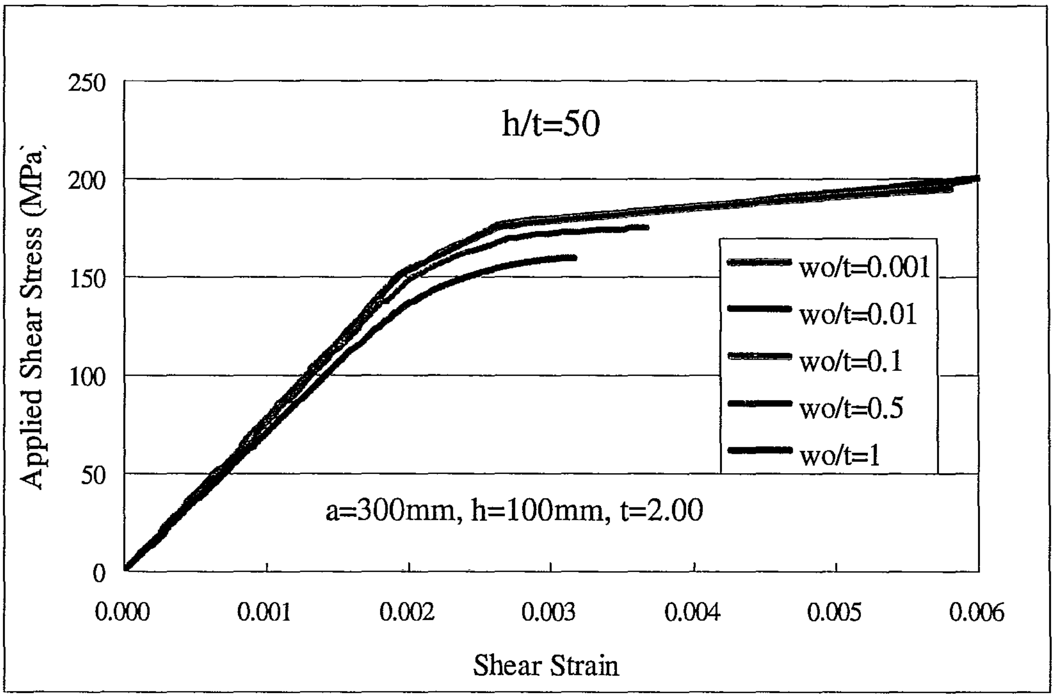

Figure 4.7 Applied Average Shear Stress Versus Average Shear Strain for Thick Plates

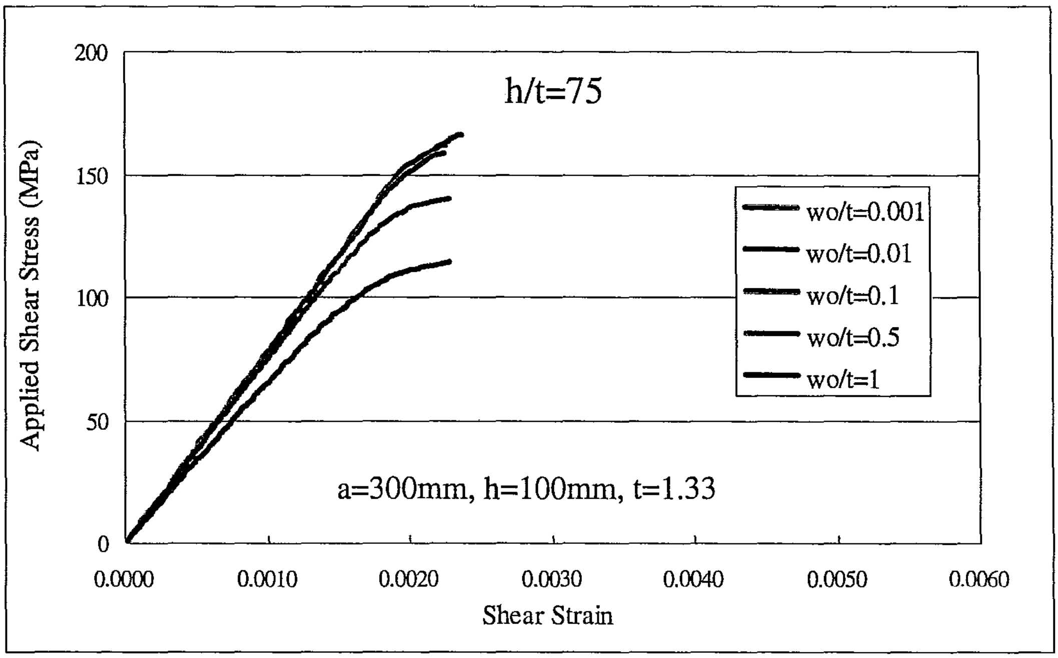

Figure 4.8 Applied Average Shear Stress Versus Average Shear Strain for Moderately Thick Plates

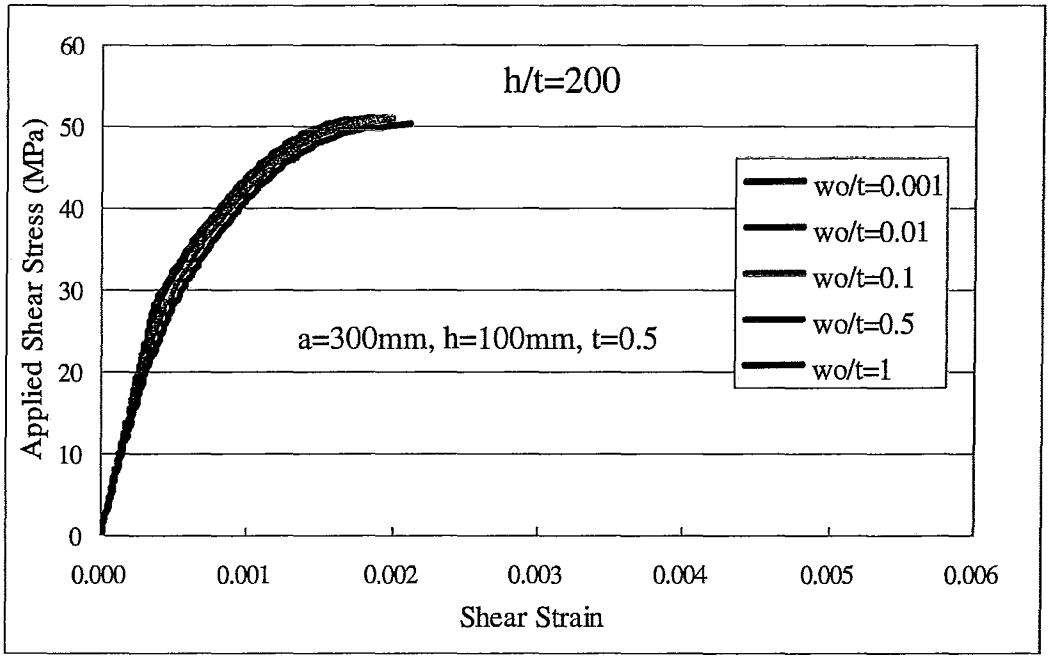

Figure 4.9 Applied Average Shear Stress Versus Average Shear Strain for Thin Plates

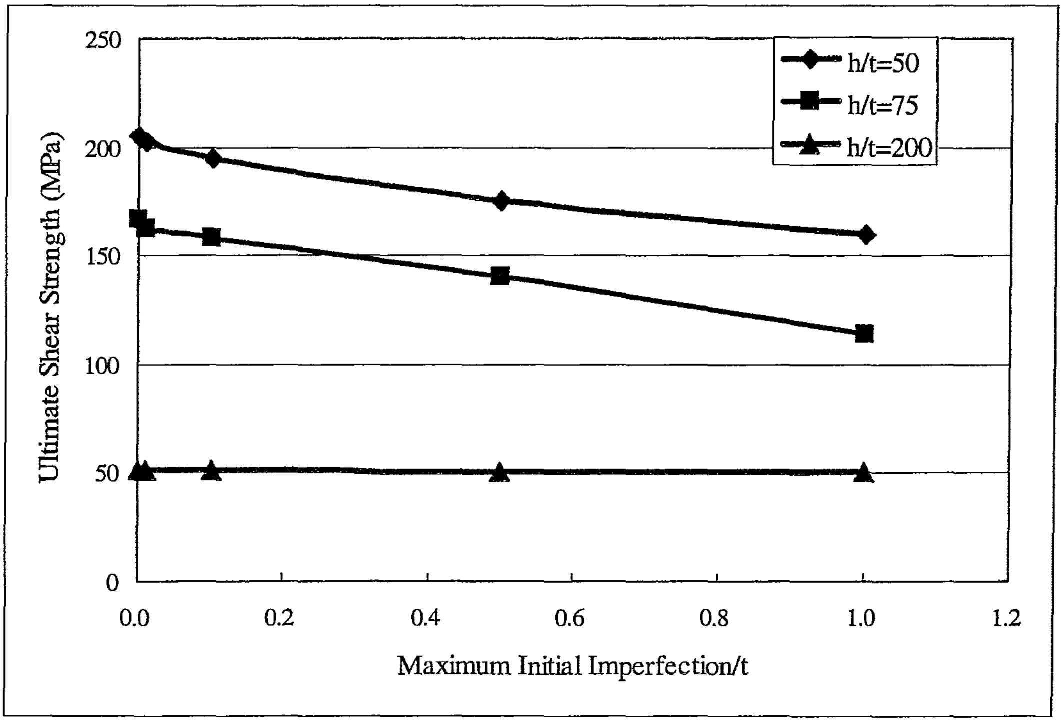

Figure 4.10 Ultimate Shear Strength Versus Maximum Initial Imperfection/Plate Thickness

[Deformation Magnification =100]

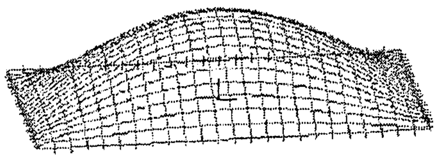

(a) a/h=1

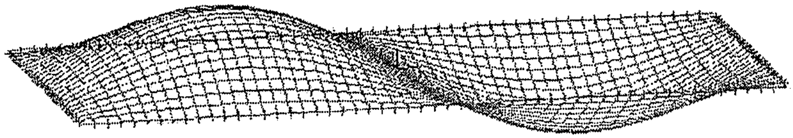

(b) a/h=2

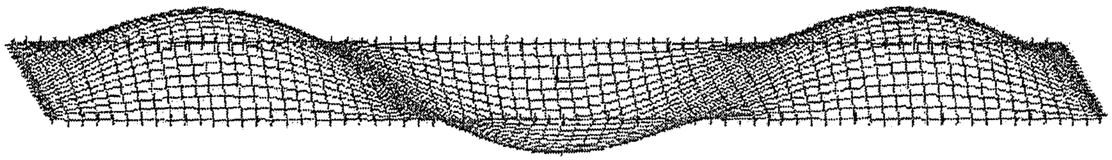

(c) a/h=3

[Deformation Magnification =100]

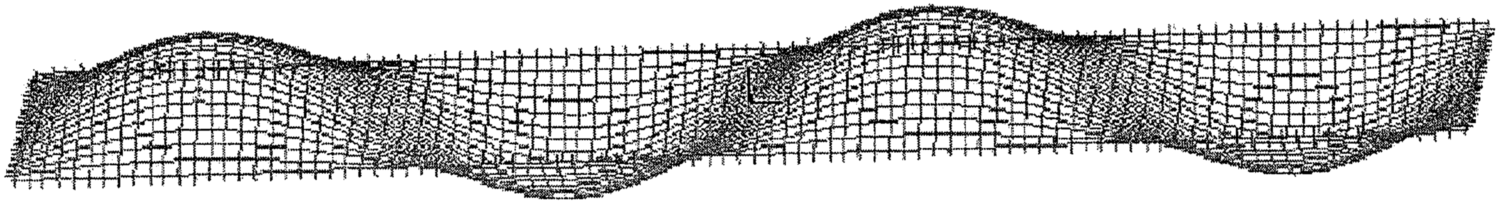

(d) a/h=4

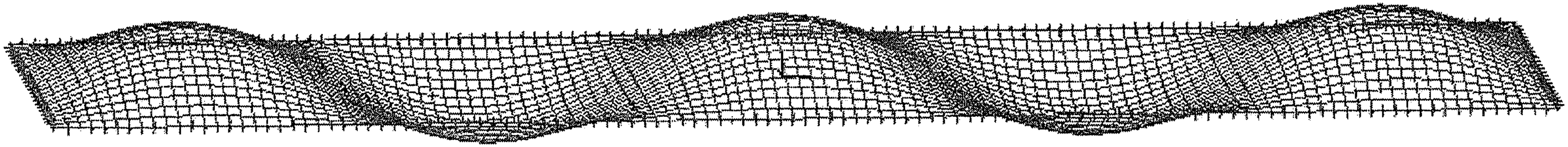

(e) a/h=5

Figure 4.11 (a) Initial Imperfection Shape for Plates with a/h=1
(b) Initial Imperfection Shape for Plates with a/h=2
(c) Initial Imperfection Shape for Plates with a/h=3
(d) Initial Imperfection Shape for Plates with a/h=4
(e) Initial Imperfection Shape for Plates with a/h=5

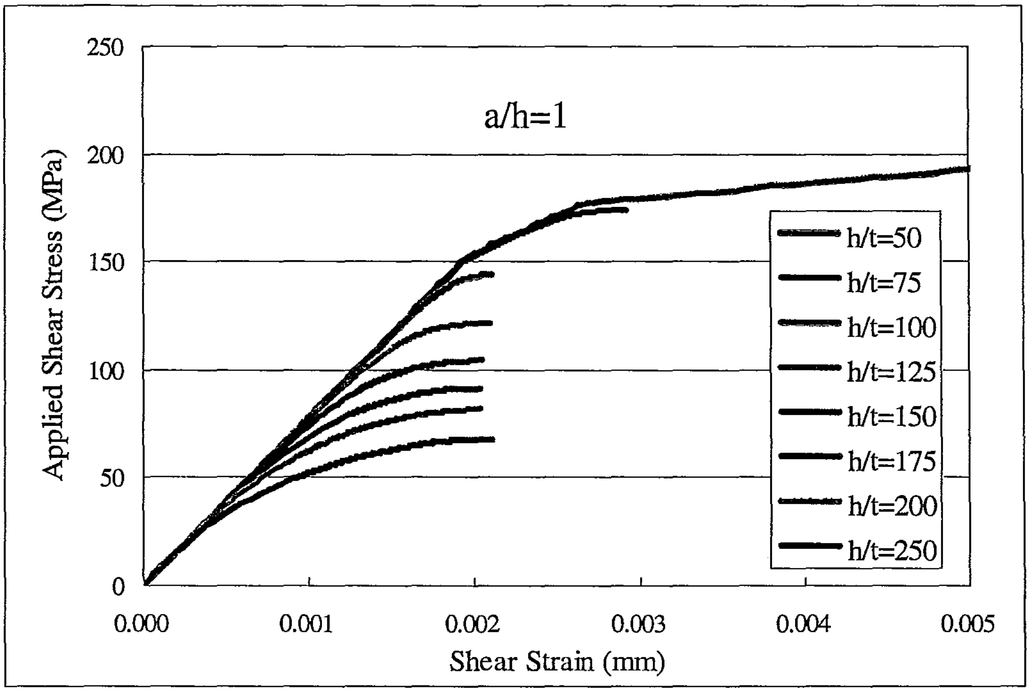

Figure 4.12 Average Applied Shear Stress Versus Shear Strain for a/h=1

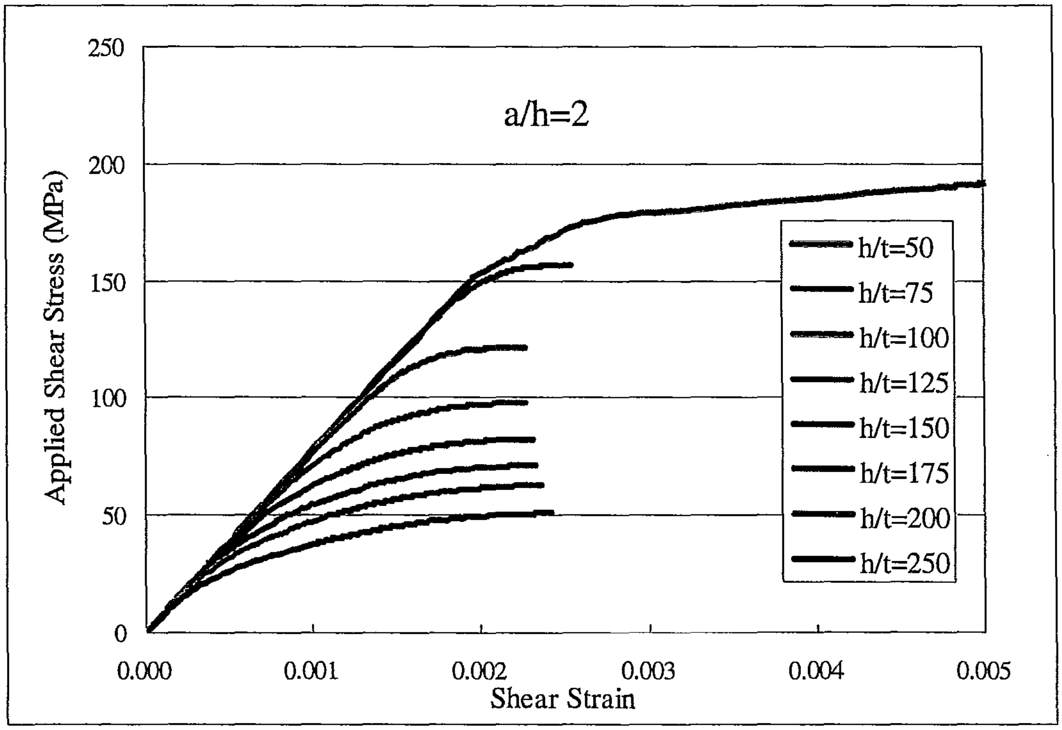

Figure 4.13 Average Applied Shear Stress Versus Shear Strain for a/h=2

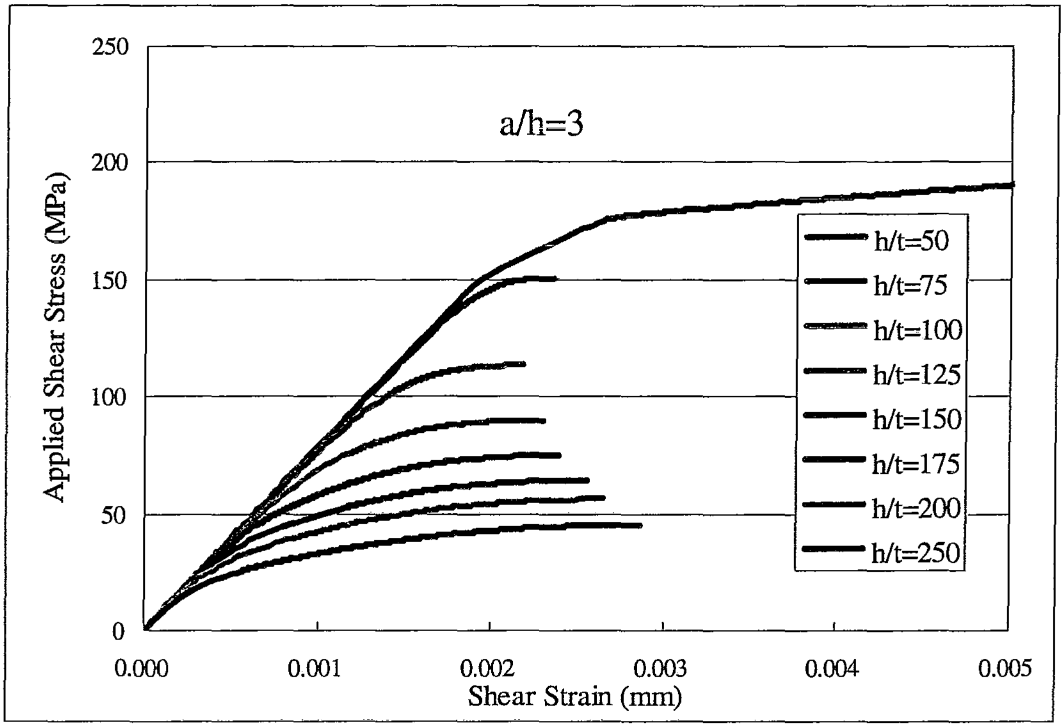

Figure 4.14 Average Applied Shear Stress Versus Shear Strain for a/h=3

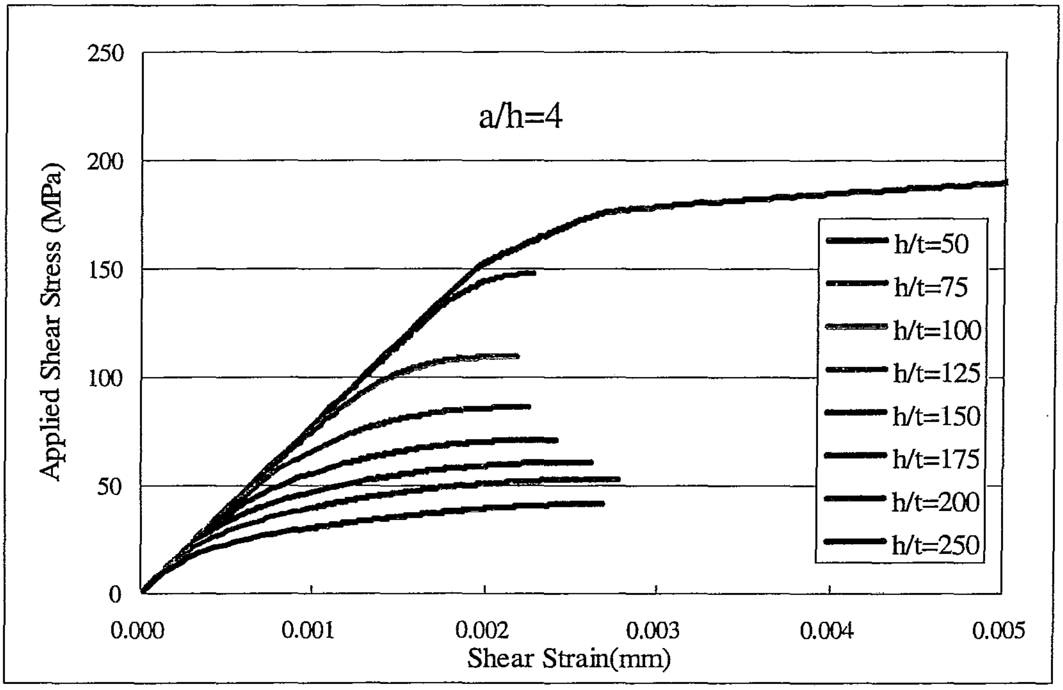

Figure 4.15 Average Applied Shear Stress Versus Shear Strain for a/h=4

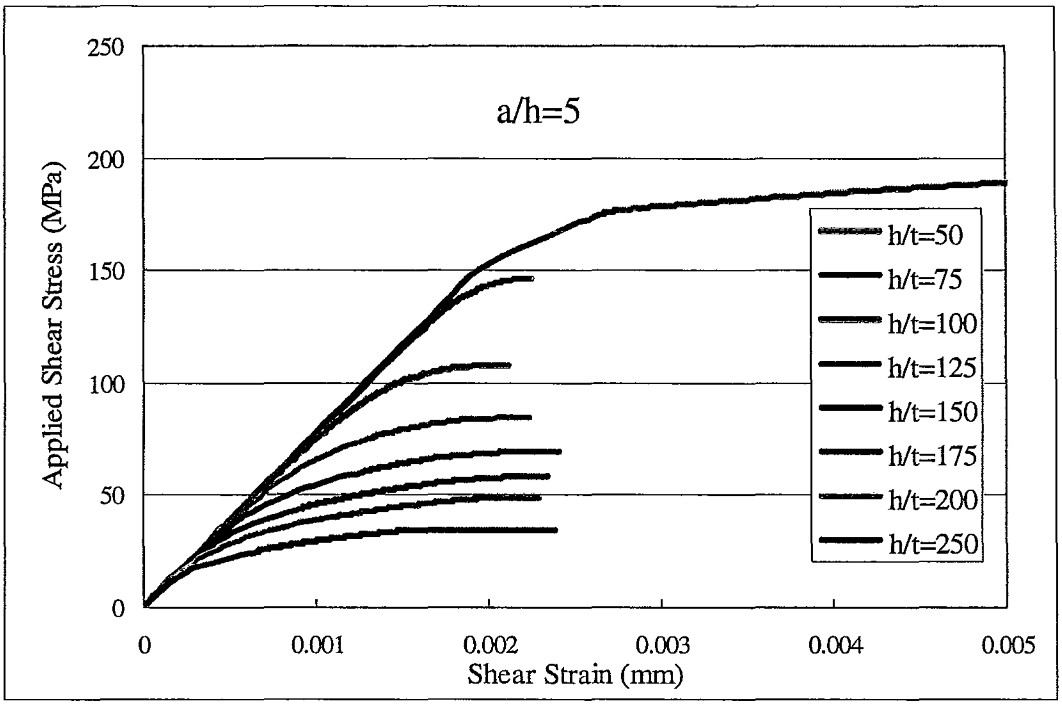

Figure 4.16 Average Applied Shear Stress Versus Shear Strain for a/h=5

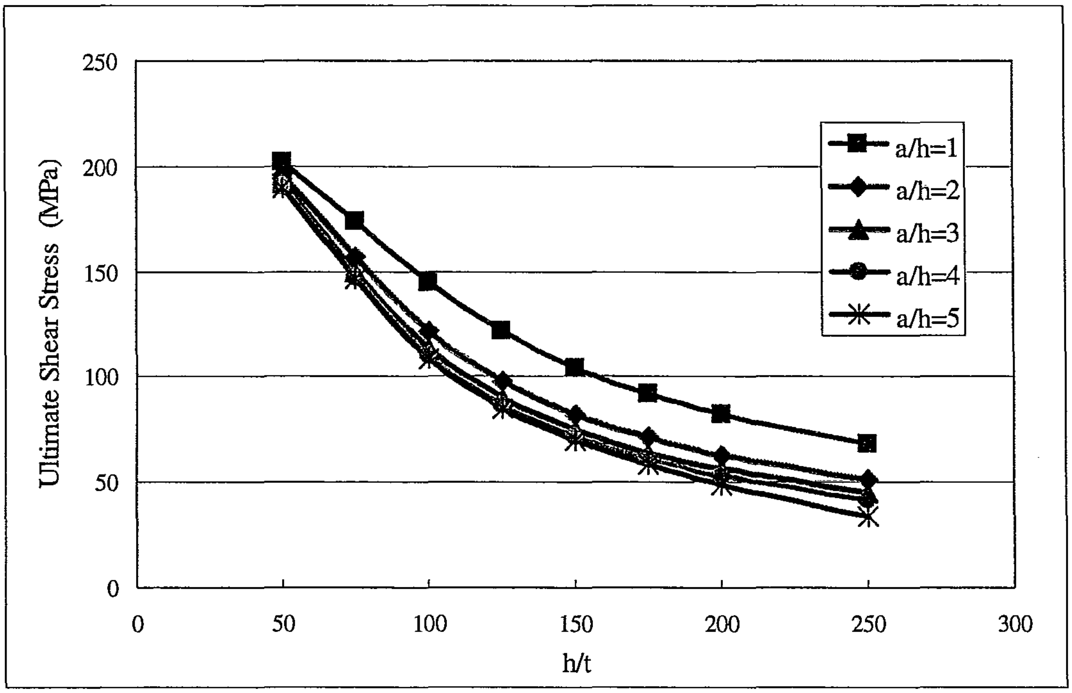

Figure 4.17 Ultimate Shear Strength Obtained from the Finite Element Analysis of Plates with Different a/h Versus h/t

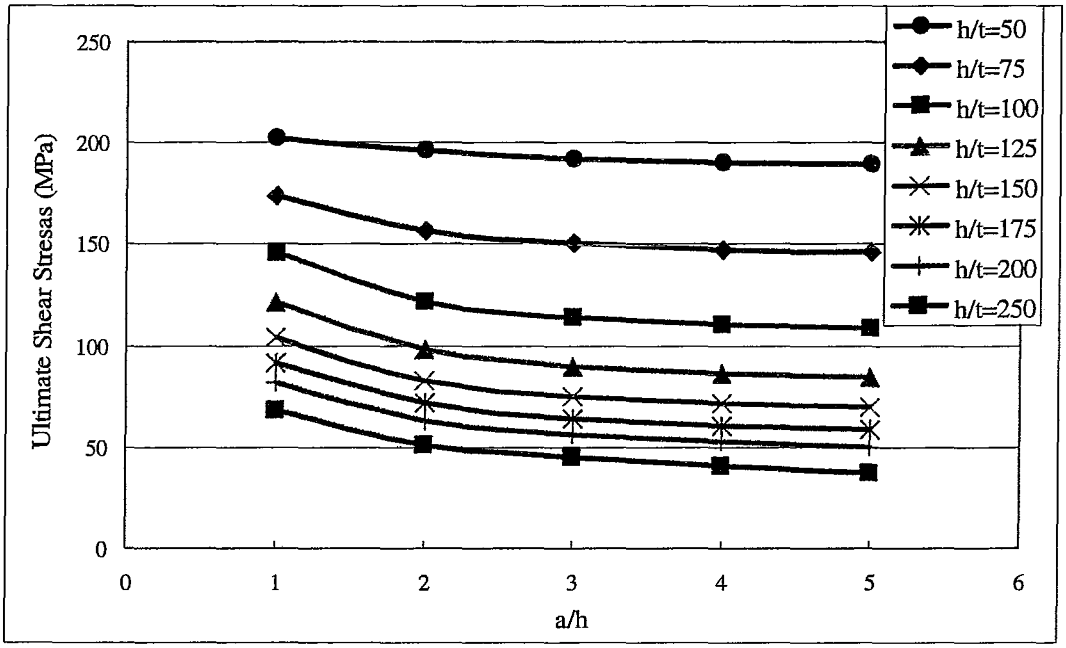

Figure 4.18 Ultimate Shear Strength of Plates Versus a/h Ratios

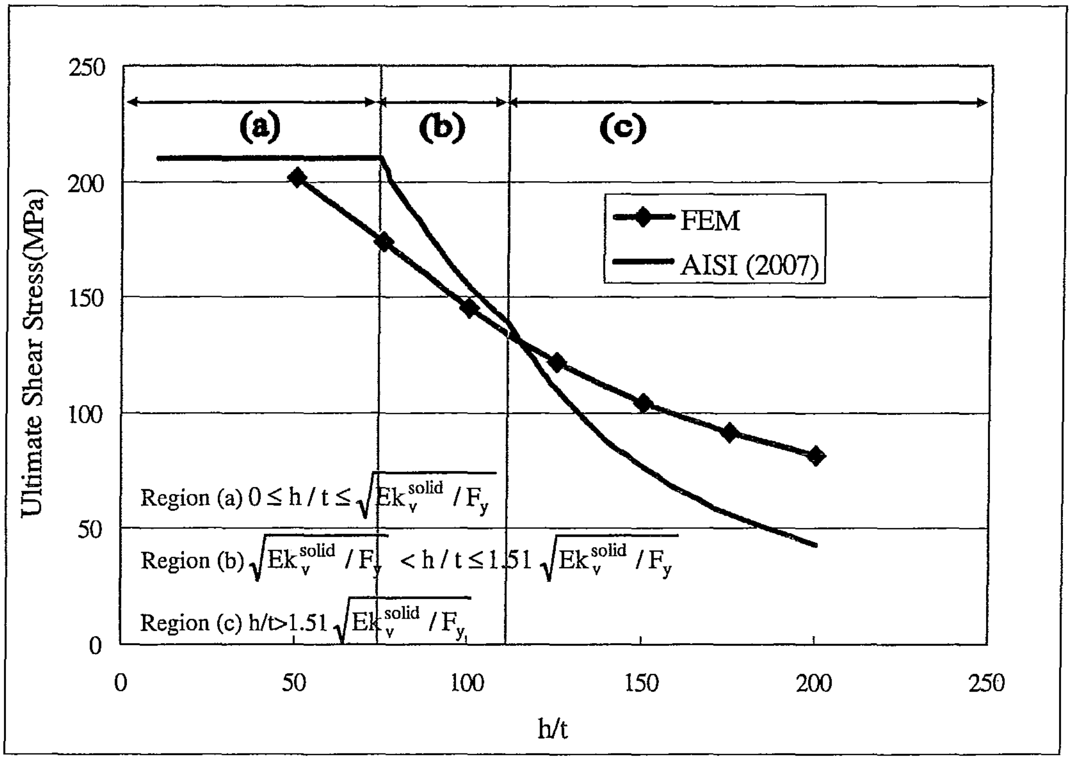

Figure 4.19 Ultimate Shear Strength Versus h/t Ratios for Plate Models with a/h=1

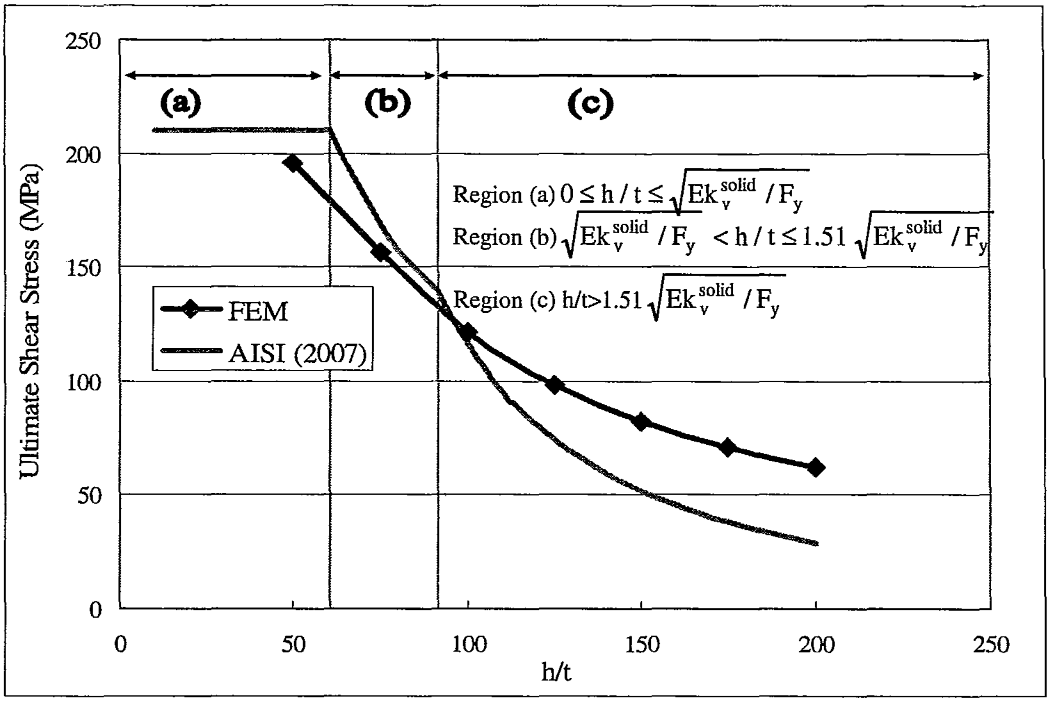

Figure 4.20 Ultimate Shear Strength Versus h/t Ratios for Plate Models with a/h=2

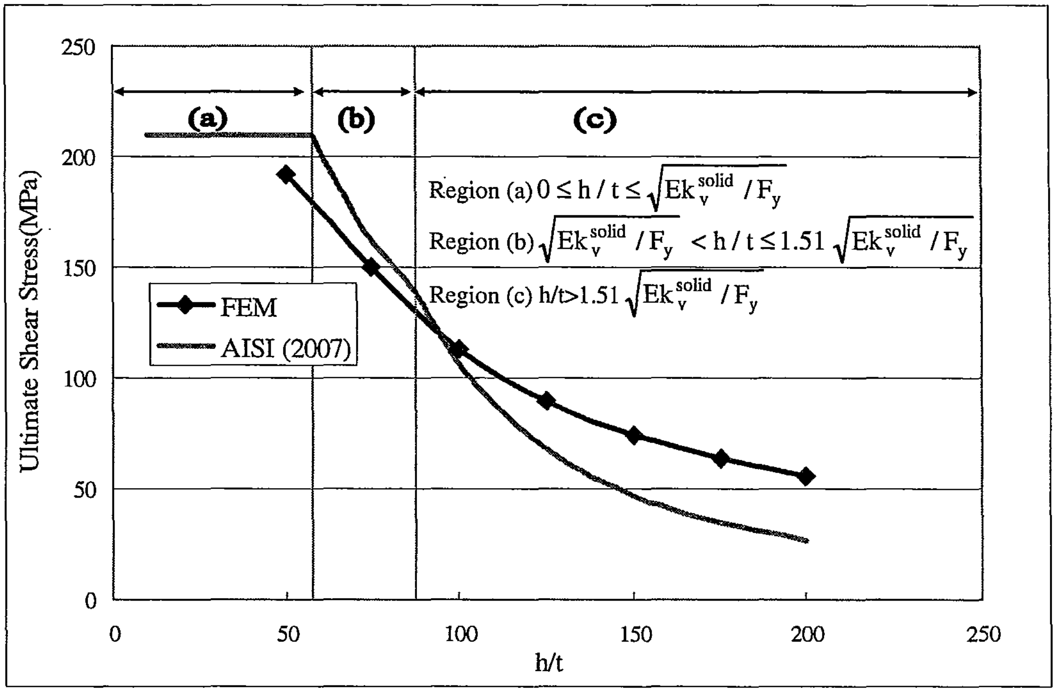

Figure 4.21 Ultimate Shear Strength Versus h/t Ratios for Plate Models with a/h=3

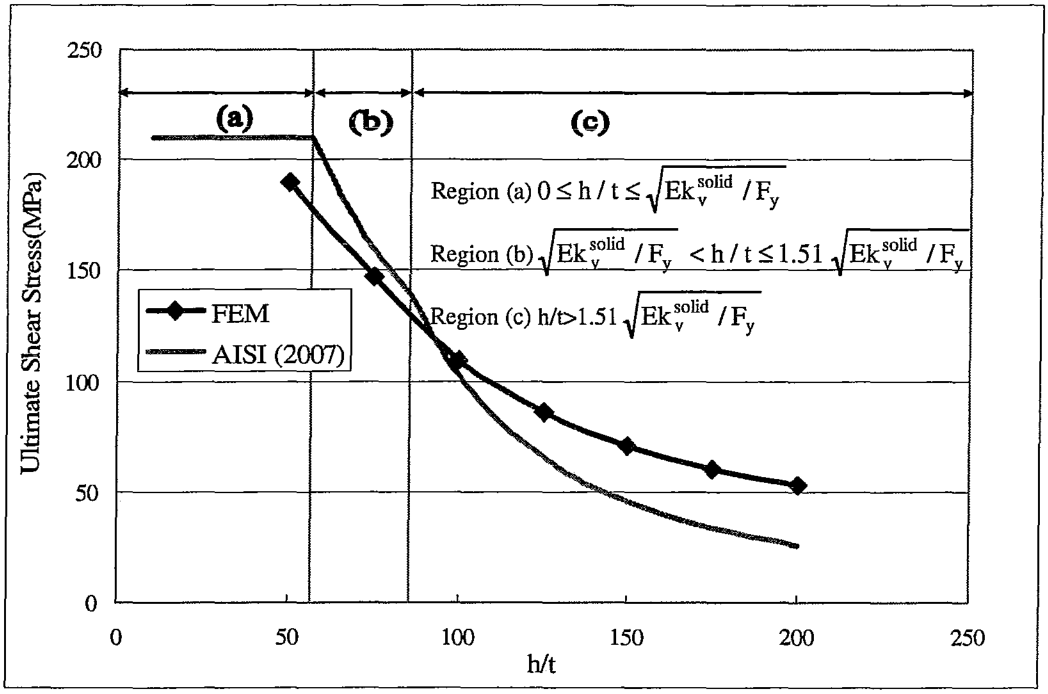

Figure 4.22 Ultimate Shear Strength Versus h/t Ratios for Plate Models with a/h=4

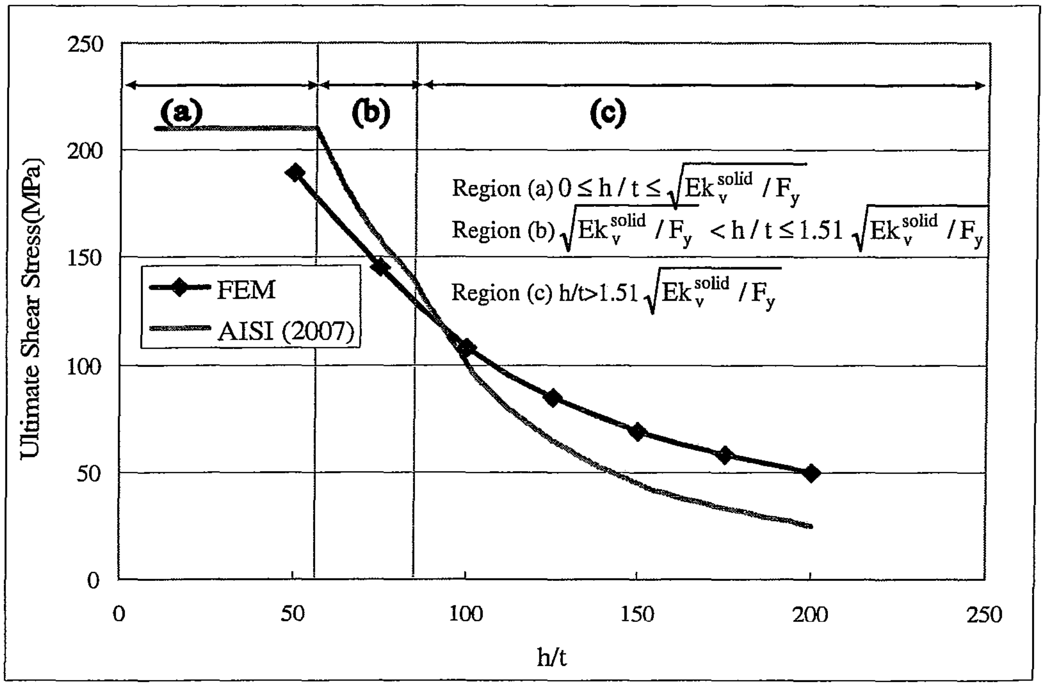

Figure 4.23 Ultimate Shear Strength Versus h/t Ratios for Plate Models with a/h=5

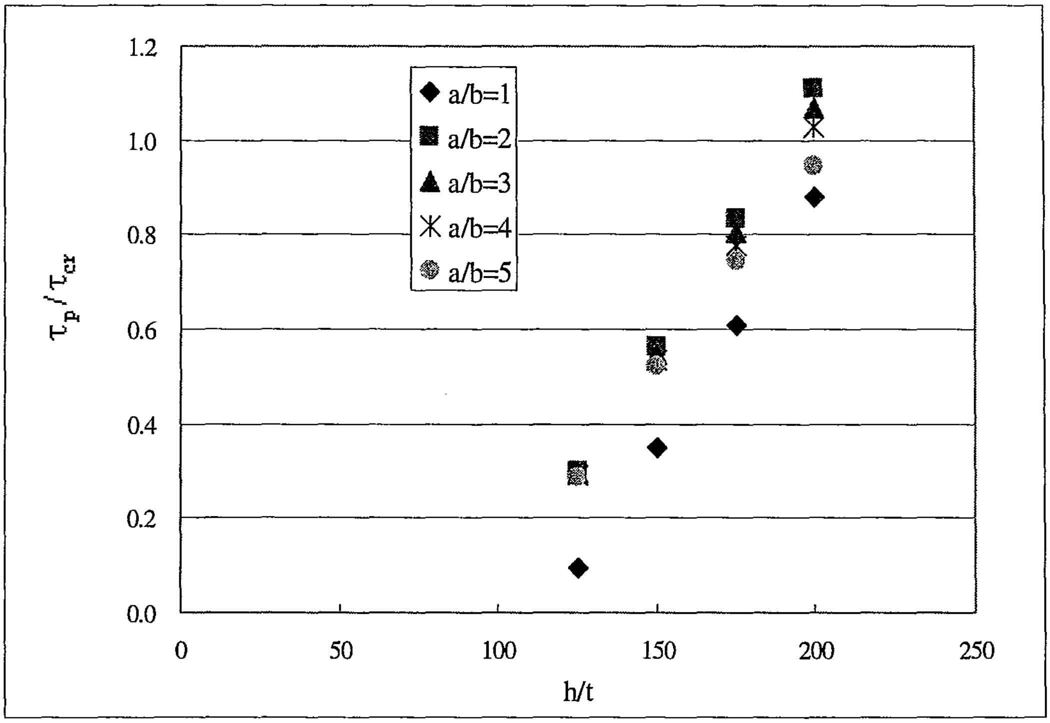

Figure 4.24 τ_p / τ_{cr} Versus h/t Ratio for Plates with Different Aspect Ratios

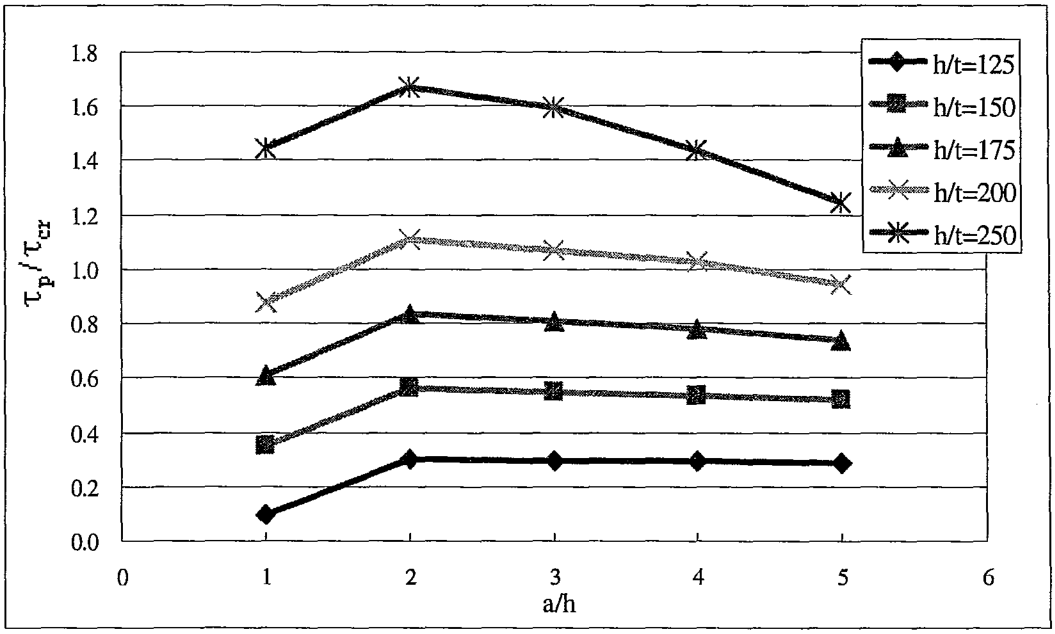

Figure 4.25 τ_p / τ_{cr} Versus a/h Ratio for Plates with Different Slenderness Ratios

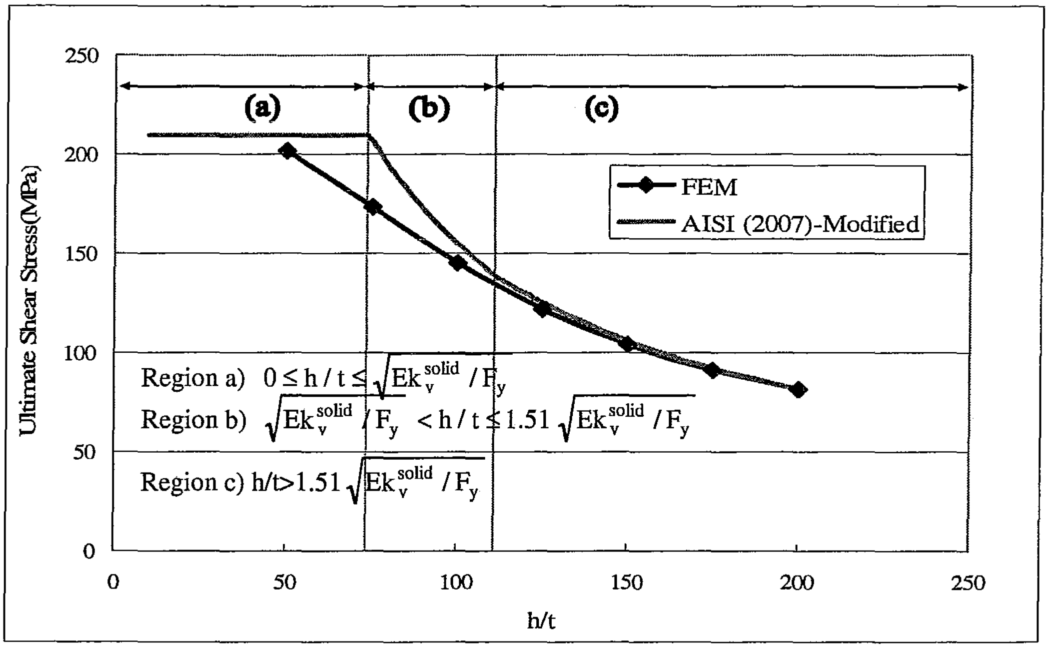

Figure 4.26 Ultimate Shear Strength Versus h/t Ratios for Plate Models with a/h=1

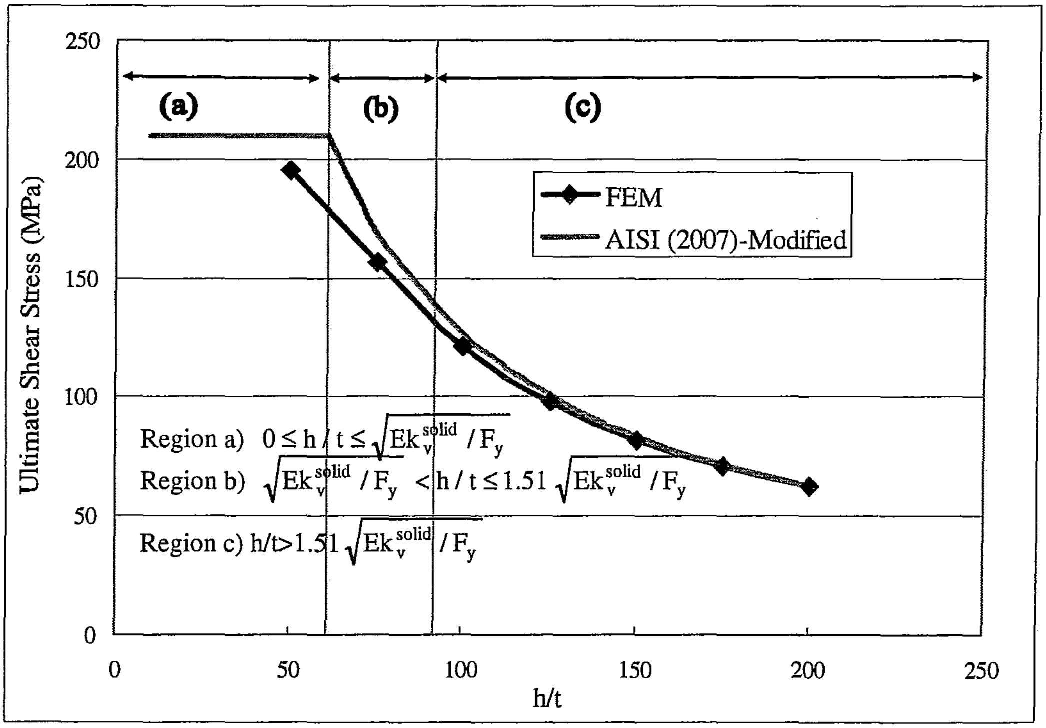

Figure 4.27 Ultimate Shear Strength Versus h/t Ratios for Plate Models with a/h=2

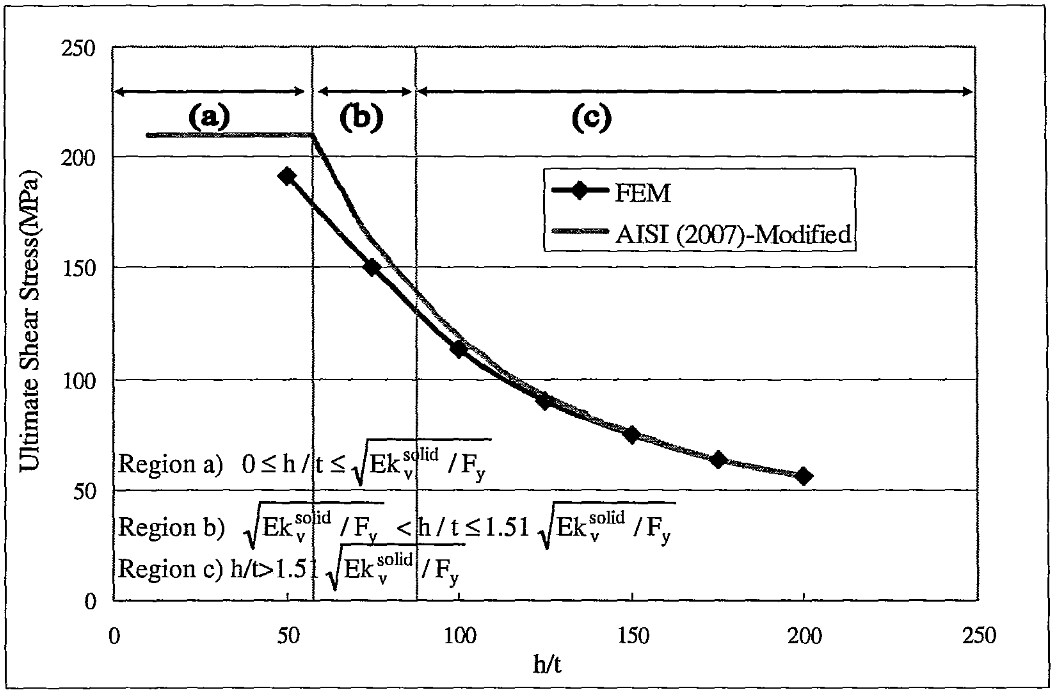

Figure 4.28 Ultimate Shear Strength Versus h/t Ratios for Plate Models with a/h=3

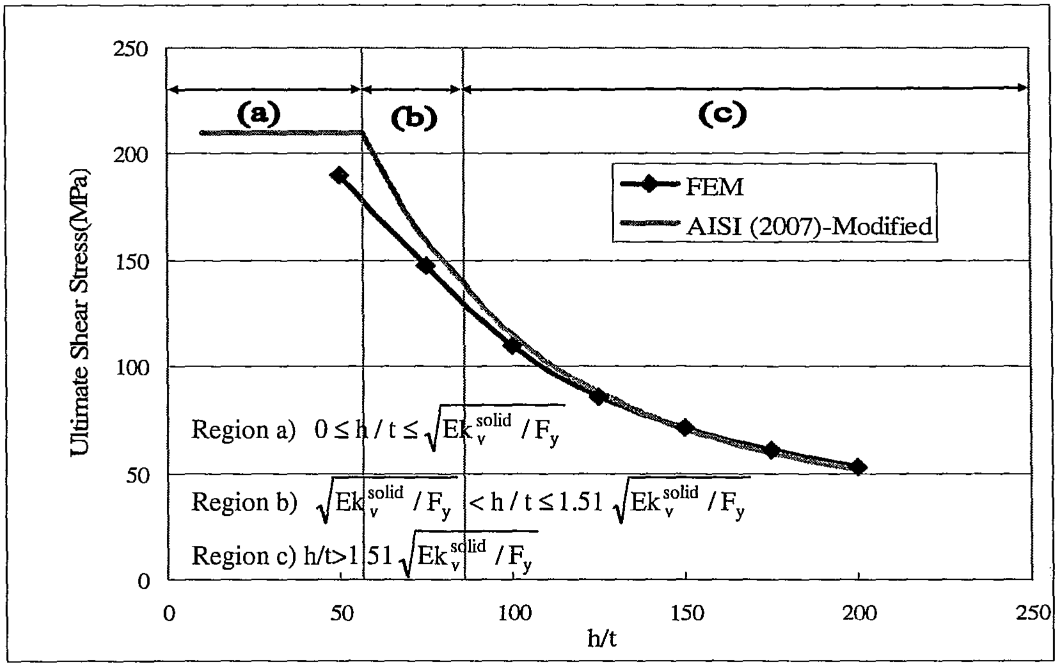

Figure 4.29 Ultimate Shear Strength Versus h/t Ratios for Plate Models with a/h=4

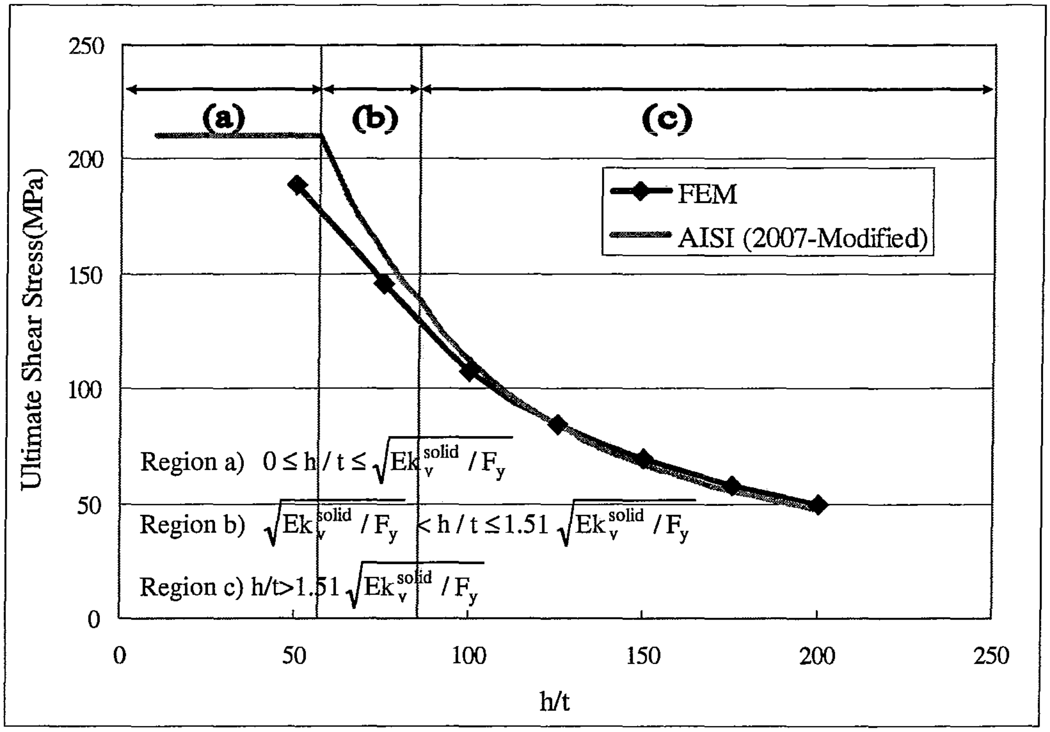

Figure 4.30 Ultimate Shear Strength Versus h/t Ratios for Plate Models with a/h=5

Chapter 5

SHEAR BEHAVIOR OF PLATES WITH OPENINGS

5.1 Introduction

Despite the fact that openings have been made in plated structures for a long time, there is very limited analytical research data exists on the buckling and ultimate strength for shear loading condition, especially for web plates with rectangular openings. This chapter will perform a systematic finite element analysis on the shear buckling and ultimate strength of web plates, ranging from thick to thin plates, with square openings located on the center of web plates. The plate under consideration is shown in Figure 5.1.

In Chapter 5, simply supported steel plates with square openings under pure shear loads will be analyzed using the commercial finite element software package ADINA8.5. The nonlinear behavior, including buckling, post-buckling and the ultimate strength of the plate will be studied through the use of finite element models. The proposed finite element model will be used to perform a parametric study on such plates. The parameters to be studied include the size of the opening (d_c / h), the slenderness ratio (h/t) and the aspect ratio (a/h) of plates. The purpose of this chapter is to establish the influence of these parameters on the ultimate shear strength of cold-formed steel plates with square openings.

The first part of this chapter will present some theoretical methods of calculating the shear critical buckling stress and the ultimate shear strength of plates with openings. In the second part, a finite element model suitable for modeling rectangular plates with square openings subjected to shear loads will be proposed. In the third part, a convergence study will be carried out to decide how many mesh elements should be used for future analysis. In the fourth part, parametric studies will be performed on plates with centrally located square openings under shear loads using the proposed finite element models. The post-buckling behavior of such plates will be studied. The parameters, as mentioned before, are the size of the opening (d_c / h), the web slenderness ratio (h/t) and the web aspect ratio (a/h). The effects from each of the parameters on the shear buckling strength and the ultimate shear capacity of plates will be evaluated and analyzed in the parametric study. The ultimate shear strengths obtained from the finite element analysis will be compared with those calculated from the AISI (2007) code method. A new equation of calculating the shear capacity of plates with centrally located square openings will then be proposed based on the results obtained from the finite element analysis. The detailed results and observations are presented in the following sections.

5.2 Background Information of Plates with Openings Subjected to Shear Loads

As mentioned in Chapter 2, the shear resistance of steel sections mainly comes from the web panel of the section. Thus openings on the web are expected to decrease the shear resistance of the steel section.

5.2.1 Shear Buckling Strength of Plates with Openings

Previous research (Narayanan and Der-Avanessian, 1984) has shown that the shear buckling strength of a plate decreases as the size of the opening on the plate increases. The equation for calculating the elastic shear buckling strength of a plate with opening can be expressed in a similar form as for the solid plate:

$$\tau_{cr}^{opening} = k_v^{opening} \frac{\pi^2 E}{12(1-\nu^2)(h/t)^2} \tag{5.1}$$

where 'E' and 'ν' are Young's modulus and Poisson's ratio respectively, while 'h' is the width of the plate and 't' is its thickness. '$\tau_{cr}^{opening}$' is the critical buckling stress for plates with openings, '$k_v^{opening}$' is the non-dimensional shear-buckling coefficient modified according to the effects of the openings. '$k_v^{opening}$' is functions of the loading and the boundary conditions, size and shape of opening, location of opening, etc.

Based on experiments, Narayanan and Der-Avanessian (1984) suggested that for centrally located rectangular holes,

when $d_c/h \leq 0.5$ and $b_c/h \leq 0.5$

$$k_v^{opening} = k_v^{solid}\left(1-\alpha_r \frac{A_{opening}}{A}\right) \tag{5.2.1}$$

when $d_c/h > 0.5$ and $b_c/h > 0.5$

$$k_v^{opening} = k_v^{solid}\left(1-\frac{d_c}{h}\right), \text{ or } k_v^{opening} = k_v^{solid}\left(1-\frac{b_c}{h}\right) \tag{5.2.2}$$

Whichever governs.

where 'd_c' is the width of the rectangular opening and 'b_c' is the length of the opening, respectively. $A_{opening}$ = area of the opening= $d_c b_c$ and A= area of the plate= h·a. α_r = 1.5 for simply supported edges and 1.25 for clamped edges.

5.2.2 Ultimate Shear Strength of Plates with Openings

The existence of a web opening can decrease the shear strength of a cold-formed steel web plate. To account for the effects caused by openings on the ultimate shear strength of web plates, a shear reduction factor is usually applied on the nominal shear strength of a solid web panel. The North American Specification (AISI, 2007) provides procedures to estimate the ultimate shear capacity of C-section webs with web openings. The specific procedure is presented below.

AISI (2007)-C3.2.2 Shear Strength [Resistance] of C-Section Webs with Holes

(Note: some symbols haves been changed in order to be consistent with the symbols used in this research)

These provisions shall be applicable within the following limits:

(1) $d_c/h \leq 0.7$

(2) $h/t \leq 200$

(3) Holes centered at mid-depth of web

(4) Clear distance between holes ≥ 18 in. (457mm)

(5) Non-circular holes, corner radii $\geq 2t$

(6) Non-circular holes, $d_c \leq 2.5$ in. (64mm) and $b_c \leq 4.5$ in. (114mm)

(7) Circular holes, diameter ≤ 6 in. (152mm)

(8) $d_c \geq 9/16$ in. (14mm)

The nominal shear strength [resistance], V_n, determined by Section C3.2.1 shall be multiplied by q_s:

(Note: Nominal shear strength V_n is given in Section 4.2.2)

When $c/t \geq 54$

$$q_s = 1.0 \tag{5.3.1}$$

When $5 \leq c/t < 54$

$$q_s = c/(54t) \tag{5.3.2}$$

where

$$c = h/2 - d_c/2.83 \quad \text{for circular holes} \qquad [5.3.3(a)]$$

$$= h/2 - d_c/2 \quad \text{for non-circular holes} \qquad [5.3.3(b)]$$

d_c = Depth of web hole

b_c = Length of web hole

h =Depth of flat portion of web measure along plane of web

The AISI (2007) divides the openings into circular and non-circular. From Equation 5.3.3(a) and Equation 5.3.3(b), it can be seen that according to AISI (2007), the non-circular openings cause larger reduction in shear strength than the circular opening does. Moreover, the AISI (2007) method does not include the length of the plate (a) in the equations of calculating the shear reduction factor. In other words, if the width (h) of the plate is fixed, the effect from the aspect ratio (a/h) is not included. The ultimate shear strength of the plate with square openings as functions of the openings size and the slenderness ratio according to the AISI (2007) procedure are shown in Figure 5.2.

5.3 Finite Element Model for Plates with Square Openings under Shear Loads

In this section, a general finite element model for analyzing the post-buckling behavior of a simply supported rectangular plate with a square opening subjected to pure shear loads is proposed. As explained in Section 3.3, the quadrilateral four-node shell elements are used in this model. The automatic-time-step (ATS) is used as the analysis method, and the linearized-buckling-analysis is used to obtain the critical buckling strength of plates in this chapter. Again, as stated in Section 3.3.2, at least 100 load steps are used for each loading process to insure sufficient numbers of data point for the load-displacement diagram. Moreover, the proposed finite element model uses an idealized stress-strain relationship for cold-formed steel proposed by Sivakumaran and Abdel-Rahman (1997). See Section 4.3.2 for the details about the material model used. The model has included the effects of the geometrical initial imperfection, but has ignored the effects of the residual stress for simplicity. The reason for neglecting residual stresses was stated in Section 4.3.4.

5.3.1 Finite Element Model and Boundary Conditions

Figure 5.1 shows the dimensions and the loading conditions of plates needed to be studied. A simply supported rectangular plate, with length 'a', width 'h', thickness 't' and a centered square opening with a side length of 'd_c', is subjected to pure shear loads along the edges. Again, the x-y plane is at the middle plane of the plate. The z-plane is perpendicular to the plate and is zero at the geometric center of the plate.

The finite element model of such a plate with the boundary details and the loading conditions are shown in Figure 5.3. In this figure, 'U_1', 'U_2' and 'U_3' are the displacements in 'x', 'y' and 'z' directions respectively, while 'θ_1', 'θ_2' and 'θ_3' are the rotations in 'x', 'y', and 'z' directions respectively. 'L1', 'L2', 'L3' and 'L4' are the four edges of the plate. Unless otherwise specified, all nodes are fixed in the z-direction rotation (θ_3) to restrain the rigid body rotation about z-axis, and are free in all other degree of freedoms. The boundary conditions for the four edges, namely 'L1', 'L2', 'L3' and 'L4' in Figure 5.3, are the same as the boundary conditions for the four edges of a solid plate described in Section 4.3.1. The four edges of the opening are left free. The loading conditions are the same as the loading condition for a solid plate, which is again described in detail in Section 4.3.1.

5.3.2 Initial Geometric Imperfections

Similar with Chapter 4, an imperfection is introduced in the finite element model for plate with openings. In order to be realistic, the initial geometric imperfection is superimposed on a solid plate before openings are made. This is enabled by forming surfaces with a initial imperfection for a solid plate, but only mesh the surfaces outside of the opening. As in Chapter 4, a double sine function is used to present the shape of the initial imperfection, and the maximum value of the imperfection is calculated as (1/2)*(Equation 4.8).

5.4 Convergence Study

As stated before, convergence study should be performed on each separate model prior to further analysis to insure the accuracy of the analysis. In this research, convergence studies will be performed on plates with different aspect ratios. For plates having the same aspect ratio, the convergence study will be carried out for the thinnest plate having the smallest opening. This is because thin plates may experience more non-linearity because of the large deformations they undergo during the loading process; and as the size of the opening increases, fewer mesh elements are needed for plates. Furthermore, the mesh configurations are also controlled so that the ratio of the longest edge to the shortest edge of the element is less than 5. In this section, a sample convergence study will be carried out for shear plates with a/h=3, h/t=200 and d_c/h=0.2, while suitable mesh configurations will also be selected for plates with each different aspect ratio.

The dimensions of the plate model for this convergence study is shown in Figure 5.1, with a=300mm, h=100mm and d_c=20mm. The slenderness ratio 'h/t' is selected to be 200, that is when t=0.5mm. The loading details and the boundary conditions for the finite element model for this plate are shown in Figure 5.3. The plate is under uniform shear loading along 4 edges. The applied loads and the boundary conditions are described in Section 5.3.1. The plate is assumed to have a multi-linear material model as described in Section 4.3.2, with F_y=350MPa and ν=0.3. The initial imperfection is imposed as stated in Section 5.3.2, with the amplitude of the initial imperfection calculated from (1/2)*(Equation 4.8), which is w_0= (1/2)*(0.006h) =0.3mm.

The analysis includes 5 identical models with the only change is the mesh densities. Figure 5.4(a) shows a general mesh pattern for plate with an aspect ratio of 3 and d_c/h=0.2. It can be seen that a finer mesh was generated closer to the opening region to handle the expected stress concentrations and high stress variations around the opening region. Figure 5.4(b) shows all the lines that need to be divided in order to discretize the plate into finite elements. In this study, each line is divided into the same numbers of divisions. Thus this analysis includes 5 identical models with only change the number of divisions in each line. Models number 1 to 5 will have the numbers of divisions on each line being 10, 16, 20, 24 and 28 respectively. Thus models 1 to 5 have an increasing number of total mesh elements. The shear buckling loads are obtained through the linearized-buckling analysis and the ultimate strengths are obtained from the ADINA static analysis with the ATS algorithm discussed in Section 3.3. The shear buckling loads and the ultimate shear strengths of the five models are presented in the Table 5.1. The percentage change in buckling load and ultimate strength of the each model will be compared.

In Table 5.1, the first column from the left indicates the number of divisions made on each geometrical line for the 5 models. It is evident from Table 5.1 that as the mesh becomes finer (increasing total number of elements), the percentage differences in both the buckling loads and ultimate strengths between two adjacent plates become smaller. Aagin, as suggested by Thangavadivel (2003), the percentage difference of less 5% for both the buckling and ultimate load is considered as acceptable for analysis purpose in this study. Therefore, from Table 5.1, it is shown that a geometrical line division of 20, 24 and 28 are all qualified. However, since the models for a/h=3 will include plate models with changing plate thickness, in order to be more conservative, the 24-division mesh configuration with 3456 elements in total will be used as the mesh density for plates with a aspect ratio of 3.

Similar convergence studies were also performed on plates with aspect ratios of 1 and 5 and d_c/h=0.6, since for plates with a/h=1 and 5, only d_c/h=0.6 will be considered in this study. Figure 5.5(a) and (b) show the lines needed to be divided in order to discretize the plate into finite elements for plates with a/h=1 and a/h=5, respectively. Based on the convergence studies, for plates with a/h=1, lines 1 to 12 were divided into 24 divisions; for plates with a/h=5, lines 1 to 14 were divided into 24 divisions and lines 15 to 17 were divided into 48 divisions.

5.5 Parametric Study on Plates with Square Openings Subjected to Shear Loads

In this section, parametric studies will be performed on simply supported plates with openings. The parameters of interest are the size of the opening (d_c/h), the slenderness ratio of the plate (h/t) and the aspect ratio of the plate (a/h). In this parametric study, a total of 42 plates will be modeled. The width of the plates were kept constant as h=100mm. First of all, 28 plates with a/h=3 will be modeled to study the effects on the ultimate shear capacity of plates caused by changing the opening size (d_c/h) and the slenderness ratio (h/t) of plates. Because the AISI (2007) limits the h/t for an unreinforced flexural web panel to a maximum value of 200, the selected slenderness ratios are h/t=50, 75, 100, 125, 150, 175 and 200. These slenderness ratios are also selected so that they are consistent with the slenderness ratios used in Chapter 4. The selected square opening sizes were 20mm, 40mm, 60mm and 80mm, which translate into 'd_c/h' values of 0.2, 0.4, 0.6 and 0.8, respectively. Even though the AISI (2007) has limited the maximum d_c value to be less than 64mm for non-circular openings, an 80mm opening will be also studied as an extreme case. For parametric study on the aspect ratio (a/h), the opening size of the plate will be fixed as d_c/h=0.6. Three groups of plates with aspect ratios of a/h=1, 3 and 5 will be studied. For each group of plates, seven plates with different slenderness, namely h/t=50, 75, 100, 125, 150, 175 and 200, were studied.

The finite element model described in Section 5.3 will be used for the parametric study. The loading conditions and the boundary details were described in Section 5.3.1 and are shown in Figure 5.3. The plate is assumed to have a multi-linear material model with F_y =350MPa and ν =0.3. The mesh configurations to be used for plates with different aspect ratios are selected through the convergence studies. The initial imperfection is imposed as described in Section 5.3.2.

5.5.1 The Effect of the Opening Size (d_c/h) on the Ultimate Shear Strength of Plates

The behavior of the plates studied during the loading process are illustrated through the applied shear stress versus the average shear strain diagrams. Figure 5.6 shows how the average shear strains are calculated. The average shear strain is calculated by dividing the y-displacement of the lower right corner of the plate by the length (a) of the plate. Figures 5.7 to 5.10 show the applied shear stress versus the average shear strain diagram as the 'd_c/h' values change from 0 to 0.8 for plates with h/t=50, 100, 150 and 200 respectively.

Figures 5.11 shows the deformed shape magnified by 10% and the band plot for the effective stress at the top surface of plates with a/h=3 and h/t=50 (thick plate) having various opening sizes at the failure load. Figure 5.12 shows the deformed shape magnified by 10% and the band plot for the effective stress at the middle surface of plates with a/h=3 and h/t=200 (thin plate) having various opening sizes at the failure load. From Figure 5.11, it can be seen that for thick plates (h/t=50), when $d_c / h = 0.2$, the area where the effective stress is greater than the yield stress ($F_y = 350\,\text{MPa}$) occurs throughout most part of the plate. Such plates fail due to the material failure rather than the instability failure. As 'd_c/h' increases, the area where the effective stress is greater than the yield stress ($F_y = 350\,\text{MPa}$) occurs only around the opening. When $d_c / h \geq 0.6$, the area where the effective stress is greater than the yield stress ($F_y = 350\,\text{MPa}$) occurs clearly at the four corners of the square opening. This is due to the stress concentration at the corners of the square opening. A similar situation happened for thin plates (h/t=200). From Figure 5.12, it can be seen that when $d_c / h \leq 0.2$, the area where the effective stress is greater than the yield stress ($F_y = 350\,\text{MPa}$) occurs at places where the out-of-plane deflection is the most, this indicates a stability type of failure for such plate. As 'd_c/h' increases, the area where the effective stress is greater than the yield stress ($F_y = 350\,\text{MPa}$) occurs only around the opening. Again, when $d_c / h \geq 0.6$, the area where the effective stress is greater than the yield stress ($F_y = 350\,\text{MPa}$) occurs clearly at the four corners of the square opening. Therefore, for plates with large openings, failure occurs in areas close to the openings, especially at points where stress concentration may occur. Thus, in order to increase or restore the shear capacity of plate with openings, reinforcement must be placed around the openings.

Table 5.2 records the ultimate shear capacity of plates with openings and a/h=3 obtained from the finite element analysis. As introduced before, seven groups of plates with different slenderness ratios (h/t) were studied. For each h/t value, Table 5.2 lists the '$\tau_{ul}^{opening}$' and '$\frac{\tau_{ul}^{opening}}{\tau_{ul}^{solid}}$' for plates with different opening sizes (d_c/h). It can be seen that for each slenderness ratio (h/t), the opening significantly reduces the ultimate shear strength of the plate. This can be explained by the fact that, as the opening size increases, less material is left to resist the shear loading. In the extreme case, where d_c/h=0.8, the reduction in the ultimate shear strength compared with solid plate can be as large as more than 90% for all plates studied. Figure 5.13 shows the '$\tau_{ul}^{opening}$' versus 'd_c/h' for plates with various h/t value and with a/h=3. It again shows that the ultimate shear strength decreases as the opening size (d_c/h) increases. Figure 5.14 shows the '$\tau_{ul}^{opening}$' versus 'h/t' for Plates with various opening sizes (d_c/h). It can be seen from Figure 5.14 that the openings have more effects on the ultimate shear capacity of thick plates than thin plates.

5.5.2 The Effect of the Slenderness Ratio (h/t) on the Ultimate Shear Strength of Plates

Table 5.2 and Figure 5.14 also show that as h/t increases, the ultimate shear strength of the plate decreases. Moreover, it can be seen from Figure 5.14 that as the size of the opening (d_c/h) increases, the effect caused by the slenderness ratio (h/t) decreases. This can be explained by the fact that thick plates fail mainly due to material failing; reduction in material in such plates will have more effect on the ultimate strength than that in the thin plates, which fail mainly due to loss of stability. This is why when large openings exist, the strength difference between thick and thin plates fades out since the strength reduction in thick plates is much greater than that in thin plates. Thus, plates with higher slenderness ratio experience lower effects on the ultimate shear capacity from centrally located openings.

5.5.3 The Effect of the Aspect Ratio (a/h) on the Ultimate Shear Strength of Plates

To study the effect on the ultimate shear strength of plates caused by the aspect ratio (a/h), the opening size is kept constant as $d_c/h=0.6$. The results used for the parameter study on the aspect ratio (a/h) of plates are listed in Table 5.3. It can be seen that for each slenderness ratio (h/t), the ultimate shear strength increases as the aspect ratio (a/h) increases, but only to a small amount. For example, for a plate with h/t=50, the difference in the ultimate shear strength between a/h=1 and a/h=5 is only about 2.3%. Figure 5.15 shows the ultimate shear capacity of plates with square openings as a function of the plate aspect ratio (a/h). It can be seen from Figure 5.15 that as the aspect ratio increases, the ultimate shear strengths of such plates tend to increase. However, for all of these models, the effect caused by changing the aspect ratio is relatively small compared with the effects caused from the openings size (d_c/h) and the slenderness ratio (h/t).

5.5.4 Comparison between the Ultimate Shear Capacities Obtained from the Finite Element Method and the AISI (2007) Method

Figures 5.16 to 5.19 show the ultimate shear capacities of plates with openings as a function of the size of the openings (d_c/h) obtained from both the finite element method and the AISI (2007) code method (Eq.5.3.1 to 5.3.3) for plates with h/t=50, 100, 150 and 200, respectively. Where $q_s = \frac{\tau_{ul}^{opening}}{\tau_{ul}^{solid}}$. It is evident from these figures that the AISI (2007) tends to underestimate the ultimate shear strength of thick to moderate thick plates with square openings, but overestimate the ultimate shear strength of thin plates with square openings. A new equation of estimating the shear reduction factor (q_s) for web plates with centrally located square opening will be proposed based on the finite element analysis.

The new proposed equation is derived by curve fitting the finite element data for plates with $h/t \leq 200$ and $d_c/h \leq 0.8$. Figure 5.20 shows the shear reduction factor (q_s) as a function of the opening size (d_c/h) for plates with different slenderness ratios (h/t). Thus, according to Figure 5.20, a third power polynomial equation can be used to represent the relationship between the shear reduction factor (q_s) and the opening size (d_c/h) of plates. The equation is presented as the following:

$$q_s = [3.55\left(\frac{d_c}{h}\right)^3 - 4.77\left(\frac{d_c}{h}\right)^2 + 0.39\left(\frac{d_c}{h}\right) + 1] - 20[-\left(\frac{d_c}{h} - 0.5\right)^2 + 0.25] / \left(\frac{h}{t}\right) \qquad (5.4)$$

Figures 5.21 to 5.24 show the shear reduction factor of plates with square openings as a function of their opening size (d_c/h) obtained from the finite element analysis and from Equation 5.4 for plates with h/t=50, 100, 150 and 200, respectively. It can be seen that Equation 5.4 is able to better estimate the ultimate shear strength of plates with centralized square opening.

5.6 Conclusion

In this chapter, simply supported plates with centrally located square openings were modeled using the finite element method. The non-linear behavior and ultimate shear capacity of such plates were analyzed using the commercial three dimensional finite element analysis software ADINA8.5. The proposed finite element models were used to carry out parametric studies on the ultimate shear capacity of plate with square openings. The parameters selected are the size of the openings (d_c / h), the plate slenderness ratio (h/t) and the plate aspect ratio (a/h).

The parametric study has shown that the centrally located square opening significantly reduces the ultimate shear strength of the plate. Based on the parametric study, it can be concluded that the opening size is the primary parameter influencing the ultimate shear strength of plate. The reduction in the ultimate shear strength displays an approximately linear relationship with the increase of the opening sizes. It was also found that as the slenderness of the plate increases, the ultimate shear strength decreases. However, the extent of the effect on the ultimate shear strength of plate decreases as the openings size increases. The last parameter, which is the plate aspect ratio, was found to affect the ultimate shear strength of plate with square opening to some extent. When holding the opening size unchanged, the ultimate shear strength of plates with square openings tends to increase as the plate aspect ratio increases. However, as the aspect ratio increases, that is when the plate becomes very long; the rate of increase in the ultimate shear strength tends to decrease and eventually fades out. Thus compared to the other two parameters, the aspect ratio is the least significant parameter in the sense of affecting the ultimate shear strength of plates with square opening.

Table 5.1 Buckling and Ultimate Strengths of Plates with Openings with Different Mesh Densities (a/b=3, h/t=200, $d_c / h = 0.2$)

		Shear Buckling Strength		Ultimate Load	
Number of Divisions On Each Line	Total Number of Elements	σ_{cr} (FEM) (MPa)	%diff.	σ_{ul} (FEM) (MPa)	%diff.
10	600	23.29		58.52	
			2.15		8.09
16	1536	22.80		54.14	
			0.62		2.48
20	2400	22.66		52.83	
			0.35		2.03
24	3456	22.58		51.78	
			0.31		0.52
28	4704	22.51		51.51	

Table 5.2 Ultimate Shear Strength of Plates with Different Opening Sizes and Slenderness Ratios for Plates with a/h=3

	h/t=50		h/t=75		h/t=100		h/t=125	
dc/h	$\tau_{ul}^{opening}$ (MPa)	$\frac{\tau_{ul}^{opening}}{\tau_{ul}^{solid}}$	$\tau_{ul}^{opening}$ (MPa)	$\frac{\tau_{ul}^{opening}}{\tau_{ul}^{solid}}$	$\tau_{ul}^{opening}$ (MPa)	$\frac{\tau_{ul}^{opening}}{\tau_{ul}^{solid}}$	$\tau_{ul}^{opening}$ (MPa)	$\frac{\tau_{ul}^{opening}}{\tau_{ul}^{solid}}$
0.00	191.55	1.00	149.98	1.00	113.12	1.00	89.72	1.00
0.20	151.10	0.79	124.22	0.83	97.00	0.86	79.46	0.89
0.40	89.25	0.47	73.22	0.49	59.10	0.52	50.33	0.56
0.60	31.10	0.16	26.84	0.18	23.59	0.21	21.05	0.23
0.80	7.22	0.04	6.21	0.04	5.55	0.05	5.53	0.06
	h/t=150		h/t=175		h/t=200			
dc/h	$\tau_{ul}^{opening}$ (MPa)	$\frac{\tau_{ul}^{opening}}{\tau_{ul}^{solid}}$	$\tau_{ul}^{opening}$ (MPa)	$\frac{\tau_{ul}^{opening}}{\tau_{ul}^{solid}}$	$\tau_{ul}^{opening}$ (MPa)	$\frac{\tau_{ul}^{opening}}{\tau_{ul}^{solid}}$		
0.00	74.46	1.00	63.82	1.00	55.96	1.00		
0.20	67.11	0.90	58.31	0.91	51.78	0.93		
0.40	44.41	0.60	39.71	0.62	35.86	0.64		
0.60	19.31	0.26	18.01	0.28	16.97	0.30		
0.80	5.502	0.07	5.00	0.08	4.704	0.08		

Table 5.3 Ultimate Shear Strength of Plates with Slenderness Ratios and Aspect Ratio (d_c/h =0.6)

$\tau_{ul}^{opening}$ (MPa)	h/t=50	h/t=75	h/t=100	h/t=125
a/h=1	30.75	25.88	21.96	19.64
a/h=3	31.10	26.84	23.59	21.05
a/h=5	31.45	28.13	25.21	22.32
$\tau_{ul}^{opening}$ (MPa)	h/t=150	h/t=175	h/t=200	
a/h=1	17.70	16.76	16.08	
a/h=3	19.31	18.01	16.97	
a/h=5	20.31	18.81	17.46	

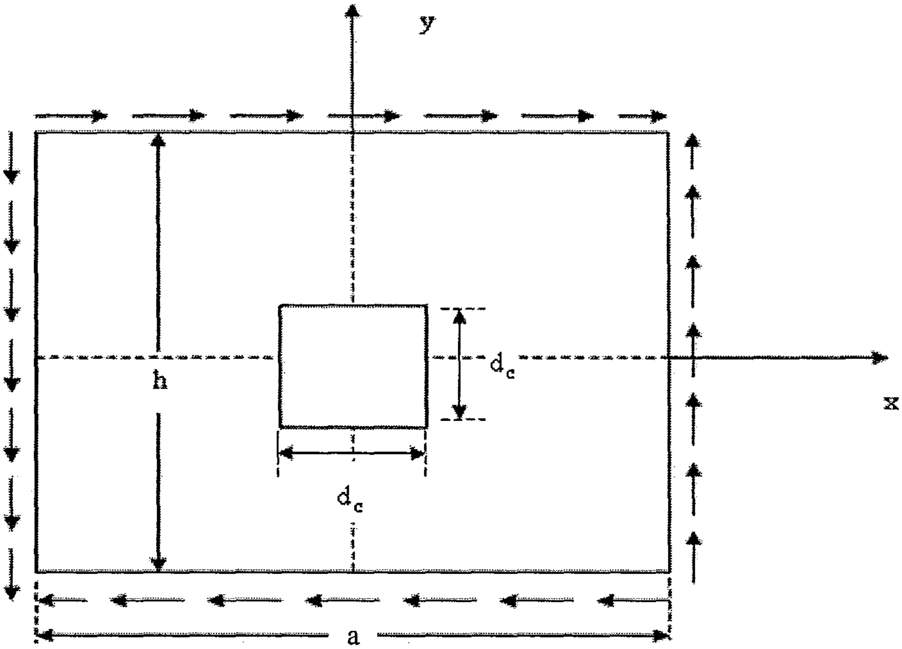

Figure 5.1 Simply Supported Plate with Centered Square Opening Subjected to Uniform Edge Shear

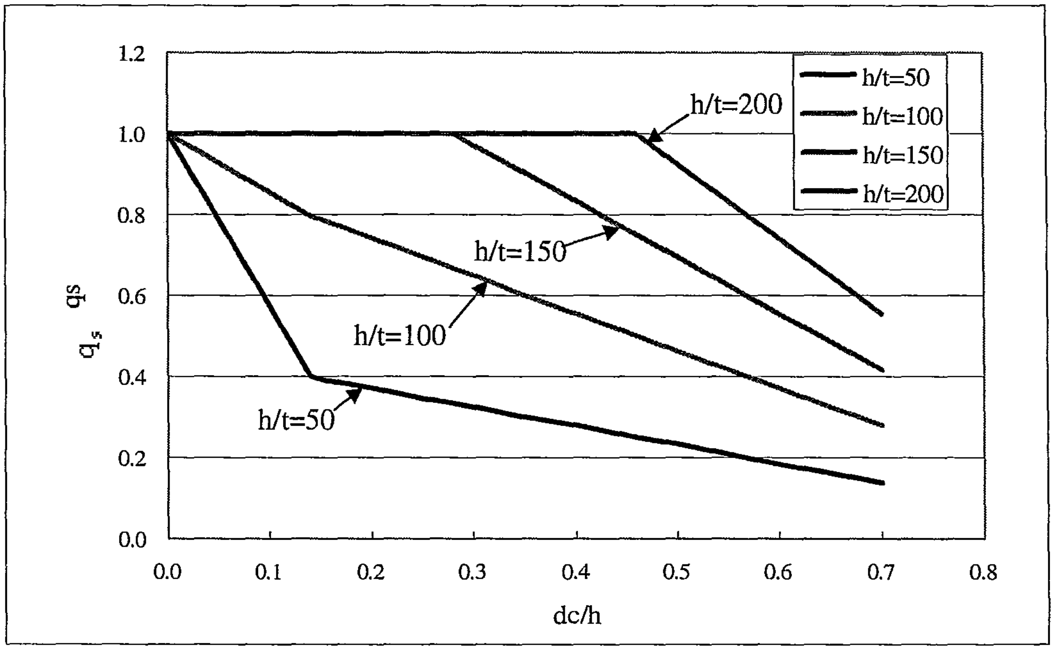

Figure 5.2 Shear Reduction Factor q_s as a Function of d_c/h Calculated According to the AISI (2007) Specification (Equation 5.3.1 to 5.3.3)

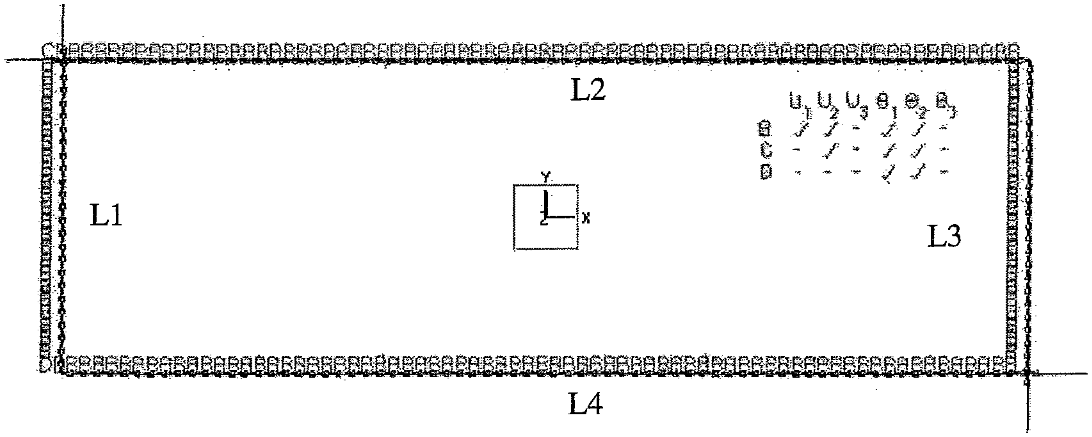

Figure 5.3 Finite Element Model with Load & Boundary Conditions of A Plate with Square Opening Subjected to Edge Shear Loading

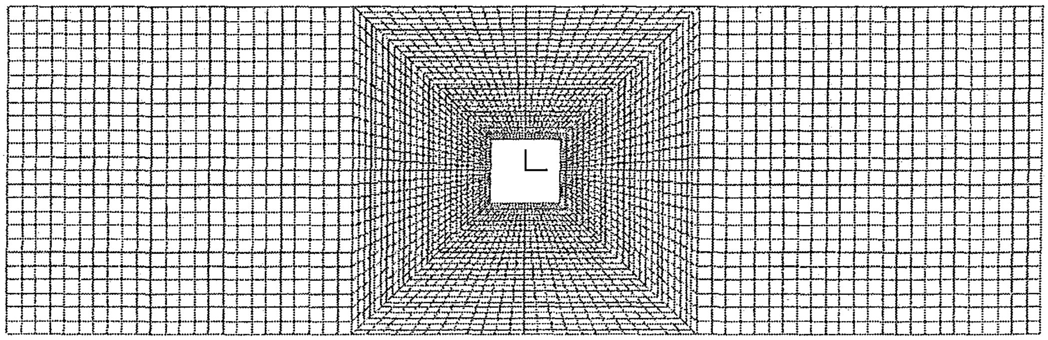

(a)

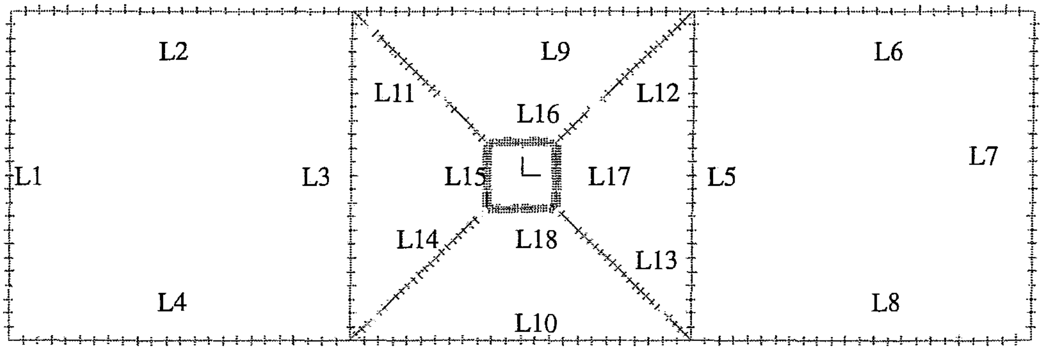

(b)

Figure 5.4 (a) Typical Mesh Pattern for A Rectangular Plate with $a/h=3$, $d_c/h=0.2$

(b) Rectangular Plate with $a/h=3$ and $d_c/h=0.2$ with Lines Being Divided According to Specified Mesh Density

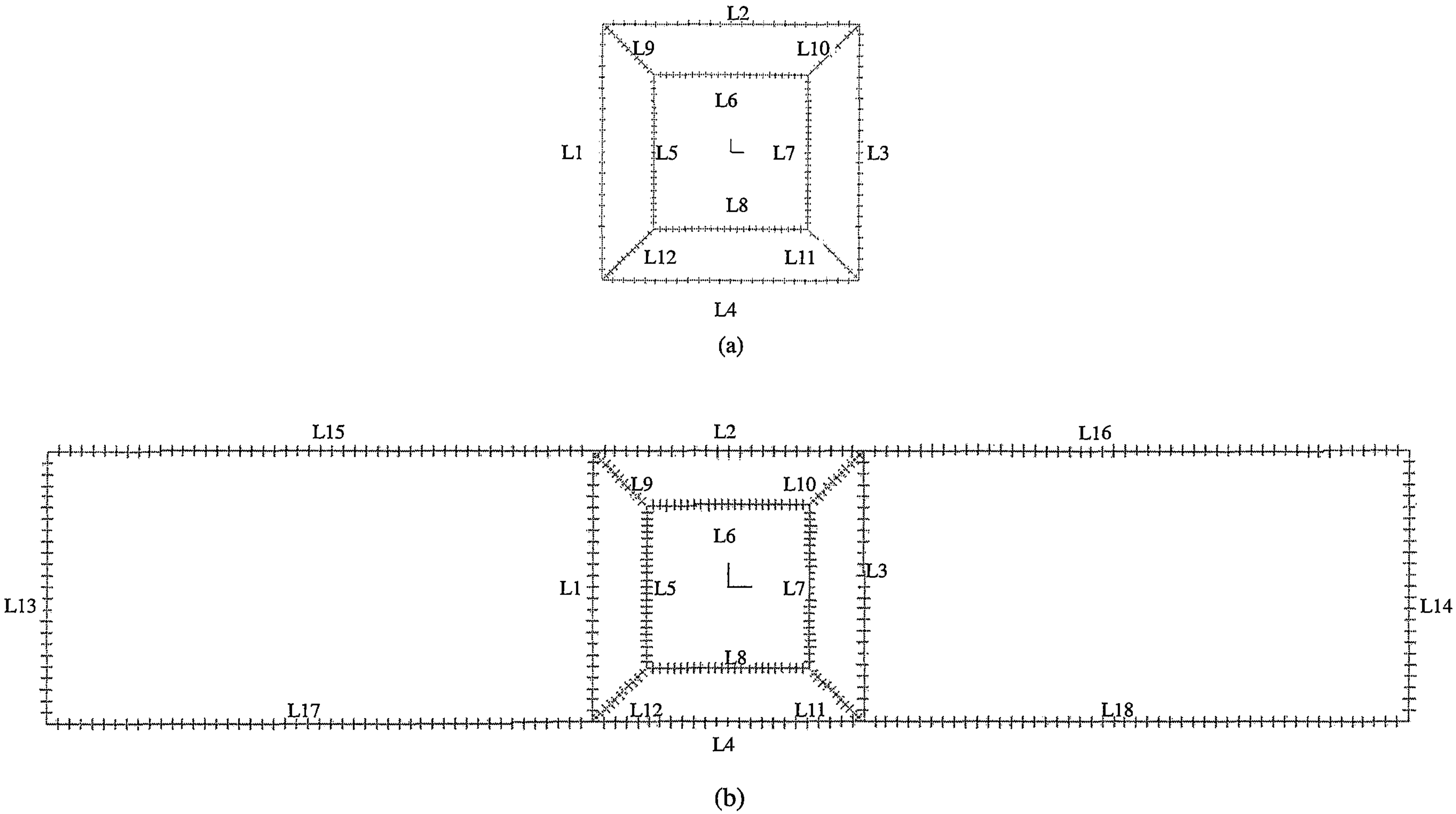

Figure 5.5 Rectangular Plate with Lines Being Divided According to Specified Mesh Density
(a) a/h=1 and $d_c/h=0.6$ (b) a/h=5 and $d_c/h=0.6$

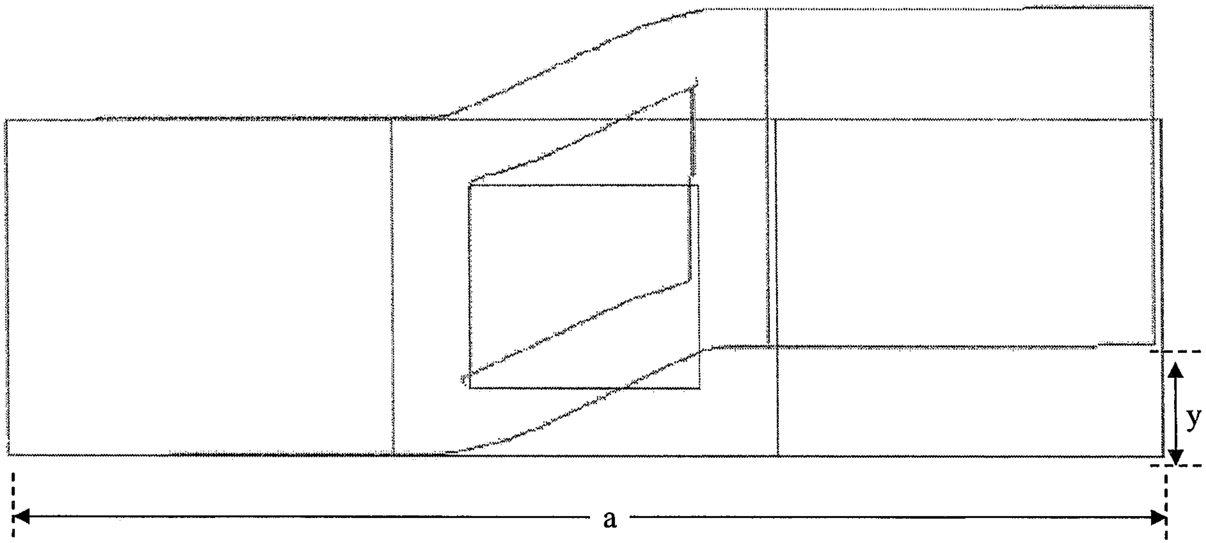

Figure 5.6 Illustration of Calculation of the Average Shear Strain of Plates with Openings

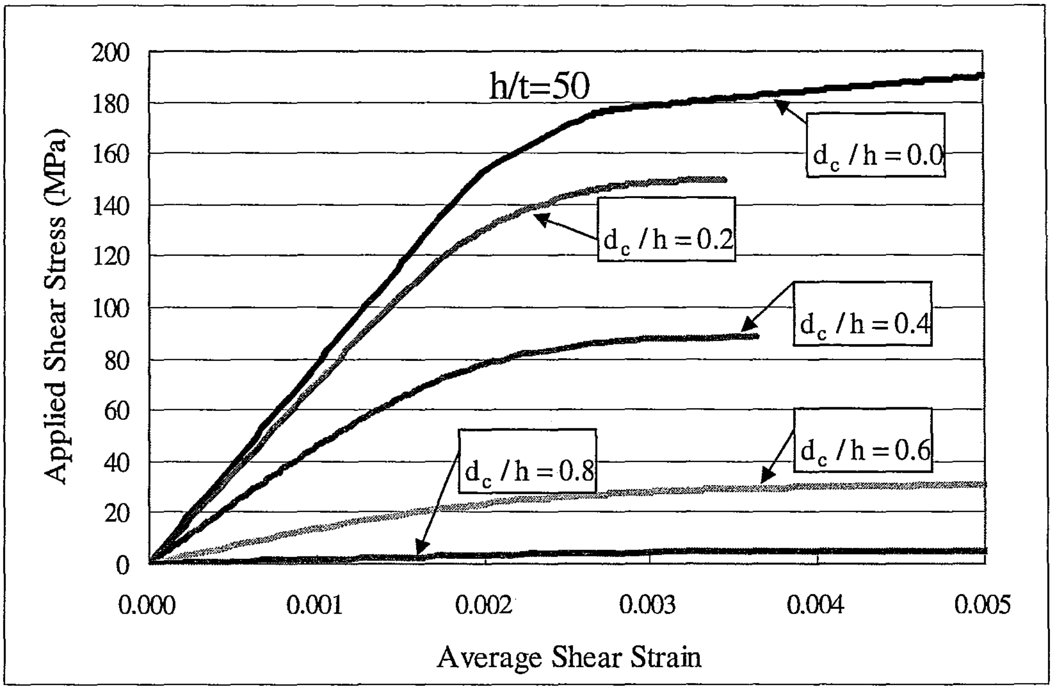

Figure 5.7 Applied Shear Stress Versus Average Shear Strain for h/t=50

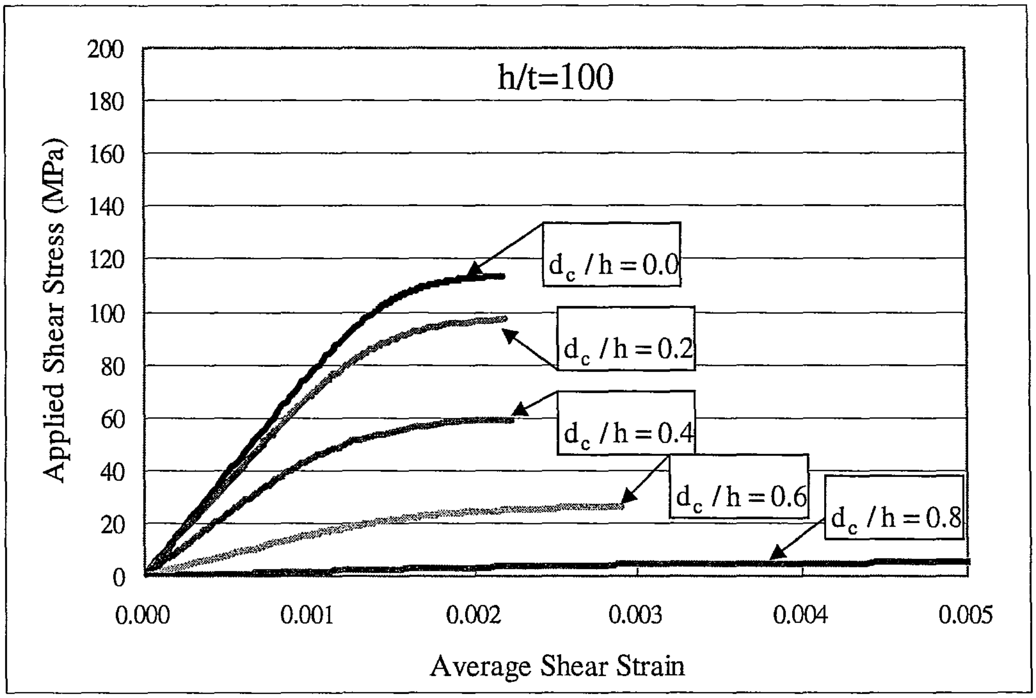

Figure 5.8 Applied Shear Stress Versus Average Shear Strain for h/t=100

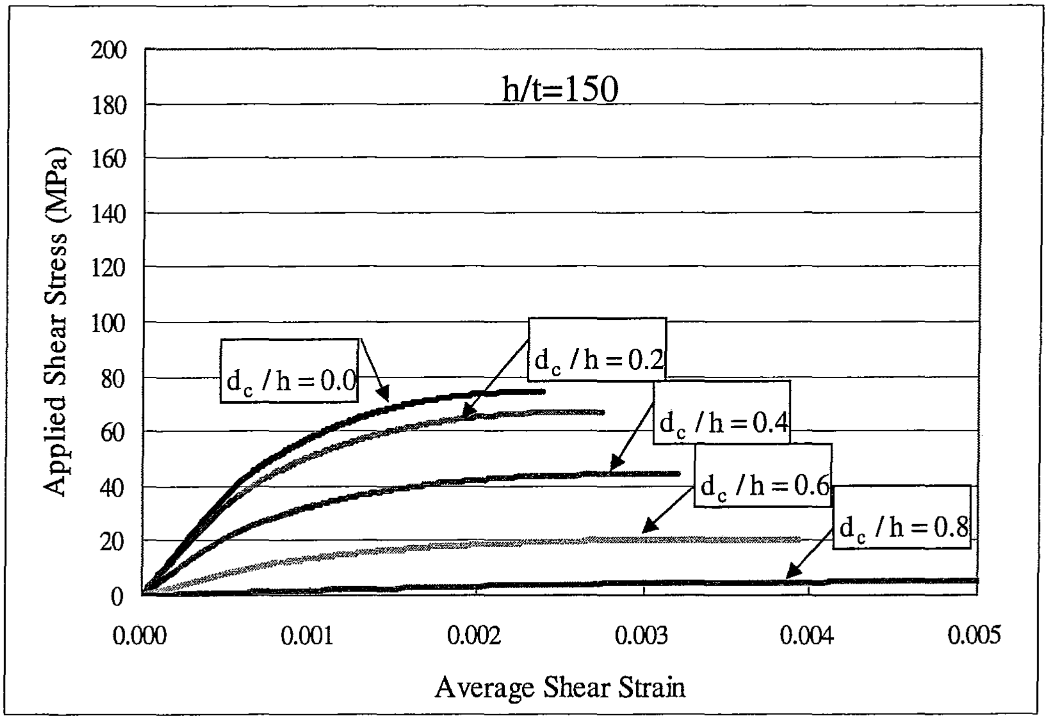

Figure 5.9 Applied Shear Stress Versus Average Shear Strain for h/t=150

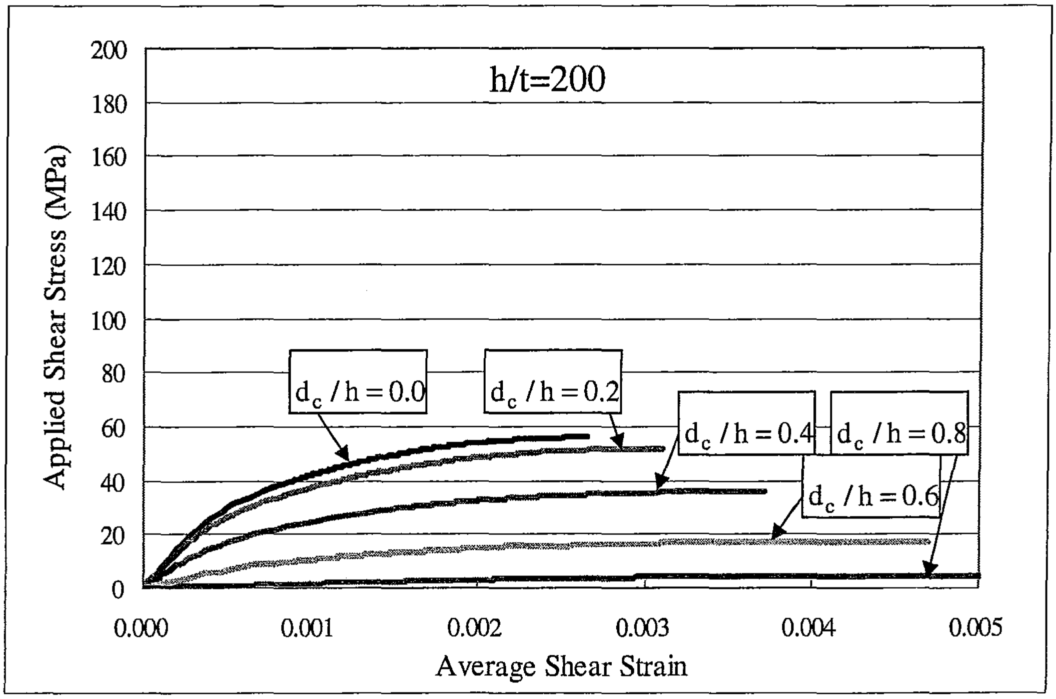

Figure 5.10 Applied Shear Stress Versus Average Shear Strain for h/t=200

<table>
<tr><th>Opening Size</th><th>Effective Stress Band Plots and Deformed Shape Magnified by 10% at the Failure Load Level for Thick Plates (h/t=50)</th><th>Failure Descriptions</th></tr>
<tr><td rowspan="2">$d_c / h = 20$</td><td>x-y View:
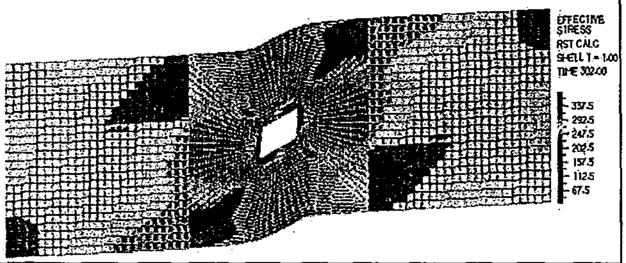
</td><td rowspan="2">

- Failure initiated at the four corners of the opening
- Diagonal shear failure at the opening region
- Plasticity spread throughout the plate

</td></tr>
<tr><td>Iso-View:
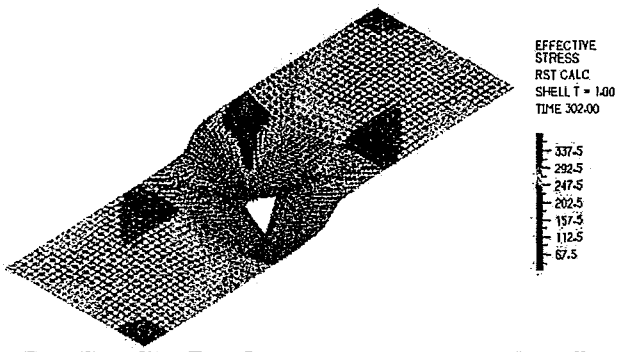
</td></tr>
<tr><td rowspan="2">$d_c / h = 40$</td><td>x-y View:
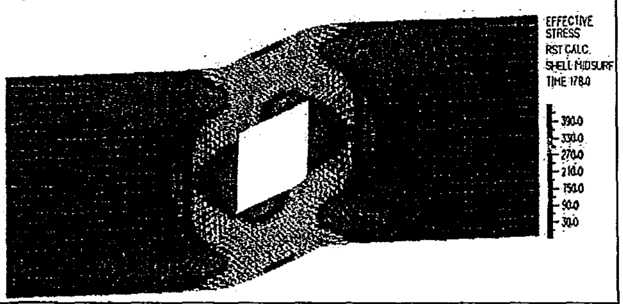
</td><td rowspan="2">

- Failure initiated at the four corners of the opening
- Diagonal shear failure at the opening region
- Plasticity occurs around the opening region

</td></tr>
<tr><td>Iso-View:
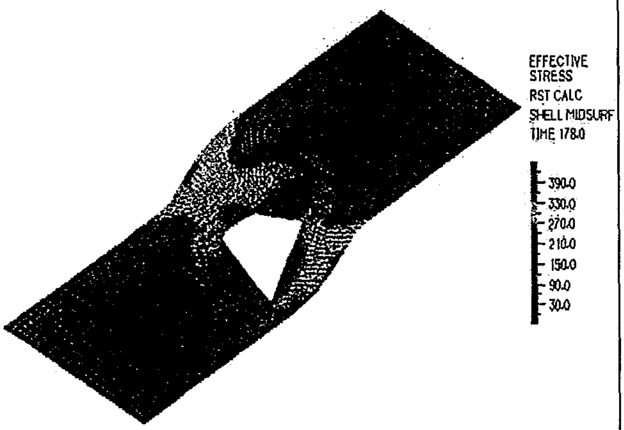
</td></tr>
</table>

<table>
<tr>
<td rowspan="2">$d_c / h = 60$</td>
<td>x-y View:
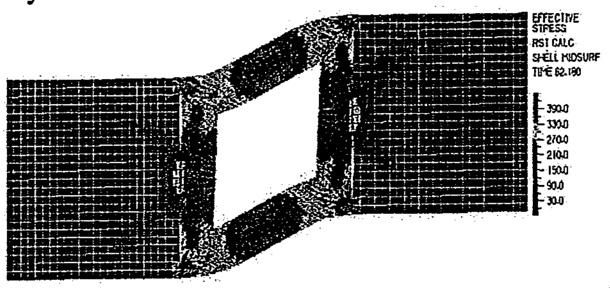
</td>
<td rowspan="2">• Failure initiated at the four corners of the opening
• Diagonal shear failure at the opening region
• Plasticity occurs around the four corners of the opening</td>
</tr>
<tr>
<td>Iso-View:
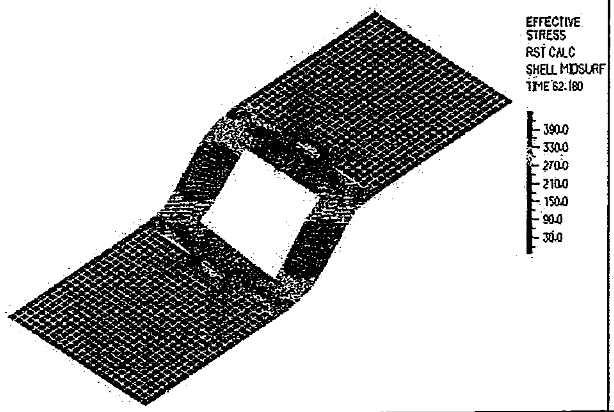
</td>
</tr>
<tr>
<td>$d_c / h = 80$</td>
<td>x-y View:
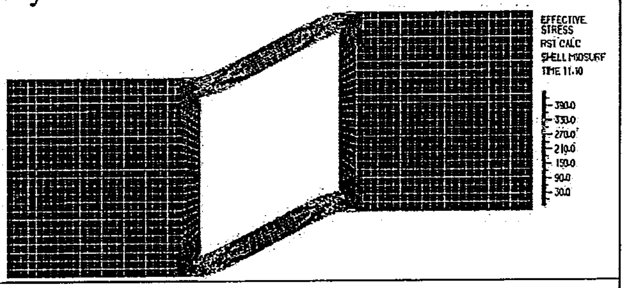
</td>
<td rowspan="2">• Failure initiated at the four corners of the opening
• Diagonal shear failure at the opening region
• Plasticity occurs only at the four corners of the opening</td>
</tr>
<tr>
<td></td>
<td>Iso-View:
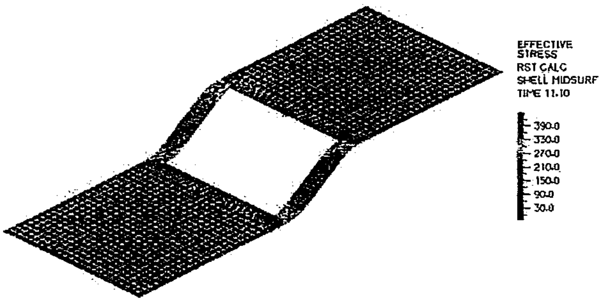
</td>
</tr>
</table>

Figure 5.11 Effective Stress Band Plots and Deformed Shape for Plates with a/h=3, h/t=50 (Thick Plates) at Failure Loads

<table>
<tr>
<td rowspan="2">$d_c / h = 60$</td>
<td>x-y View:
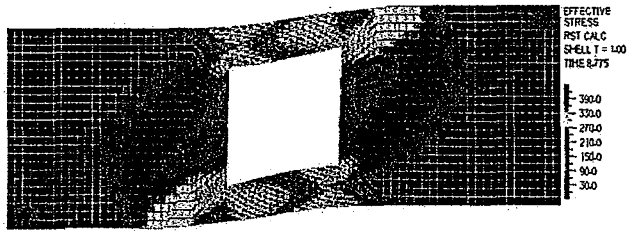</td>
<td rowspan="2">Failure initiated at the four corners of the opening
Diagonal shear failure at the opening region
Plasticity occurs around the corners of the opening</td>
</tr>
<tr>
<td>Iso-View:
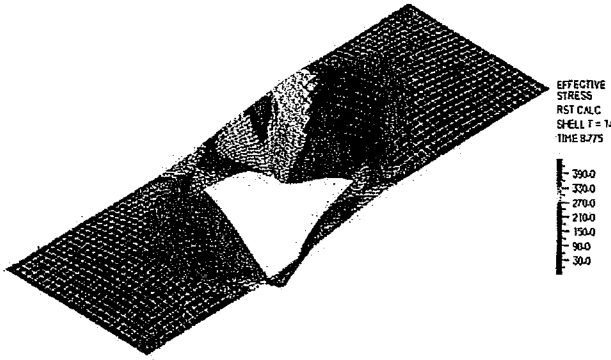</td>
</tr>
<tr>
<td>$d_c / h = 80$</td>
<td>x-y View:
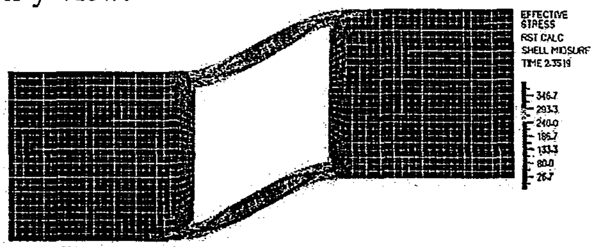</td>
<td rowspan="2">Failure initiated at the four corners of the opening
Diagonal shear failure at the opening region
Plasticity occurs only at the corners of the opening</td>
</tr>
<tr>
<td></td>
<td>Iso-View:
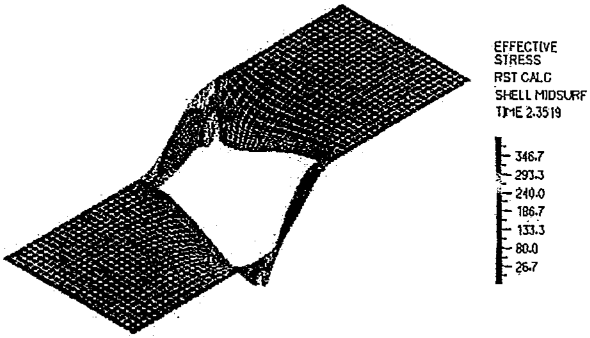</td>
</tr>
</table>

Figure 5.12 Effective Stress Band Plots and Deformed Shape for Plates with a/h=3, h/t=200 (Thin Plates) at Failure Loads

<table>
<tr><th>Opening Size</th><th>Effective Stress Band Plots and Deformed Shape Magnified by 10% at the Failure Load Level for Thin Plates (h/t=200)</th><th>Failure Descriptions</th></tr>
<tr><td rowspan="2">$d_c / h = 20$</td><td>x-y View:
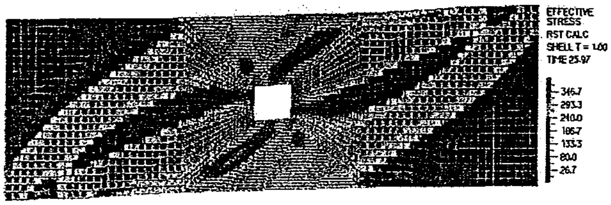
</td><td rowspan="2">

- Failure initiated at the four corners of the opening
- Plate buckled
- Plasticity occurs at the tension fields and the corners of the opening

</td></tr>
<tr><td>Iso-View:
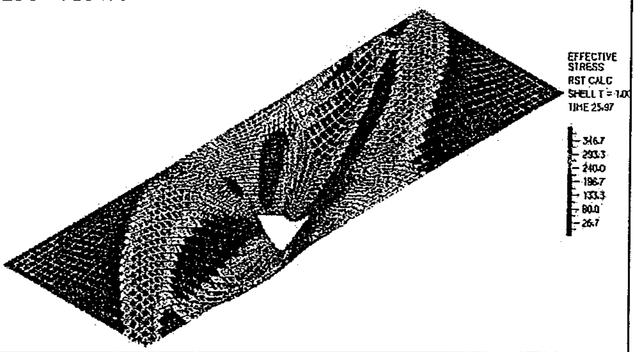
</td></tr>
<tr><td rowspan="2">$d_c / h = 40$</td><td>x-y View:
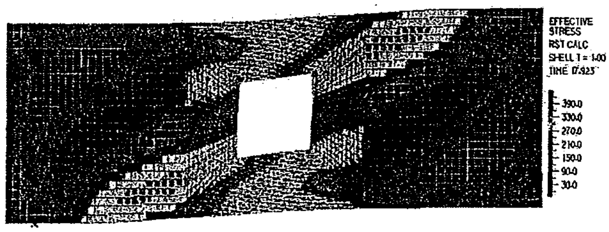
</td><td rowspan="2">

- Failure initiated at the four corners of the opening
- Diagonal shear failure at the opening region
- Plasticity occurs at the tension fields and around the corners of the opening

</td></tr>
<tr><td>Iso-View:
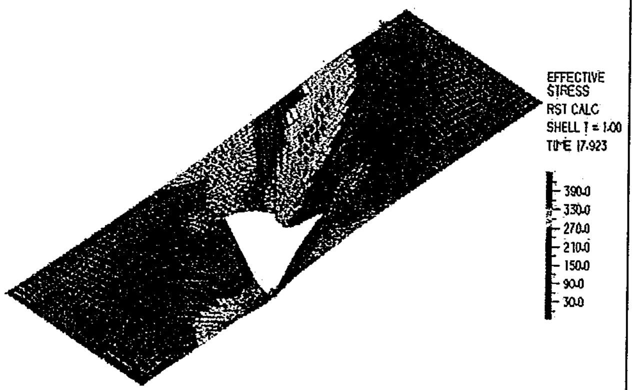
</td></tr>
</table>

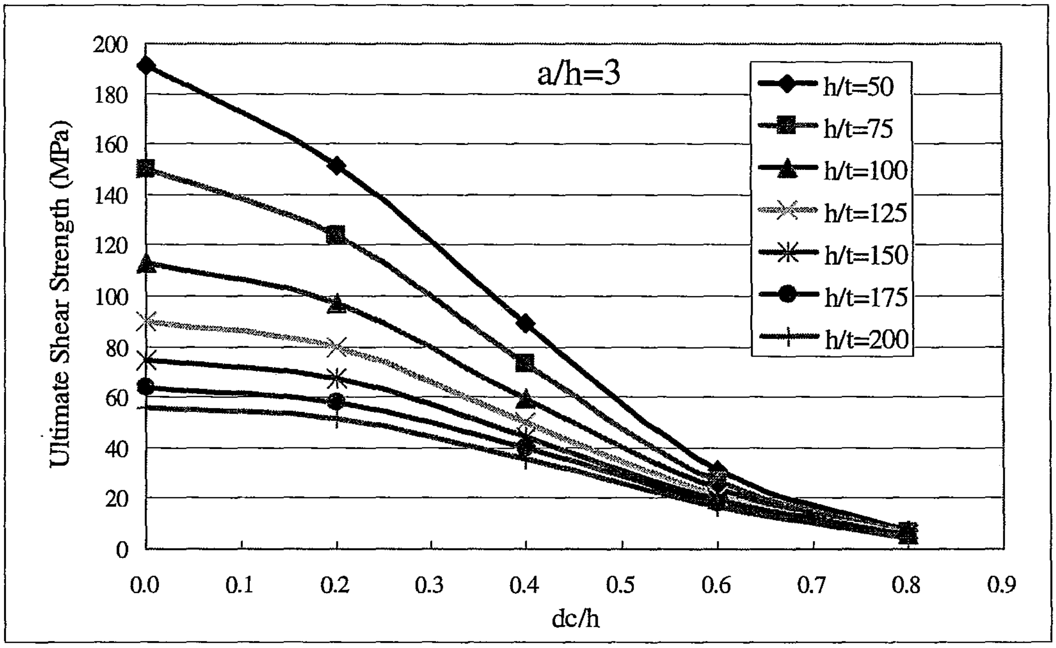

Figure 5.13 Ultimate Shear Strength of Plates Versus d_c/h for Plates with Various h/t Values (a/h=3)

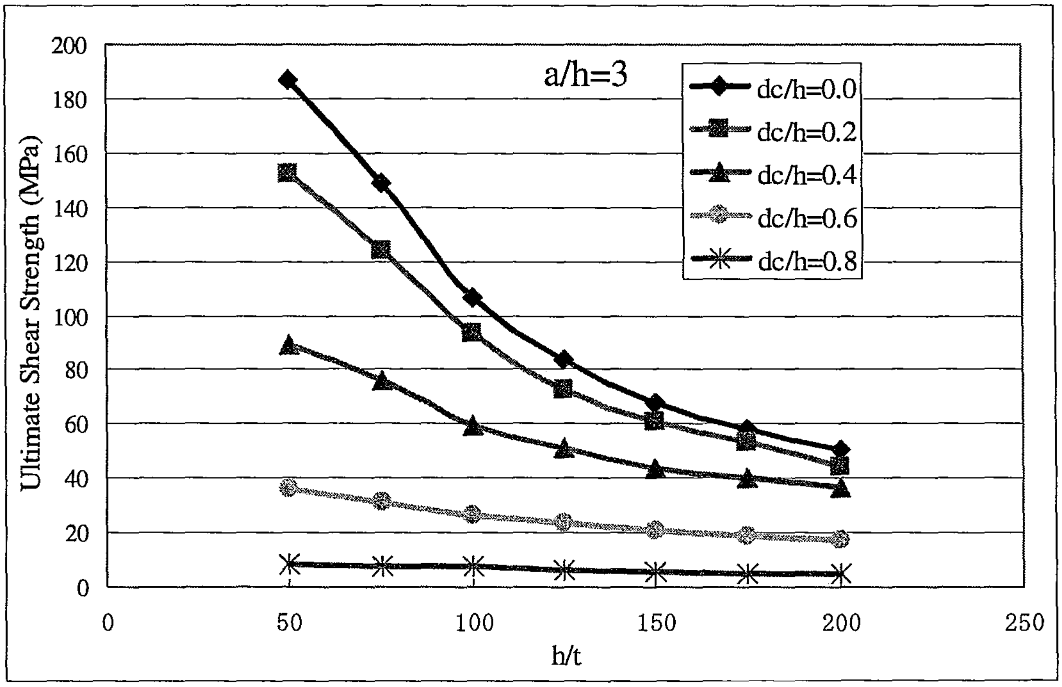

Figure 5.14 Ultimate Shear Strength of Plates with Different Opening Sizes Versus h/t (a/h=3)

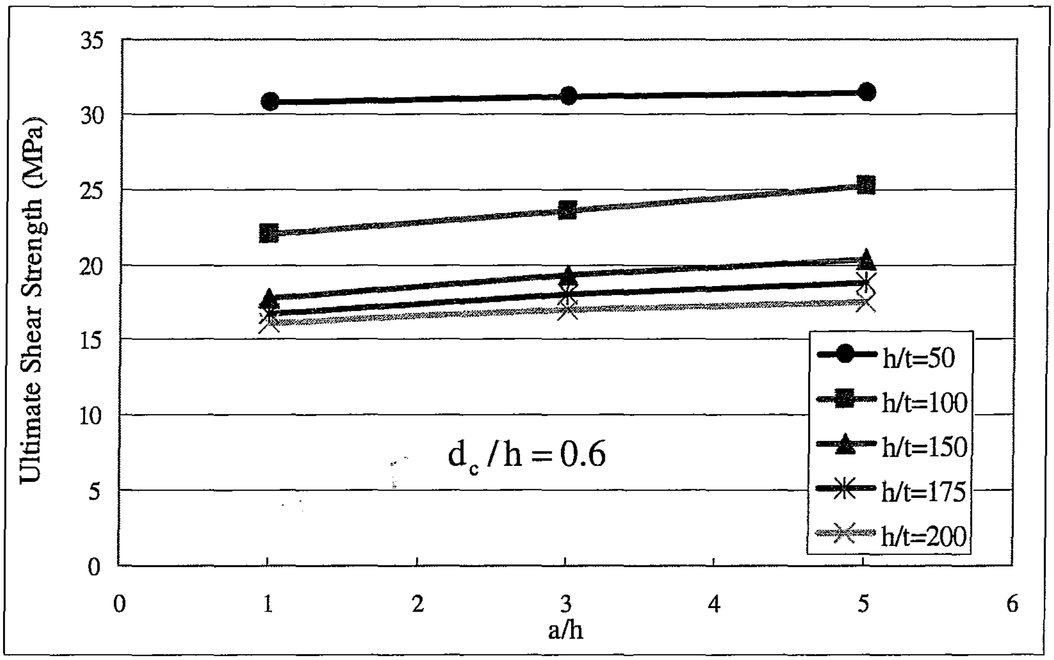

Figure 5.15 Ultimate Shear Strength of Plates with Different Slenderness Ratios Versus a/h ($d_c/h = 0.6$)

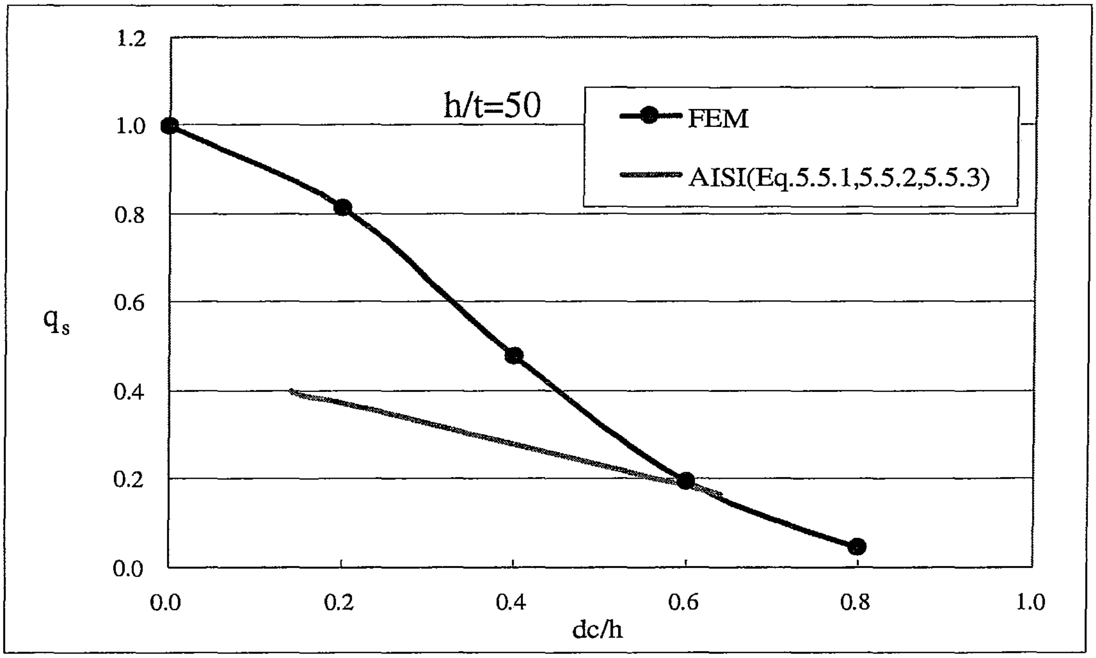

Figure 5.16 Ultimate Shear Strength of Plates with Openings/Ultimate Shear Strength of Solid Plate Versus d_c/h for Plates with a/h=3 and h/t=50

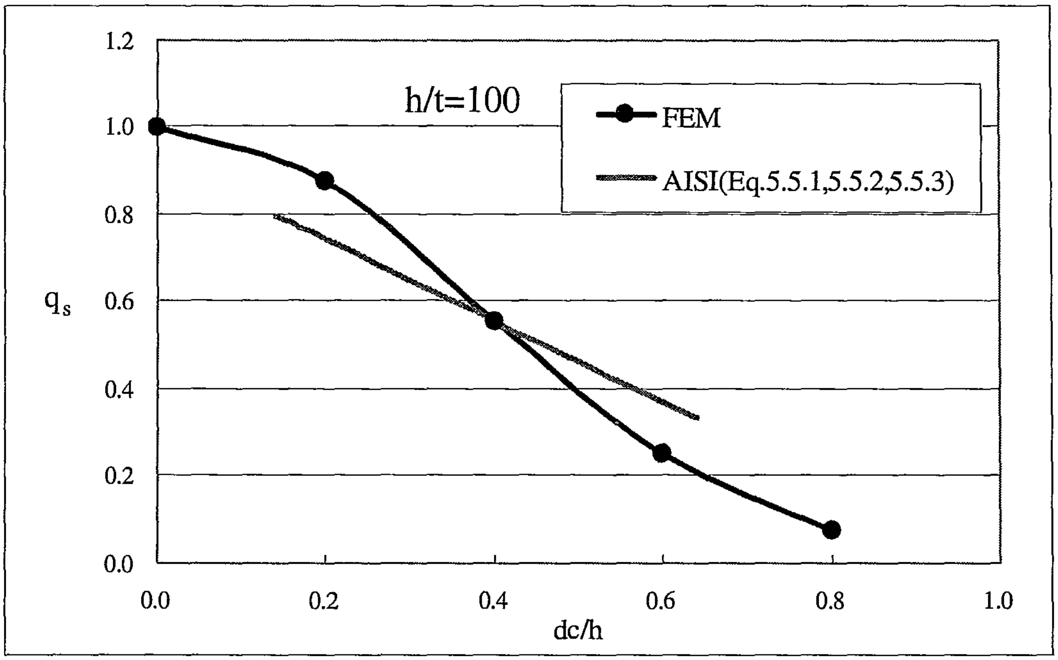

Figure 5.17 Ultimate Shear Strength of Plates with Openings/Ultimate Shear Strength of Solid Plate Versus d_c/h for Plates with a/h=3 and h/t=100

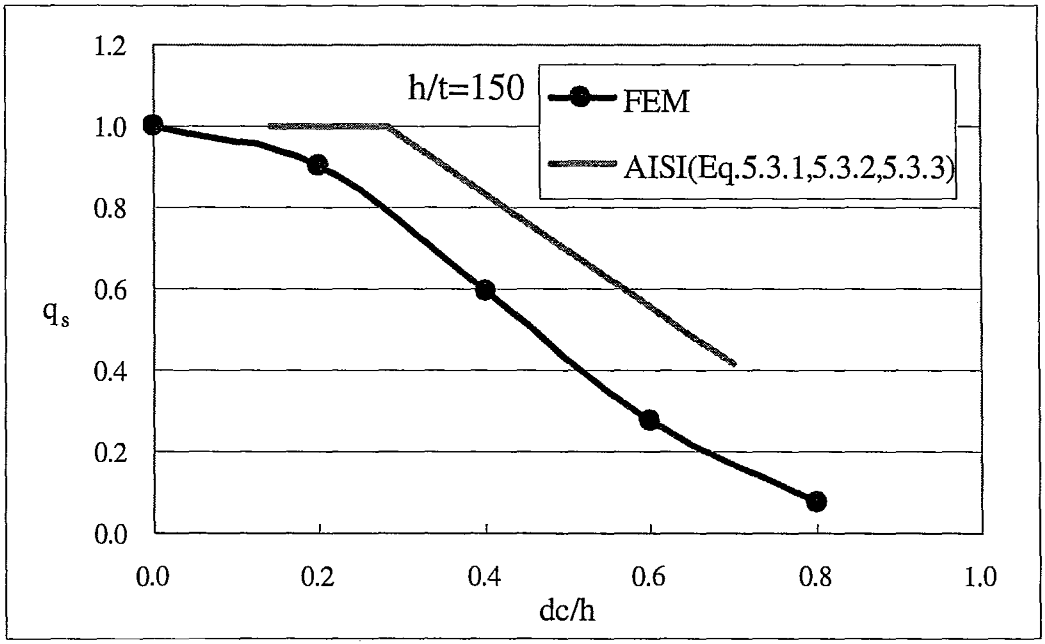

Figure 5.18 Ultimate Shear Strength of Plates with Openings/Ultimate Shear Strength of Solid Plate Versus d_c/h for Plates with a/h=3 and h/t=150

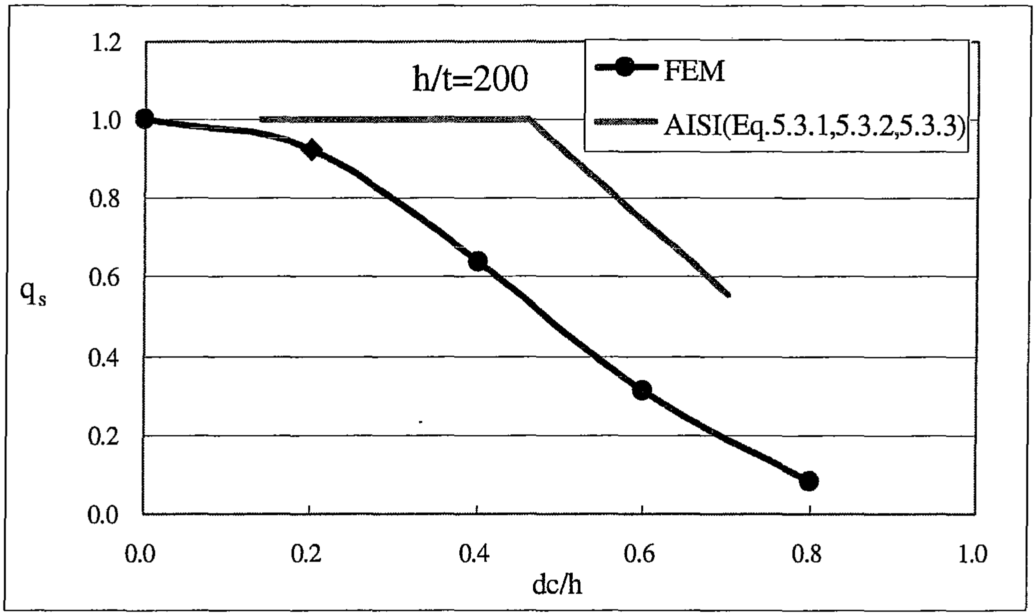

Figure 5.19 Ultimate Shear Strength of Plates with Openings/Ultimate Shear Strength of Solid Plate Versus d_c / h for Plates with a/h=3 and h/t=200

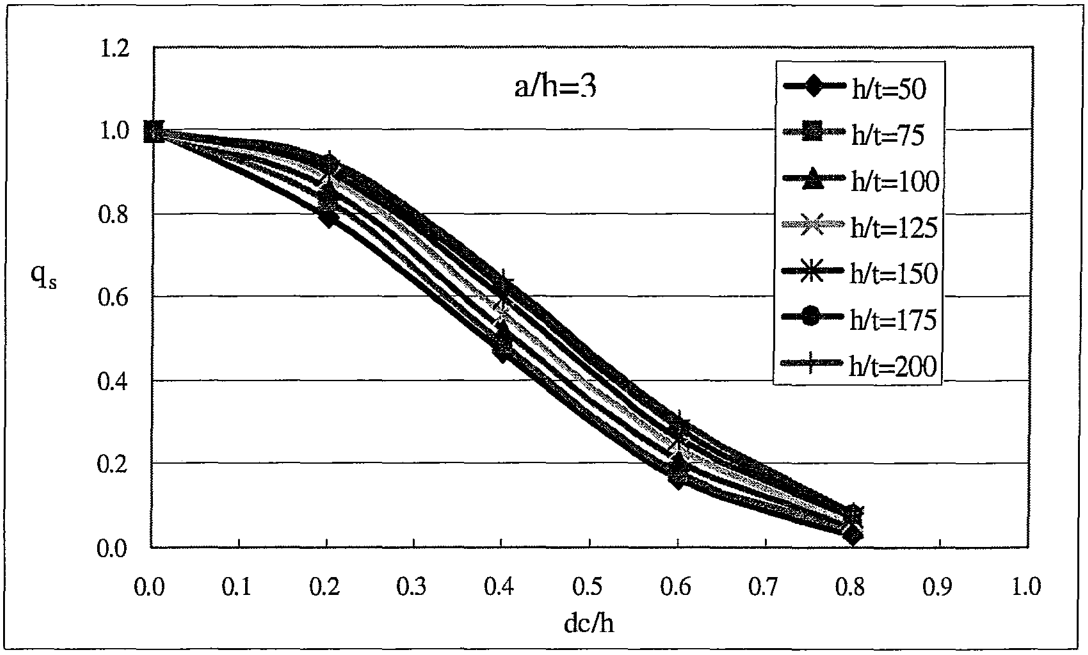

Figure 5.20 Ultimate Shear Strength of Plates with Openings/Ultimate Shear Strength of Solid Plate Versus d_c / h for Plates with Various h/t Values (a/h=3)

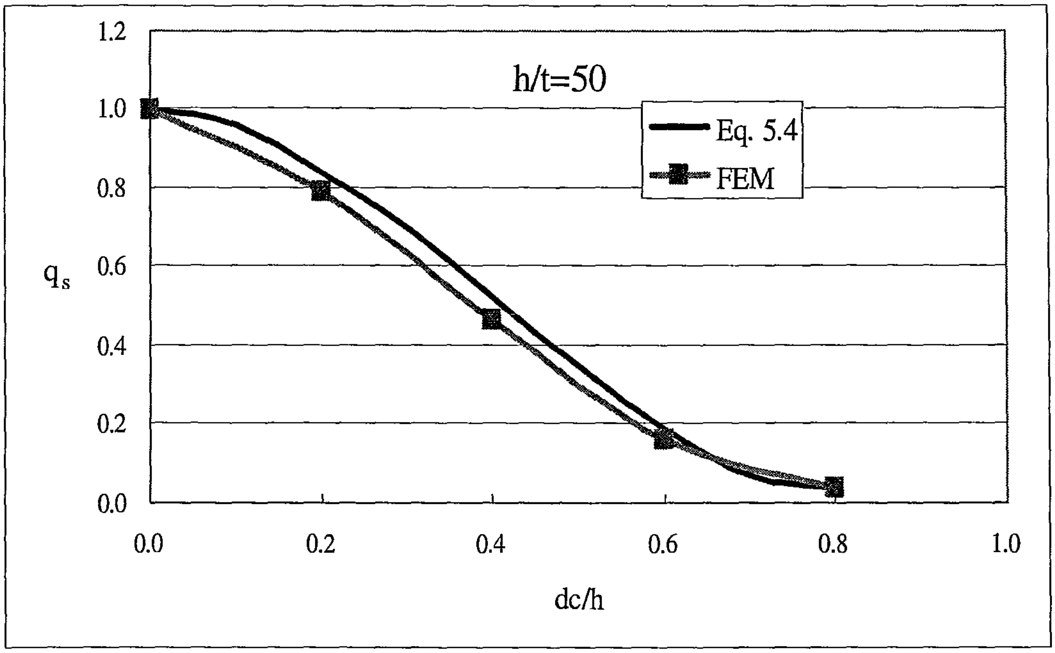

Figure 5.21 Ultimate Shear Strength of Plates with Openings/Ultimate Shear Strength of Solid Plate Versus d_c/h for Plates with a/h=3 and h/t=50

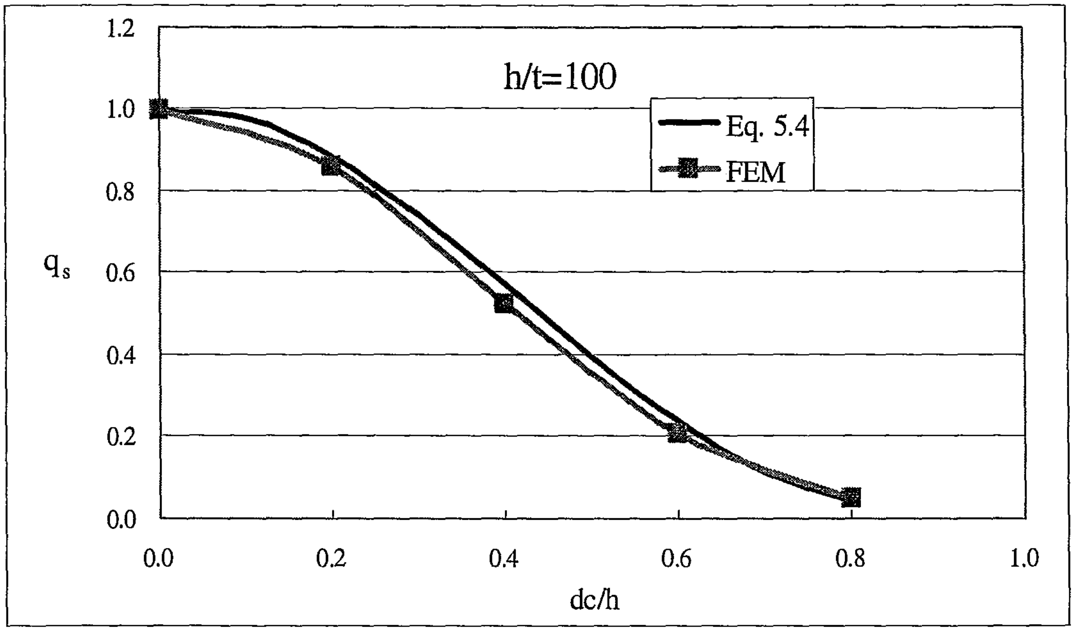

Figure 5.22 Ultimate Shear Strength of Plates with Openings/Ultimate Shear Strength of Solid Plate Versus d_c/h for Plates with a/h=3 and h/t=100

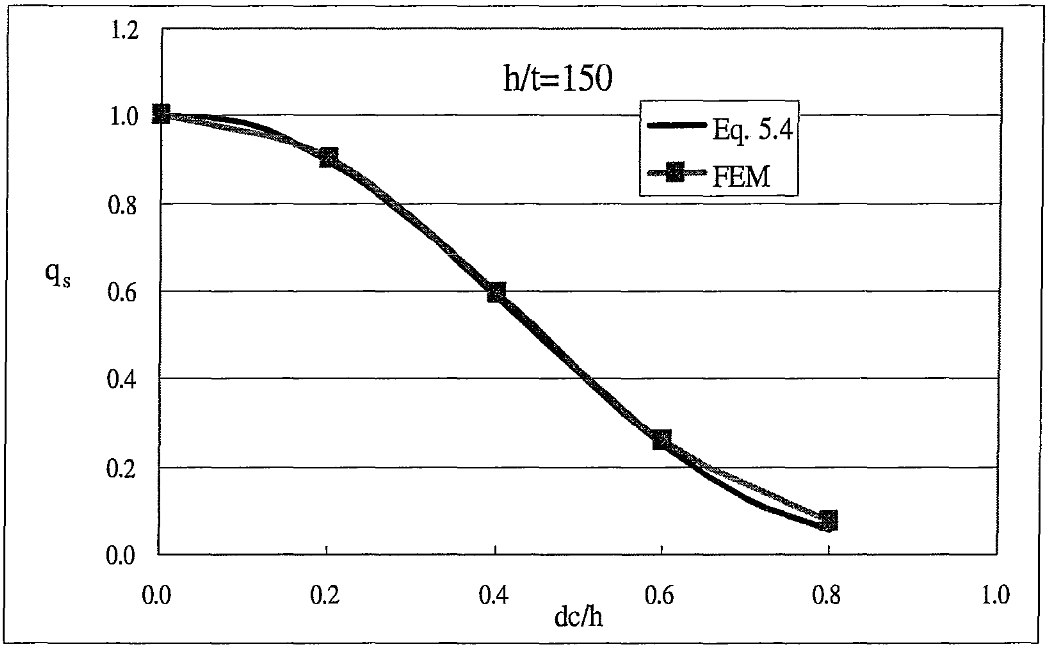

Figure 5.23 Ultimate Shear Strength of Plates with Openings/Ultimate Shear Strength of Solid Plate Versus d_c / h for Plates with a/h=3 and h/t=150

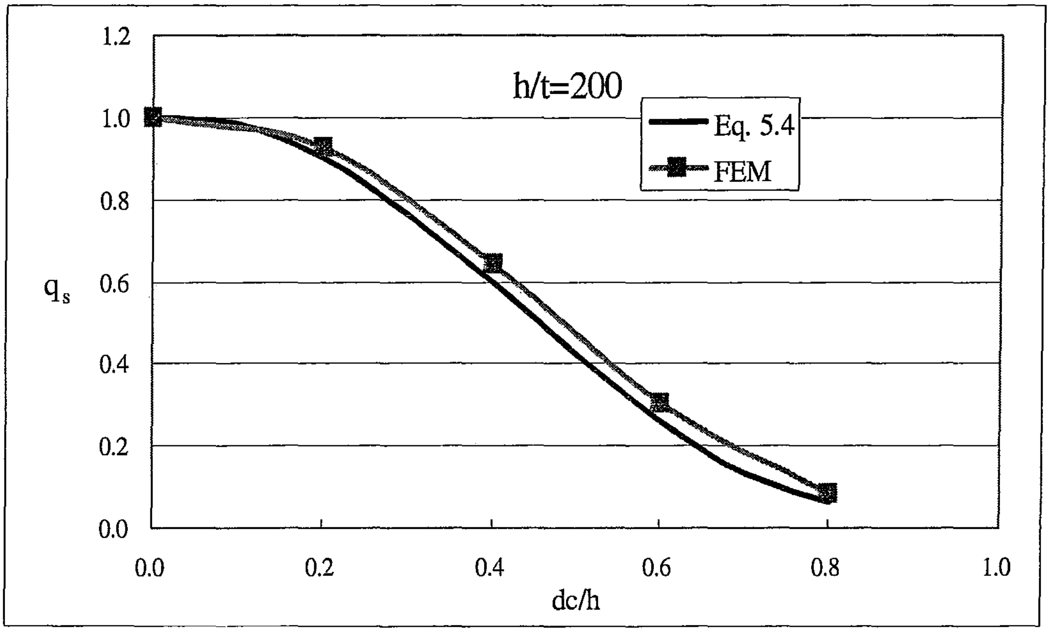

Figure 5.24 Ultimate Shear Strength of Plates with Openings/Ultimate Shear Strength of Solid Plate Versus d_c / h for Plates with a/h=3 and h/t=200

Chapter 6

SHEAR BEHAVIOR OF PLATES WITH REINFORCED OPENINGS

6.1 Introduction

Studies in Chapter 5 have shown that the presence of a square opening with the sides of the opening larger than 20% of the web height in a simply supported plate can significantly reduce the shear strength of that plate. Obviously the reduction is more severe when the opening becomes larger. For example, when the side length of the square opening is 80% of the height of the plate, the shear strength of the plate can be reduced up to 96% of its original shear capacity as a solid plate. To compensate the reduction in the shear strength of steel plates due to the presence of large openings, reinforcements may be considered. Studies in chapter 5 have shown that the failures of plates with large square openings are initiated around the openings. Thus, in this chapter, the impact of reinforcements positioned near the openings on the shear strength is considered. These results are compared to the shear strength of solid plates in order to establish the efficiency of such reinforcements. With appropriate reinforcements, a plate with an opening may recover or even exhibit increased shear capacity as compared to the shear strength of the corresponding solid plate. In order to better understand the shear behavior of plates with reinforced openings, thus to find a more efficient way to reinforce the opening, this chapter will perform finite element method based studies on the shear strength of plates with reinforced square openings.

In this chapter, a simply supported steel plate with an aspect ratio of 3 (a/h=3) and having a 60% reinforced square opening (d_c / h =0.6) under pure shear loads will be analyzed using the finite element analysis package ADINA 8.5. Three different reinforcement schemes, namely [a] flat-reinforcement, [b] lip-reinforcement and [c] angle-reinforcement will be considered in this study. The three reinforcement schemes under consideration are as shown in Figure 6.1. In this figure, ' h_r ' is the total width of the reinforcing plate which is kept constant for all three reinforcement schemes. However, the investigation considered increasing thicknesses for the reinforcements. The ultimate shear strengths of plates with each reinforcement scheme will be established through the use of finite element models, and will be compared to corresponding plates with no openings. The purpose of this chapter is to evaluate the efficiency of the three reinforcement schemes in restoring the shear capacity of plates with square openings.

The first part of this chapter presents some background information about plates with reinforced openings. In the second part, a general finite element model suitable of modeling a simply supported rectangular plate with a reinforced square opening subjected to shear loads is introduced. In the third part, results from a series of finite element analysis performed on steel plates with aforementioned three different reinforcement schemes are presented. For each reinforcement scheme, the ultimate shear strengths of plates with different reinforcement sizes

(t_r/t) will be investigated. Here, 't_r' is thickness of the reinforcement and 't' is the thickness of the base plate. The efficiency of each reinforcement scheme is established at the end of the investigation.

6.2 Background Information of Plates with Reinforced Openings Subjected to Shear Loads

Reinforcements on hot-rolled steel members have been studied in detail for a reasonably long time. Segner (1964) conducted experimental studies on hot-rolled plate girders with reinforced rectangular openings subjected to varying combinations of bending and shearing loads. The reinforcement schemes used in Segner's (1964) experiments included horizontal bars placed above and below the openings, combination of the horizontal bars and the vertical bars placed around the openings, combination of the horizontal bars and the inclined bars placed around the openings, etc. Segnar (1964) found that in high bending moment zones, horizontal bars attached to above and below the openings are the most efficient reinforcement scheme; however, in high shear zones, combination of the horizontal bars and the inclined bars are more efficient.

Redwood and Shrivastava (1980) proposed design recommendations for hot-rolled W-shaped sections with unreinforced and reinforced openings. Based on experiments, Narayanan and Der-Avanessian (1984) proposed an equilibrium solution to predict the strength of webs containing reinforced rectangular openings.

The reinforcements considered by Narayanan and Der-Avanessian (1984) were welded flat reinforcements placed symmetrically above and below the openings. In 1985, Narayanan and Der-Avanessian (1985) further proposed the design steps on using the welded flat reinforcements to restore the shear buckling strength of hot-rolled plates with openings to the buckling strength of such plates without openings.

In terms of shear reinforcements on cold-formed steel webs, very limited research can be found. Pennock (2001) carried out experimental studies on cold-formed steel joists with reinforced and unreinforced web openings subjected to bending and the combined effect of bending and shear. Both circular and square openings were considered in the study. The reinforcement scheme used in Pennock's (2001) experiments was a joist with a web opening having the same size and shape as the opening on the main joist. Pennock (2001) found that such reinforcement was inefficient for openings located both in high bending and shearing zones.

Acharya (2009) performed both the experimental study and the finite element analysis on reinforcement schemes for cold-formed steel joists having large web openings. He carried out experimental studies on reinforcement schemes for cold-formed steel joists with openings in both flexural and shear zones, but only considered the flexural reinforcement schemes in the finite element analysis.

Three reinforcement schemes were considered in Acharya's (2009) study for the shear reinforcement. Two of them are the reinforcement schemes recommended by the AISI (2001), which are a steel plate having the same size and shape of the opening as the main joist and a cold-formed steel stud section having the same size and shape of the opening as the main joist, respectively. The third reinforcement scheme considered by Acharya (2009) was to have four channel sections placed around the opening. Acharya's (2009) study concluded that only the reinforcement scheme using the channel sections was adequate to restore the shear strength of cold-formed steel joists having web openings.

The AISI (2001) has suggested that if web holes violating the requirements provided in the AISI (2001)-A4.4, then the web holes should be reinforced according to the AISI (2001)-A4.5.

AISI (2001)-A4.4 Web Holes

Holes in webs (also referred to as punchouts or perforations) of structural members shall comply with the limitations of Figure A4-1 (for floor and ceiling joists) and A4-2 (for studs and other structural members) and all of the following requirements:

Web holes shall have center-to-center spacing of not less than 610 mm (24 inches).

Web hole width for floor and ceiling joists shall not be greater than 0.5 times the member depth, d, or 64.5mm (2-1/2 inches).

Web hole width for studs and other structural members shall not be greater than 0.5 times the member depth, d, or 38.1mm (1-1/2 inches).

Web hole length shall not exceed 114mm (4-1/2 inches).

Minimum distance between the end of the member or edge of bearing and the near edge of the web hole shall be 240mm (10 inches).

Members with holes violating the above requirements shall be patched in according with Section A4.5 or designed in accordance with accepted engineering practices.

AISI (2001)-A4.5 Hole Patching

Web holes violating the requirements of Section A4.4 shall be patched if the depth of the hole does not exceed 70% of the flat width of the web and the length of the hole measured along the web does not exceed 254 mm (10 inches) or the depth of the web, which ever is greater. The patch shall be a solid steel plate stud section, or track section in accordance with Figures A4-3 or A4-4. The steel patch shall be of a minimum thickness as the receiving member and shall extend at least 25.4 mm (1 inch) beyond all edges of the hole. The steel patch shall be fastened to the web of the receiving member with NO.8 screws spaced no greater than 25.4 mm (1 inch) center-to-center along the edges of the patch with minimum edge distance of 12.7 mm (1/2 inch).

Figure 6.2 shows the reinforcement configurations recommended by the AISI (2001).

6.3 Finite Element Model for Plates with Reinforced Square Openings Subjected to Shear Loads

In this section, a general finite element analysis model is proposed to investigate the behavior of plates with reinforced square openings subjected to pure shear loads. The analysis can capture the pre-buckling, post-buckling and the ultimate load level behavior of such plates. The automatic-time-step (ATS) is used as the analysis method. This analysis method was presented in previous chapters. The model consists of two components, the main plate and the reinforcements. As explained in Section 3.3, the quadrilateral four-node shell element is used for both the main plate and the reinforcements, since both of them are plated elements. The details about the shell elements and the ATS were presented in chapter 2. Moreover, the main plate and the reinforcement plate are assumed to have the same material properties. Thus, the idealized multi-linear stress-strain relationship for cold-formed steel proposed by Abdel-Rahman and Sivakumaran (1997) is used for both the main plate and the reinforcement plate. See Section 4.3.2 for the details about the material model.

6.3.1 The Finite Element Models for the Reinforcements

The reinforcements are assumed to be fully attached to the main plate with no additional constraints. Thus, though screws are widely used in construction practice, here, no screw will be modeled. Figure 6.3 shows the surfaces formed in a general finite element model applicable to all three reinforcement configurations. Only selected surfaces will be meshed in order to model each specific reinforcement configuration. For example, for plates with flat-reinforcements, surfaces S1 to S10 (see Figure 6.3) will be meshed. In order to incorporate the flat-reinforcement, the thickness of surfaces S3 to S10 was assigned the sum of the thickness of the main plate and the thickness of the reinforcement plate. For example, if the reinforcement thickness t_r = 2*t, then, thickness of surfaces S3 to S10 was assigned as 3*t, where, t is the thickness of the main plate.

Similarly, for plates with lip-reinforcements, surfaces S11 to S14 will be meshed. Note that surfaces S1 to S10 form the main plate, which has the original mesh with thickness t, and surfaces S11 to S14 form the lip-reinforcement, thus the thickness of surfaces S11 to S14 equals to thickness of the reinforcement t_r.

For plates with angle-reinforcements, surfaces S7 to S14 will be meshed. In order to incorporate the effect from the angle-reinforcement, the thickness of surfaces S1 to S6 equals to the thickness of the main plate; the thickness of surfaces S11 to S14 equals to the thickness of the reinforcement only; however, the thickness of surfaces S7 to S10 equals to the sum of the thickness of the main plate and the thicknesses of the reinforcement plates.

6.3.2 Loading and the Boundary Conditions

The loading conditions and the boundary conditions for the main plate is the same as those described in Section 5.3.1. The main plate is assumed to be simply supported along the four edges and is subjected to uniform distributed shear loads applied along all four edges. The edges of the opening are left to move freely. Figure 5.1 shows the dimensions and the loading conditions of the main plate, where 'a' is the length of the main plate, 'h' is the width of the main plate, 't' is the thickness of the main plate and 'd_c' is the length of the square opening. Again, the reinforcements are assumed to be fully attached to the main plate with no other additional constraints.

6.3.3 Initial Geometric Imperfections and the Residual Stresses

The model has included the effects of the geometrical initial imperfection, and has ignored the effects of residual stresses. The reason for neglecting the residual stress was stated in Section 4.3.4 in detail. Similar with Chapter 5, the initial imperfection was introduced to a solid plate before openings and reinforcements were presented. The shape of the initial imperfection is described by a double sine function and the magnitude of the imperfection is calculated as 1/2•Equation 4.8. The details about the initial imperfection were described in

Section 4.3.3.

6.3.4 Mesh Quality

The mesh configuration for surfaces S1 to S10 in Figure 6.3 is based on the convergence study performed in Section 5.4. Since this chapter considers plates with an aspect ratio of 3 (a/b=3) only, the 24-division mesh configuration with 3456 elements described in Section 5.4 will be used as the mesh configuration for surfaces S1 to S10. Figure 6.4 shows the geometric lines needed to be divided in order to discretize surfaces S11 to S14 in Figure 6.3. For lines L1 to L8, 24 divisions were made on each line; for lines L9 to L12, the mesh density was controlled so that the ratio of the longest element edge to the shortest element edge maintains inclusively less than 5. Thus, for lip-reinforcement, when the lengths of lines L9 to L12 equal to h_r=20mm, 24 divisions were made on lines L9 to L12, this gives a value of 3 for the ratio of the longest element edge to the shortest element edge for elements within surfaces S11 to S14. For angle-reinforcement, when the length of lines L9 to L12 equal to (1/2)h_r=10mm, 20 divisions were made on lines L9 to L12. This resulted in a value of 5 for the ratio of the longest element edge to the shortest element edge for elements within surfaces S11 to S14. Figure 6.5(a), (b) and (c) show typical mesh configurations for plates with flat-reinforcement, lip-reinforcement and angle-reinforcement, respectively.

6.4 Shear Behavior of Plates with Reinforced Openings

In this section, the behavior of simply supported plates with a square opening reinforced with three different reinforcement configurations is considered. The finite element model described in Section 6.3 was used to model such a plate. The multi-linear material model with F_y=350MPa and v=0.3 was used as the model material property of the plate. Same material properties were used for the reinforcements as well.

Each reinforcement configuration was applied on plates having a fixed aspect ratio (a/h=3) but varying slenderness ratios (h/t). The plate under consideration has a length of 300mm (a=300mm) and a width of 100mm (h=100mm), which gives an aspect ratio of 3 (a/h=3). Since the AISI (2007) has limited the size of the opening (d_c) to be less than 64mm and also sufficient remaining width are needed in order for the main plate to restore the strength, a 60% opening with d_c=60mm was considered in this study. Reinforcement plates with a total width of 'h_r' and a thickness of 't_r' will be used to reinforce the opening area of the plate in three different configurations discussed earlier. The three reinforcement configurations are as shown in Figure 6.1(a), (b) and (c), which are the flat-reinforcement, the lip-reinforcement and the angle-reinforcement, respectively. The total width of the reinforcement plate (h_r) was assumed to be constant as 20mm, which is the length of the remaining width of the plate above and below the opening. For the angle-reinforcement configuration, the reinforcement plates are assumed to be bent into angles with the width of each leg of the angle equals to $(1/2) \bullet h_r$=10mm.

Plates with selected slenderness ratios (h/t) were studied for each reinforcement scheme. The slenderness ratios considered in this investigation are h/t=50, 100, 150 and 200, which covers from thick plates to the thinnest plates allowed in the AISI (2007) code. In this study, considering the plate with different h/t one by one, reinforcements with increasing thickness will be applied on plates to investigate the influence of the thickness of the reinforcements on the behavior and the ultimate shear capacity of such plates. Thus, for plates with each 'h/t' value, the reinforcement thickness to the main plate thickness ratio (t_r /t) increases from zero until the increase in the ultimate shear strength of plates is less than 1.0%. Generally, ' t_r/t' was increased at an incremental step of one for each 'h/t' value. However, intermediate steps may also be applied when needed.

6.4.1 Results and Discussion

The behavior of the plates considered in this section are again illustrated through the shear stress versus the average shear strain diagrams. The average shear strain in the horizontal axis is obtained as described Figure 5.6. See Section 5.5.1 for details about the calculation of the average shear strain for plates in this study. Figures 6.6 to 6.11 show the applied shear stress versus the average shear strain diagrams for both solid plates and plates with reinforced openings. The behavior of the solid plate is also shown in these diagrams, in order to compare the behavior of the reinforced plates with that of solid plates. These figures also include the behavior of plates with unreinforced openings, which corresponds to the case of $t_r/t = 0$. Essentially, thickness of the reinforcement $t_r = 0$ mm indicates no reinforcements. Figures 6.6 and 6.7 show the shear stress-strain diagrams for plates with flat-reinforcements. Figures 6.8 and 6.9 show the shear stress-strain diagrams for plates with lip-reinforcements. Figures 6.10 and 6.11 show the shear stress-strain diagrams for plates with angle-reinforcements. For each reinforcement configuration, only plates with two extreme slenderness analyzed (i.e. h/t=50 and h/t=200) are shown in these figures for the purpose of illustration. Each figure shows the shear stress-strain relationships as the size of the reinforcement (t_r/t) increases. One should note that only selected 't_r/t' values are plotted in Figures 6.6 to 6.11 for the purpose of illustration. It can be observed from Figures 6.6 to 6.11 that solid plates are generally stiffer than plates with both unreinforced and reinforced openings. In another word, openings in plates tend to decrease the stiffness of plates even though the openings were properly reinforced to recover to the ultimate shear strength of solid plates. Also in general, increasing reinforcement thickness t_r increases the stiffness as well as the strength.

Figures 6.12 and 6.13 show the deformed shapes of plates magnified by 10% and the band plots for the effective stress at the top surfaces of plates at the failure load level. Figure 6.12 is for plates with h/t=50 (thick plate) and Figure 6.13 is for plates with h/t=200 (thin plate), respectively. The plates shown in these two figures include both plates without reinforcement and plates with adequate reinforcements to restore the shear strength reduced by the opening. At this point, adequate reinforcement means a reinforcement scheme that restores the strength of the solid plate; however, later sections quantify the adequacy of reinforcements. It can be seen from Figures 6.12 and 6.13 that, before reinforcements are applied, plates with 60% openings (d_c/h=0.6) fail at the four corners of the openings for both h/t=50 and h/t=200. With adequate reinforcements, plates fail in diagonal shear failure outside of the opening region.

Tables 6.1 to 6.12 record the ultimate shear capacities of plates with reinforced openings obtained from the finite element analysis. Three reinforcement schemes were evaluated. For each reinforcement scheme, four different 'h/t' values of plates, namely h/t=50, 100, 150 and 200, were analyzed. Thus twelve tables were generated. These tables have four columns. The first column indicates the thickness of the reinforcement (t_r/t). As stated before, the 't_r/t' values were generally increased at an incremental step of one. Only for Tables 6.3 and 6.4, additional half steps were made in order to obtain enough data points for the later associated diagrams. The second column records the ultimate shear strength of plates with different amount of reinforced opening. In the third column, the ultimate shear strengths of plates with reinforced openings are normalized by the ultimate shear strength of the corresponding solid plates, in order to show the relative benefit of the reinforcement. The last column calculates the percentage increase in the ultimate shear strength of plates with increasing reinforcement size (t_r /t'). The analyses were carried until the percentage increase in the ultimate shear strength of plates is less than 1.0%, essentially, no further increase in shear strength.

Figures 6.14 to 6.17 show the plots of the ultimate shear strength of plates with reinforced openings normalized by the ultimate shear strength of the corresponding solid plates versus ' t_r /t' for plates with different reinforcement schemes. By observing the normalized shear strengths, it can be seen from these figures that, all three reinforcement schemes are capable of restoring the shear strength of plates reduced from the centrally located square openings. When enough reinforcements are applied, the ultimate shear strength of a plate with a square opening can even increase beyond its original shear strength when the plate is solid. Especially for thin plates, for example, when h/t=200, Figure 6.17 shows that the ultimate shear strength of a plate with flat-reinforcement around the opening can be as high as about 1.5 times the original shear strength of a solid plate. This can be attributed to the fact that the reinforcement actually divided the plate into three panels. Figure 6.18 shows the three parts divided by a flat-reinforcement. Part 1 and part 2 are the regions outside of the opening and part 3 is the region of the reinforced opening. In the case of this study, part 1 and 2 are square panels. When enough reinforcements are provided, the plate fails in the regions outside of the opening, which are part 1 and part 2 in Figure 6.18. The ultimate shear strength of such reinforced plate must be comparable to the ultimate shear strength of part 1 or part2, which are essentially two square panels. In Chapter 5, it was shown that the ultimate shear strength of a plate with a square opening decreases as the aspect ratio (a/h) increases. Thus, with proper opening reinforcement, the effective a/h of the plate actually decreases, causing the ultimate shear strength to increase relative to the original solid plate. For example, from Table 6.4, it can be seen that when h/t=200, with enough reinforcement (t_r/t=3.5), $\tau_{ul(reinf.)}$=84.7MPa. From Table 4.4 in Chapter 4, it can be seen that for plates with h/t=200 and a/h=1, $\tau_{ul(a/h=1)}$=81.50MPa. Thus, when enough reinforcement is applied, the ultimate shear strength of a plate with a/h=3 and reinforced opening is comparable to the ultimate shear strength of a solid plate with a/h=1.

6.4.2 Effects of Reinforcement Thickness

Tables 6.1 to 6.12 show that for all three reinforcement schemes, as the thickness of the reinforcement (t_r/t) increases, the ultimate shear strength of the reinforced plate increases. From Figures 6.14 to 6.17, it can be seen that, the ultimate shear strength of plates with reinforced openings increases approximately linearly as 't_r/t' increases at the initial portion of the diagram, but the increase in the ultimate shear strength eventually fades out as the 't_r/t' values increase further. Moreover, for thin plates, it tends to be easier to restore the shear capacity by all three reinforcement schemes. For example, for a plate with h/t=50 (Table 6.1), a flat-reinforcement with t_r/t=6 is able to restore the shear capacity of a plate with opening to the shear capacity of a solid plate. However, for a plate with h/t=200 (Table 6.4), a flat-reinforcement with t_r/t=1.5 is enough to restore the shear capacity of a plate with opening to the shear capacity of a solid plate. Similar situation happens to the lip-reinforcement and the angle-reinforcement schemes.

6.4.3 Effects of Reinforcement Configuration

Since the total width (h_r) is fixed as 20mm, and since the length of the reinforcement is approximately equal to the perimeter of the opening for all three reinforcement configurations, the reinforcement scheme with the least 't_r/t' value which can restore the shear strength of plates with openings to the shear strength of solid plates may be considered as the most effective reinforcement scheme. Figures 6.14 to 6.17 compare the ultimate shear strength of plates with different reinforcement configurations as the size of the reinforcements (t_r/t) increases. It can be seen that for plates with all 'h/t' values, the flat-reinforcement scheme can restore the ultimate shear strength of a plate with a opening to that of a solid plate

Table 6.1 Ultimate Shear Strength of Plates with Flat-Reinforcement for Different t_r/t Values (h/t=50)

Ultimate Strength of the Corresponding Solid Plate: $\tau_{ul(solid)}$=191.6 MPa			
t_r/t	$\tau_{ul(reinf.)}$ (MPa)	$\tau_{ul(reinf.)}/\tau_{ul(solid)}$	%Increase in $\tau_{ul(reinf.)}$
0.0	31.3	0.16	101.0
1.0	62.9	0.33	49.4
2.0	94.0	0.49	33.5
3.0	125.5	0.65	25.2
4.0	157.1	0.82	18.7
5.0	186.5	0.97	8.7
6.0	202.7	1.06	0.1
7.0	202.8	1.06	

Table 6.2 Ultimate Shear Strength of Plates with Flat-Reinforcement for Different t_r/t Values (h/t=100)

Ultimate Strength of the Corresponding Solid Plate: $\tau_{ul(solid)}$=113.1 MPa			
t_r/t	$\tau_{ul(reinf.)}$ (MPa)	$\tau_{ul(reinf.)}/\tau_{ul(solid)}$	%Increase in $\tau_{ul(reinf.)}$
0.0	23.6	0.21	166.6
1.0	62.9	0.56	59.0
2.0	100.0	0.88	28.8
3.0	128.8	1.14	17.2
4.0	151.0	1.33	0.9
5.0	152.4	1.35	

Table 6.3 Ultimate Shear Strength of Plates with Flat-Reinforcement for Different t_r/t Values (h/t=150)

Ultimate Strength of the Corresponding Solid Plate: $\tau_{ul(solid)}$=74.5 MPa			
t_r/t	$\tau_{ul(reinf.)}$ (MPa)	$\tau_{ul(reinf.)}/\tau_{ul(solid)}$	%Increase in $\tau_{ul(reinf.)}$
0.0	19.3	0.26	203.9
1.0	58.7	0.79	32.7
1.5	77.8	1.05	21.1
2.0	94.3	1.27	13.5
2.5	107.0	1.44	1.1
3.0	108.1	1.45	0.7
3.5	108.9	1.46	

Table 6.4 Ultimate Shear Strength of Plates with Flat-Reinforcement for Different t_r/t Values (h/t=200)

Ultimate Strength of the Corresponding Solid Plate: $\tau_{ul(solid)}$=56.0 MPa			
t_r/t	$\tau_{ul(reinf.)}$ (MPa)	$\tau_{ul(reinf.)}/\tau_{ul(solid)}$	%Increase in $\tau_{ul(reinf.)}$
0.0	17.0	0.30	101.7
0.5	34.2	0.61	46.5
1.0	50.1	0.90	32.8
1.5	66.6	1.19	19.9
2.0	79.8	1.43	4.1
2.5	83.1	1.48	1.3
3.0	84.1	1.50	0.7
3.5	84.7	1.51	

Table 6.5 Ultimate Shear Strength of Plates with Lip-Reinforcement for Different t_r / t Values (h/t=50)

Ultimate Strength of the Corresponding Solid Plate: $\tau_{ul(solid)}$=191.6 MPa			
t_r / t	$\tau_{ul(reinf.)}$ (MPa)	$\tau_{ul(reinf.)} / \tau_{ul(solid)}$	%Increase in $\tau_{ul(reinf.)}$
0.0	31.3	0.16	45.5
1.0	45.5	0.24	48.3
2.0	67.6	0.35	33.7
3.0	90.3	0.47	26.3
4.0	114.1	0.60	24.1
5.0	141.5	0.74	19.0
6.0	168.3	0.88	15.9
7.0	195.1	1.02	3.4
8.0	201.8	1.05	0.2
9.0	202.1	1.06	

Table 6.6 Ultimate Shear Strength of Plates with Lip-Reinforcement for Different t_r / t Values (h/t=100)

Ultimate Strength of the Corresponding Solid Plate: $\tau_{ul(solid)}$=113.1 MPa			
t_r / t	$\tau_{ul(reinf.)}$ (MPa)	$\tau_{ul(reinf.)} / \tau_{ul(solid)}$	%Increase in $\tau_{ul(reinf.)}$
0.0	23.6	0.21	65.9
1.0	39.1	0.35	34.4
2.0	52.6	0.47	30.7
3.0	68.8	0.61	24.3
4.0	85.5	0.76	20.4
5.0	102.9	0.91	17.8
6.0	121.3	1.07	11.4
7.0	135.1	1.19	3.7
8.0	140.1	1.24	0.3
9.0	140.6	1.24	

Table 6.7 Ultimate Shear Strength of Plates with Lip-Reinforcement for Different t_r / t Values (h/t=150)

Ultimate Strength of the Corresponding Solid Plate: $\tau_{ul(solid)}$=74.5 MPa			
t_r / t	$\tau_{ul(reinf.)}$ (MPa)	$\tau_{ul(reinf.)} / \tau_{ul(solid)}$	%Increase in $\tau_{ul(reinf.)}$
0.0	19.3	0.26	65.9
1.0	32.0	0.43	32.6
2.0	42.5	0.57	26.8
3.0	53.9	0.72	23.3
4.0	66.4	0.89	17.6
5.0	78.1	1.05	11.7
6.0	87.3	1.17	4.5
7.0	91.1	1.22	3.4
8.0	94.3	1.27	0.8
9.0	95.0	1.28	

Table 6.8 Ultimate Shear Strength of Plates with Lip-Reinforcement for Different t_r / t Values (h/t=200)

Ultimate Strength of the Corresponding Solid Plate: $\tau_{ul(solid)}$=56.0 MPa			
$t_{reinf.} / t$	$\tau_{ul(reinf.)}$ (MPa)	$\tau_{ul(reinf.)} / \tau_{ul(solid)}$	%Increase in $\tau_{ul(reinf.)}$
0.0	17.0	0.30	51.1
1.0	25.6	0.46	37.6
2.0	35.3	0.63	21.2
3.0	42.8	0.76	15.2
4.0	49.3	0.88	11.3
5.0	54.8	0.98	5.4
6.0	57.8	1.03	5.7
7.0	61.1	1.09	4.8
8.0	64.0	1.14	2.7
9.0	65.7	1.17	0.9
10.0	66.3	1.18	

Table 6.9 Ultimate Shear Strength of Plates with Angle-Reinforcement for Different t_r / t Values (h/t=50)

Ultimate Strength of the Corresponding Solid Plate: $\tau_{ul(solid)}$=191.6 MPa			
t_r / t	$\tau_{ul(reinf.)}$ (MPa)	$\tau_{ul(reinf.)} / \tau_{ul(solid)}$	%Increase in $\tau_{ul(reinf.)}$
0.0	31.3	0.16	81.5
1.0	56.8	0.30	46.3
2.0	83.1	0.43	29.9
3.0	108.0	0.56	20.2
4.0	129.8	0.68	19.6
5.0	155.3	0.81	14.7
6.0	178.1	0.93	12.1
7.0	199.6	1.04	1.1
8.0	201.8	1.05	0.3
9.0	202.4	1.06	

Table 6.10 Ultimate Shear Strength of Plates with Angle-Reinforcement for Different t_r / t Values (h/t=100)

Ultimate Strength of the Corresponding Solid Plate: $\tau_{ul(solid)}$=113.1 MPa			
t_r / t	$\tau_{ul(reinf.)}$ (MPa)	$\tau_{ul(reinf.)} / \tau_{ul(solid)}$	%Increase in $\tau_{ul(reinf.)}$
0.0	23.6	0.21	128.5
1.0	53.9	0.48	40.4
2.0	75.7	0.67	27.2
3.0	96.3	0.85	18.7
4.0	114.3	1.01	14.4
5.0	130.8	1.16	10.3
6.0	144.2	1.27	1.1
7.0	145.8	1.29	0.6
8.0	146.6	1.30	

Table 6.11 Ultimate Shear Strength of Plates with Angle-Reinforcement for Different t_r / t Values (h/t=150)

Ultimate Strength of the Corresponding Solid Plate: $\tau_{ul(solid)}$ =74.5 MPa			
t_r / t	$\tau_{ul(reinf.)}$ (MPa)	$\tau_{ul(reinf.)} / \tau_{ul(solid)}$	%Increase in $\tau_{ul(reinf.)}$
0.0	19.3	0.26	165.0
1.0	51.2	0.69	47.9
2.0	75.7	1.02	27.2
3.0	96.3	1.29	5.1
4.0	101.2	1.36	1.4
5.0	102.6	1.38	0.7
6.0	103.3	1.39	

Table 6.12 Ultimate Shear Strength of Plates with Angle-Reinforcement for Different t_r / t Values (h/t=200)

Ultimate Strength of the Corresponding Solid Plate: $\tau_{ul(solid)}$ =56.0 MPa			
t_r / t	$\tau_{ul(reinf.)}$ (MPa)	$\tau_{ul(reinf.)} / \tau_{ul(solid)}$	%Increase in $\tau_{ul(reinf.)}$
0.0	17.0	0.30	162.6
1.0	44.6	0.80	54.2
2.0	68.7	1.23	14.8
3.0	78.8	1.41	1.2
4.0	79.8	1.43	0.6
5.0	80.3	1.43	

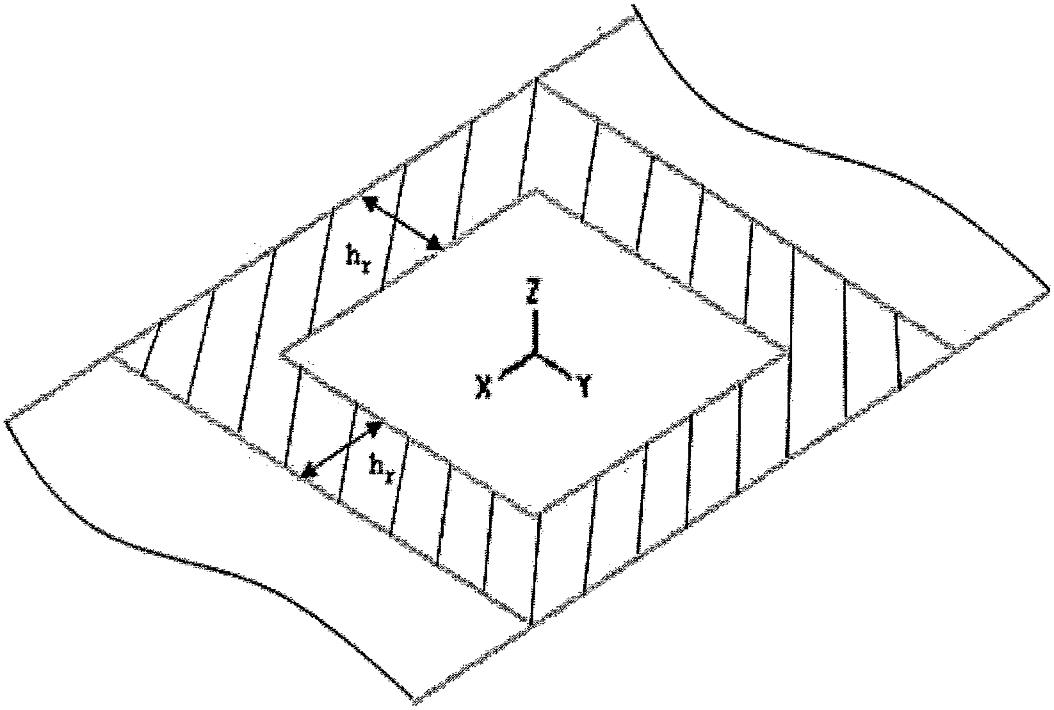

(a) Flat-Reinforcement

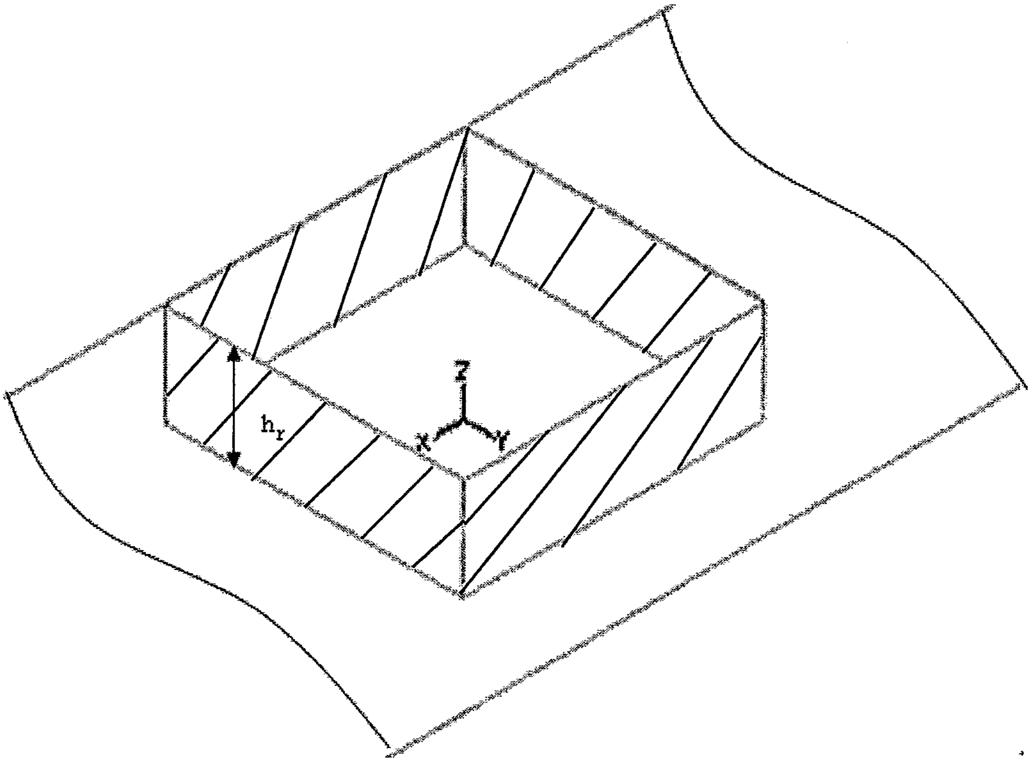

(b) Lip-Reinforcement

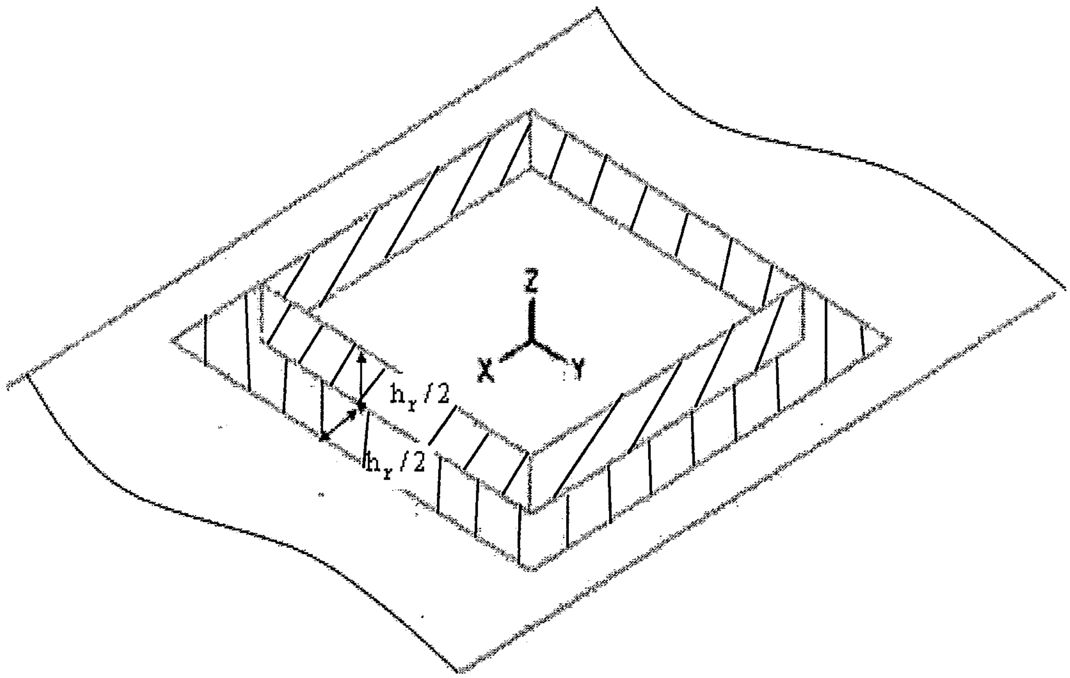

(c) Angle-Reinforcement

Figure 6.1 Shear Reinforcement Schemes (a) Flat-Reinforcement (b) Lip-Reinforcement (c) Angle-Reinforcement

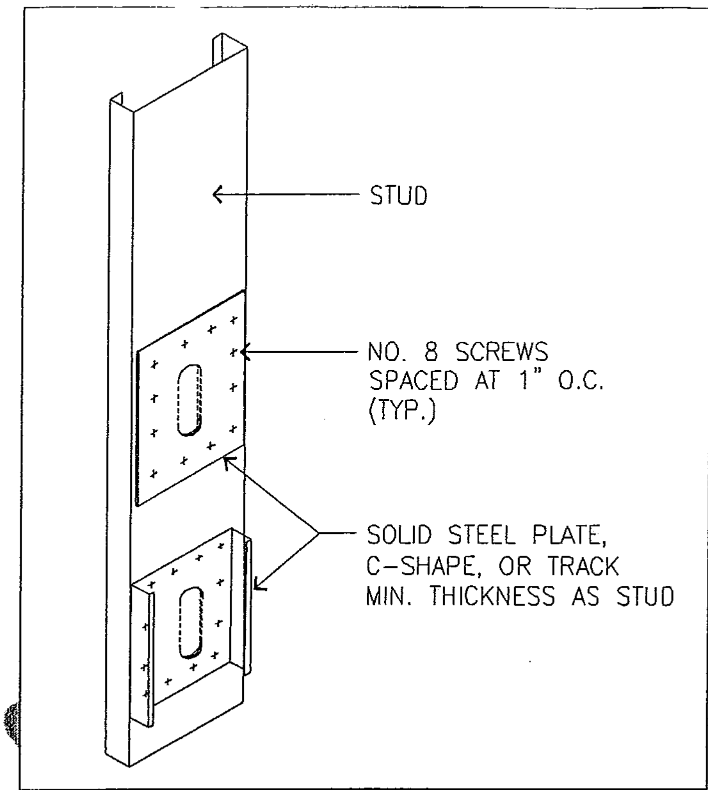

Figure A4-3 Stud Web Hole Patch

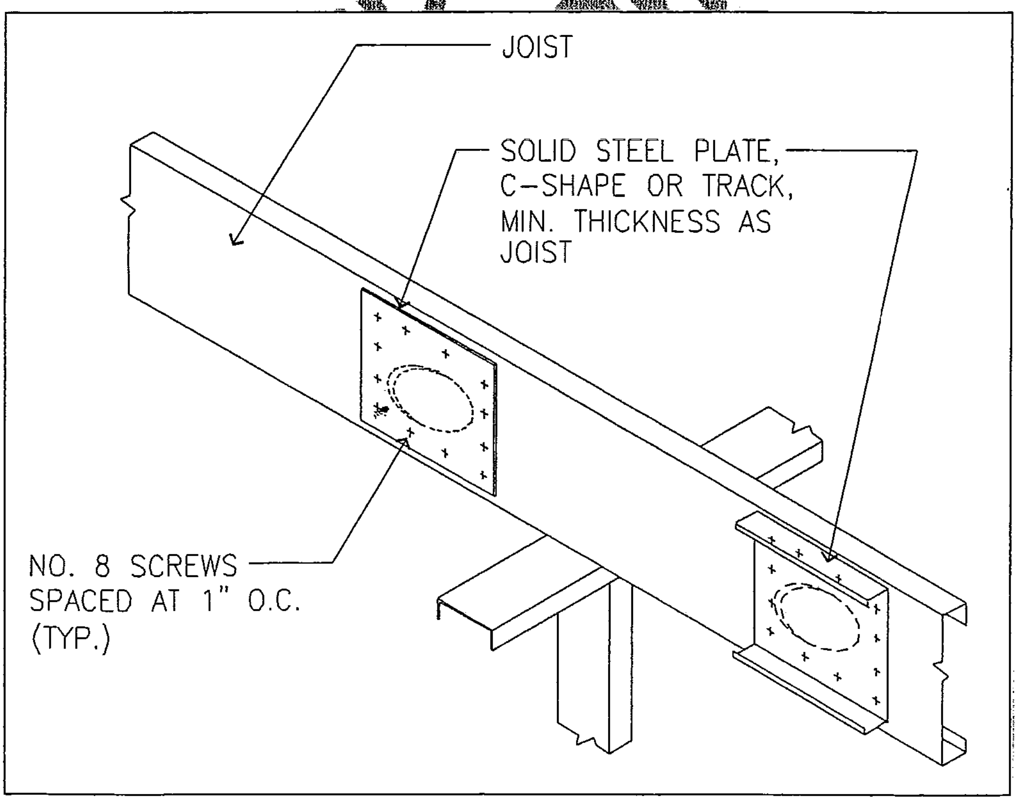

Figure A4-4 Joist Web Hole Patch

Figure 6.2 Joist Web Hole Patch Recommended by The AISI (2001) Standard

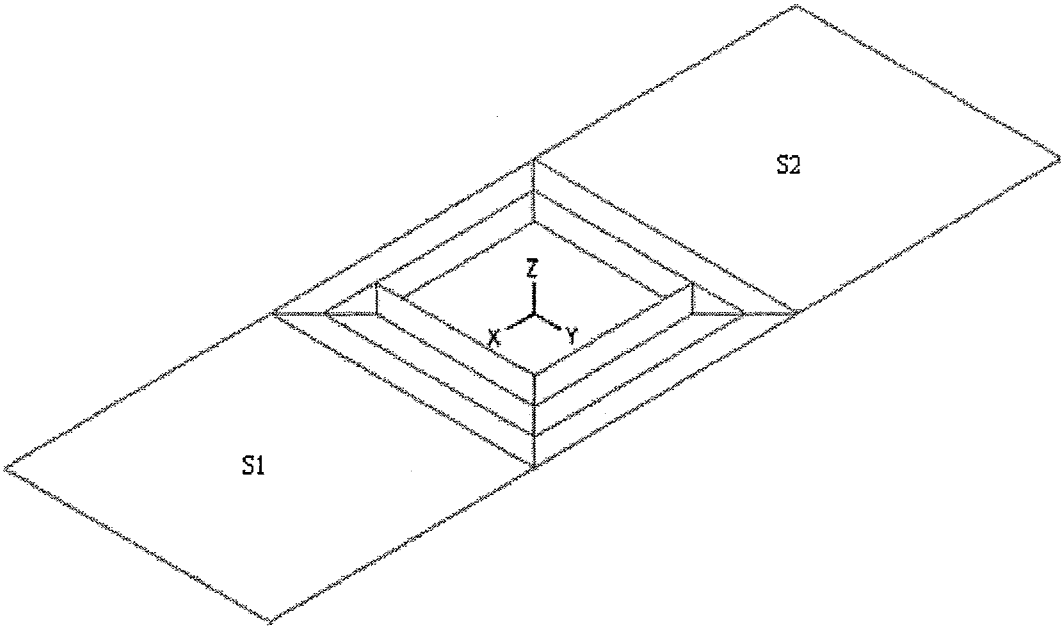

(a)

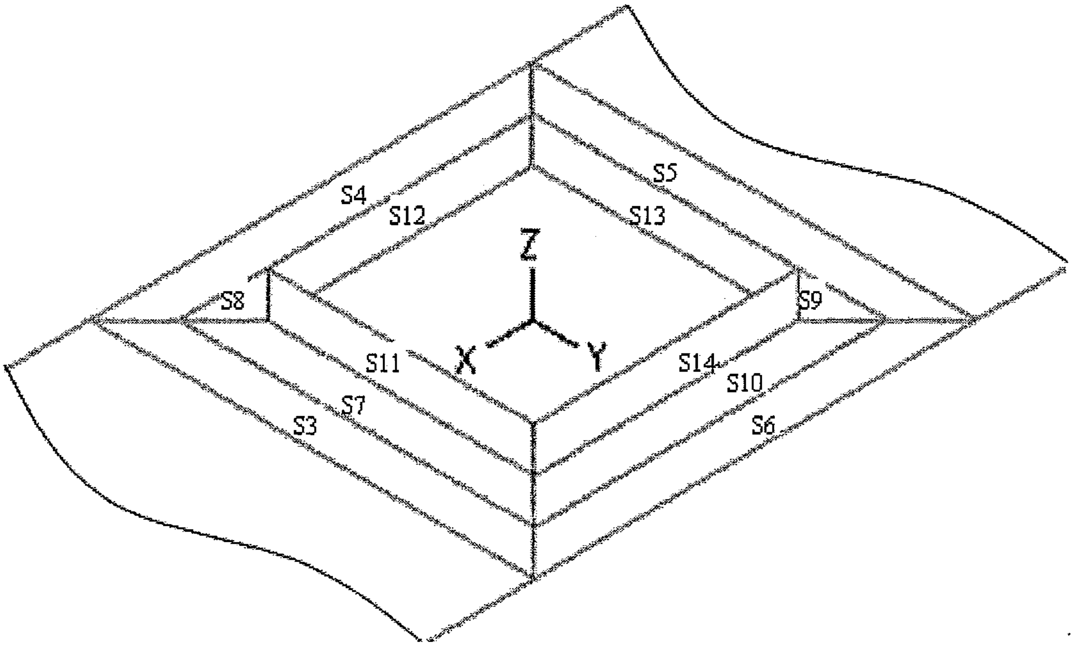

(b)

Figure 6.3 Surfaces Formed in the Finite Element Model (a) overall view (b) close-up view of the reinforced opening.

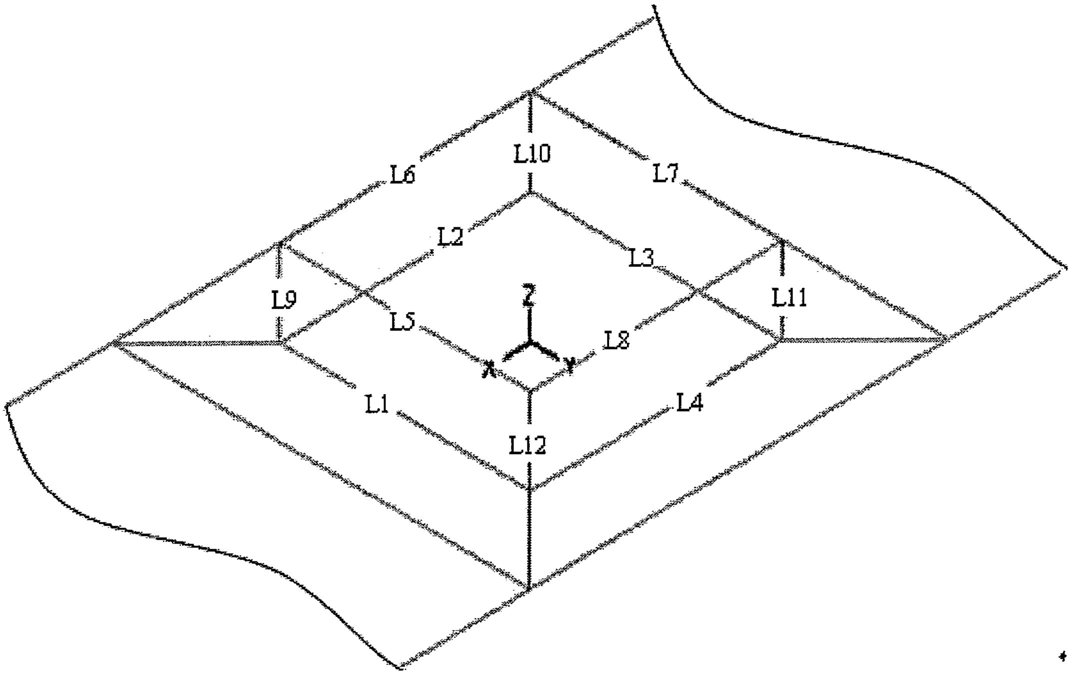

Figure 6.4 Lines Formed for the Reinforcement Lip

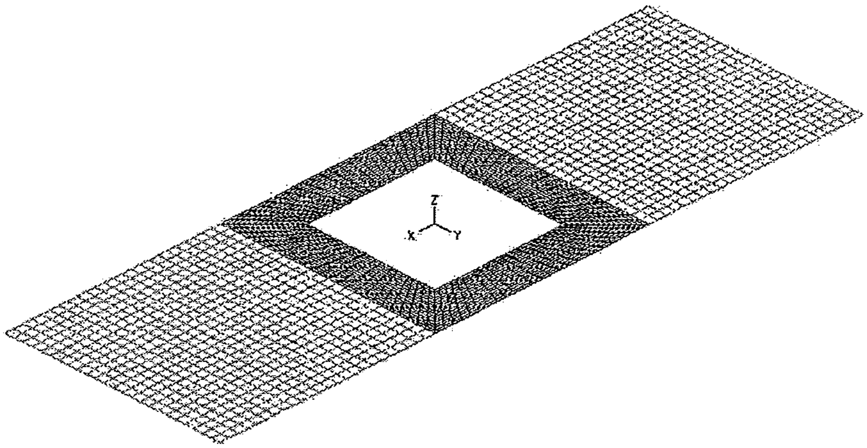

(a) Flat-Reinforcement

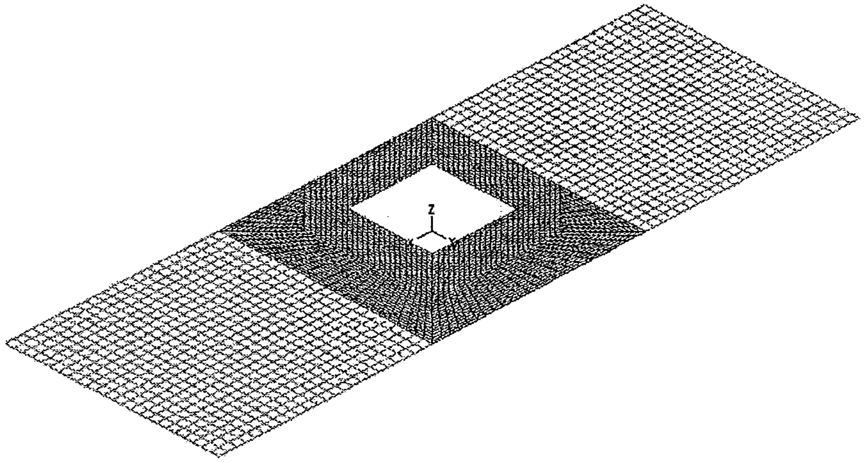

(b) Lip-Reinforcement

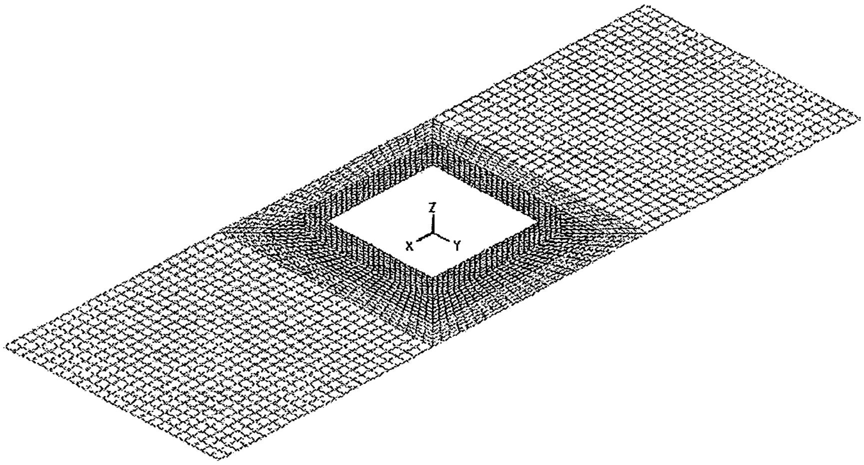

(c) Angle-Reinforcement

Figure 6.5 Mesh Configuration for Different Reinforcement Schemes

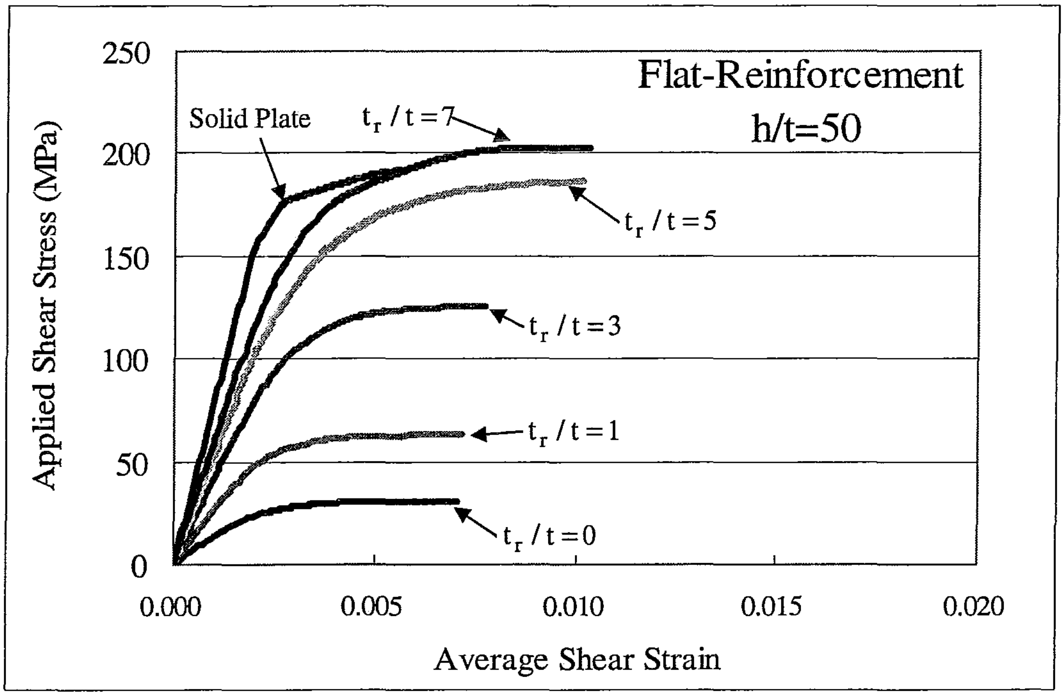

Figure 6.6 Applied Shear Stress Versus Average Shear Strain for Plates with Flat- Reinforcement (h/t=50)

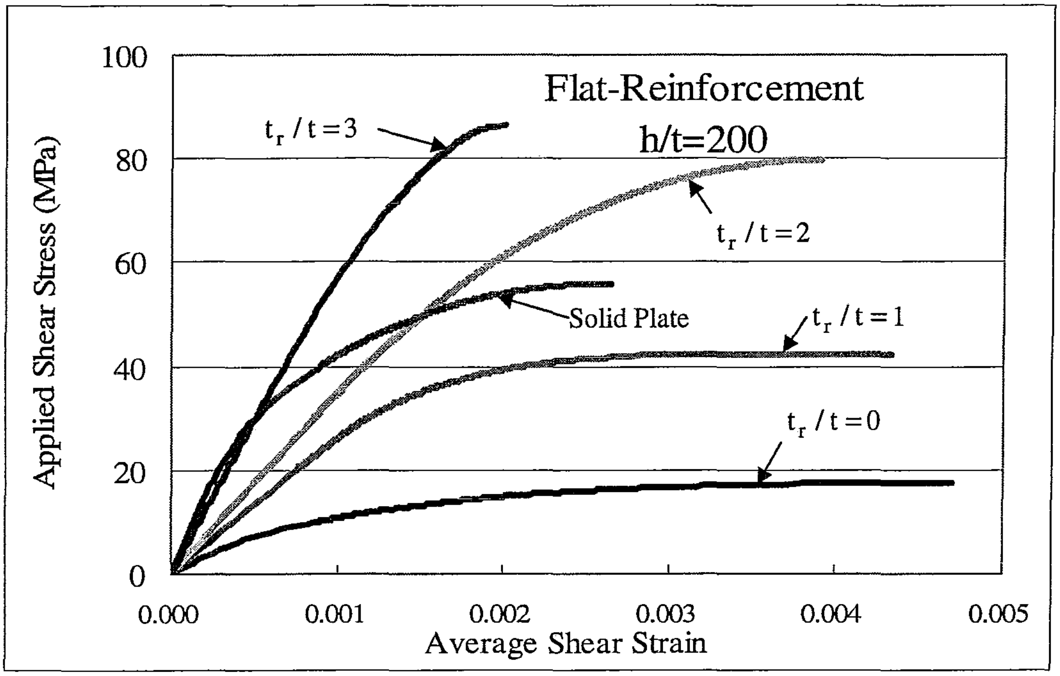

Figure 6.7 Applied Shear Stress Versus Average Shear Strain for Plates with Flat- Reinforcement (h/t=200)

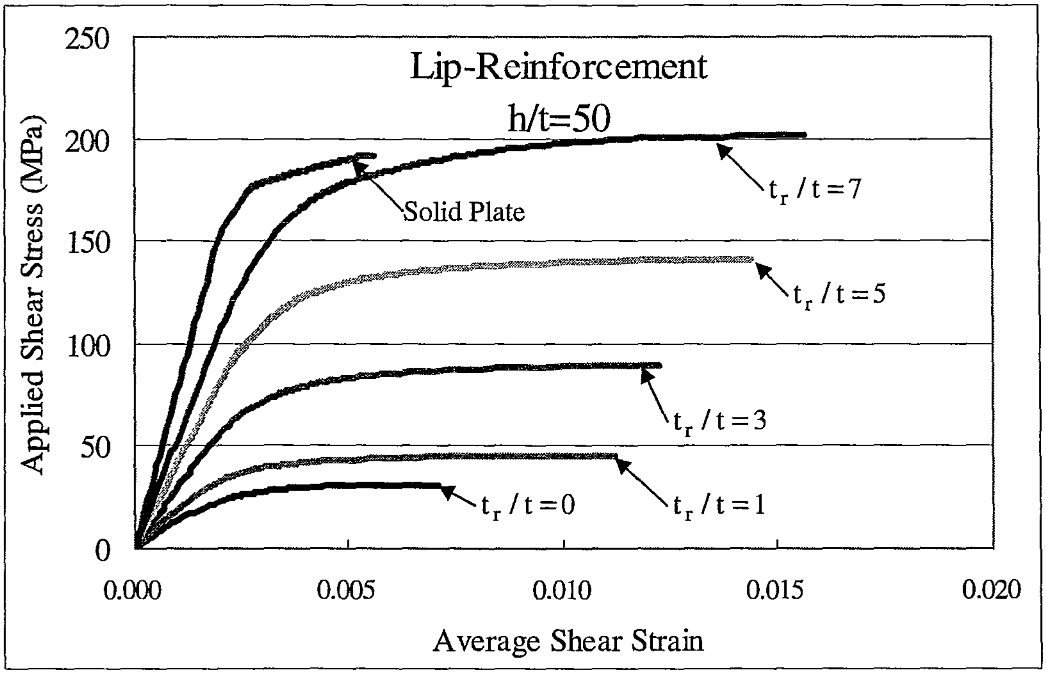

Figure 6.8 Applied Shear Stress Versus Average Shear Strain for Plates with Lip- Reinforcement (h/t=50)

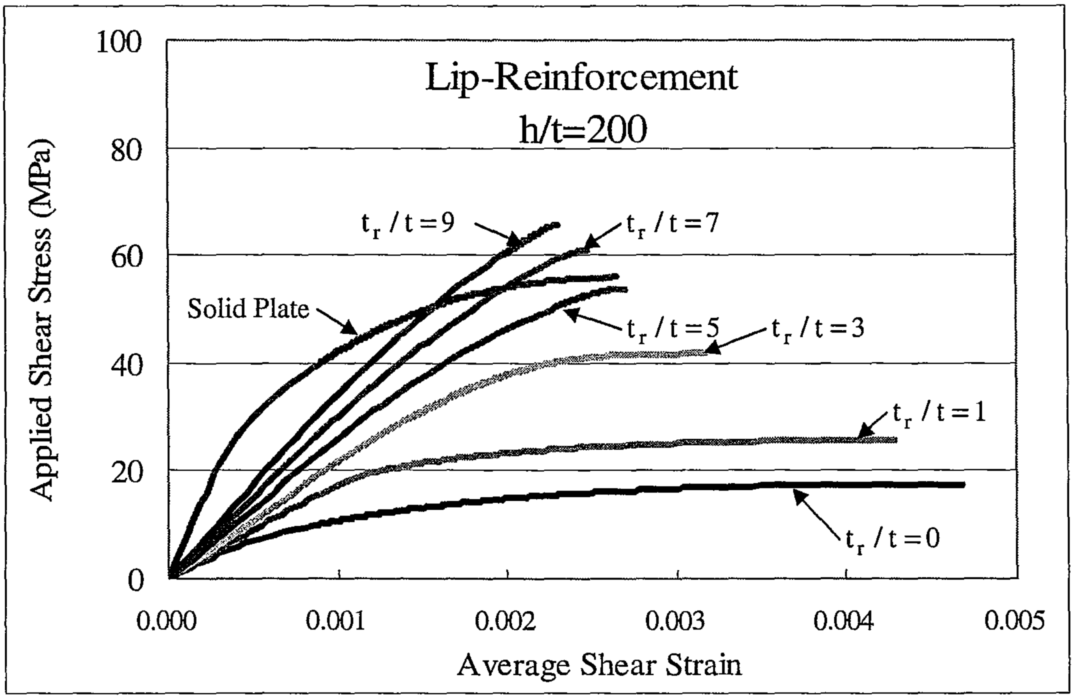

Figure 6.9 Applied Shear Stress Versus Average Shear Strain for Plates with Lip- Reinforcement (h/t=200)

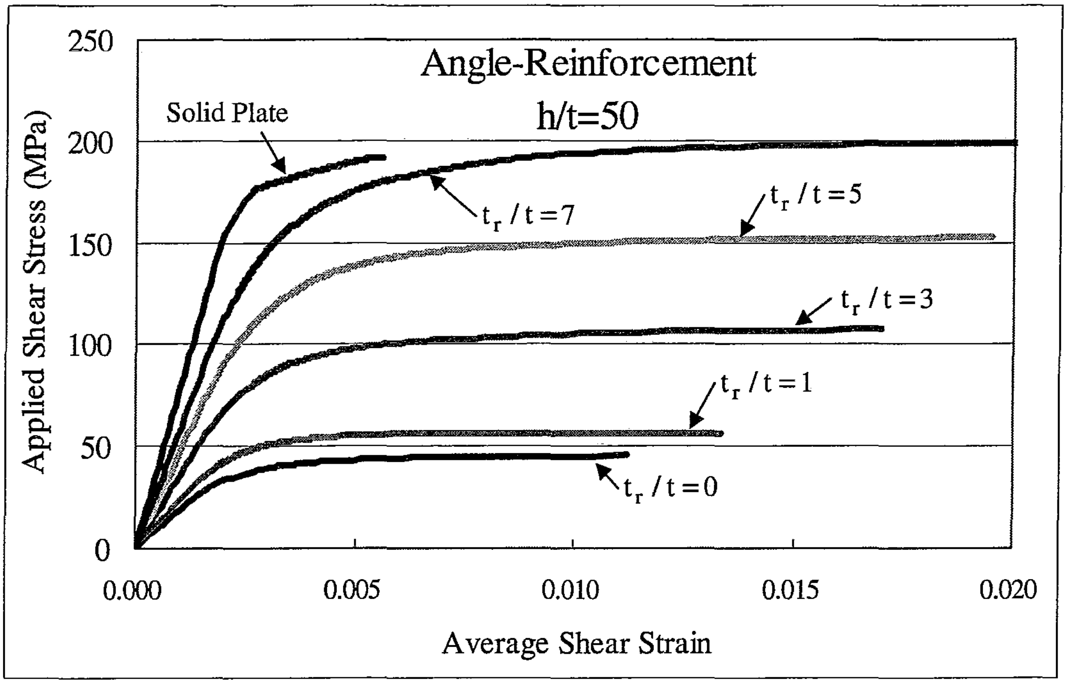

Figure 6.10 Applied Shear Stress Versus Average Shear Strain for Plates with Angle- Reinforcement (h/t=50)

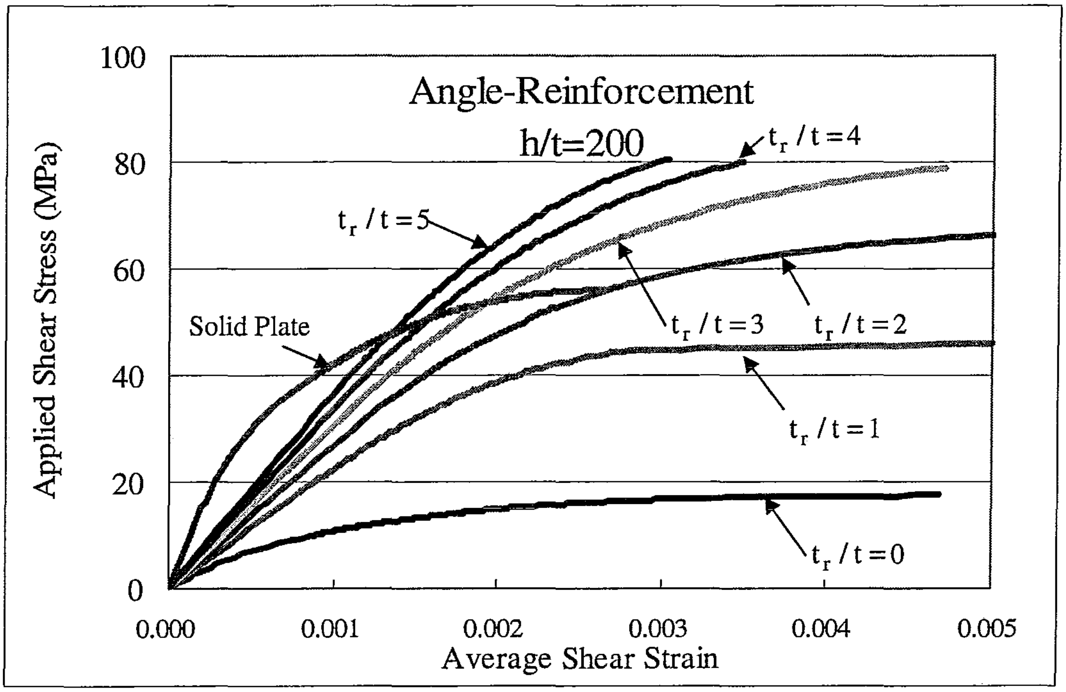

Figure 6.11 Applied Shear Stress Versus Average Shear Strain for Plates with Angle- Reinforcement (h/t=200)

Model Description	Deformed Shape and The Effective Stress at the Failure Load Level for Thick Plates (h/t=50)	Failure Descriptions
No Reinforcement	Deformed Shape Magnified by 10%: 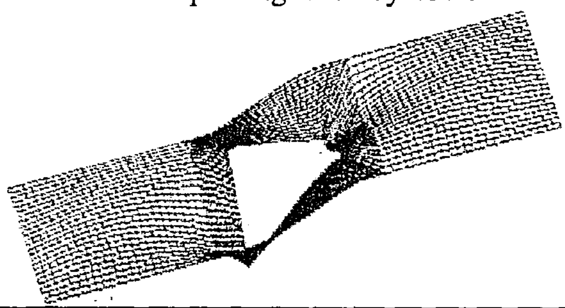	• Diagonal shear failure at the opening region • Plasticity occurs around the four corners of the opening
	Effective Stress: 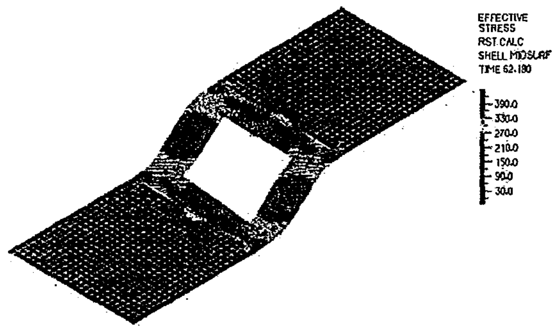	
Flat-Reinforcement $t_r/t=6$, $\frac{\tau_{ul(Reinf.)}}{\tau_{ul(Solid)}} =$ 1.058	Deformed Shape Magnified by 10%: 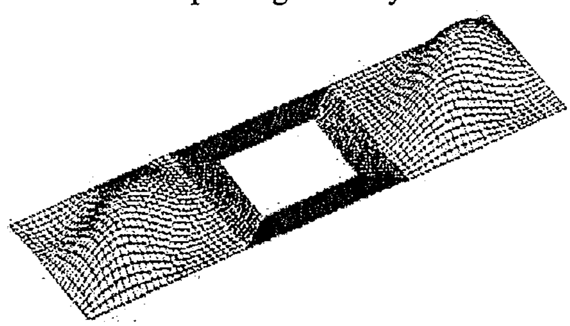	• Diagonal shear failure outside the opening region • Plasticity occurs throughout the plate
	Effective Stress: 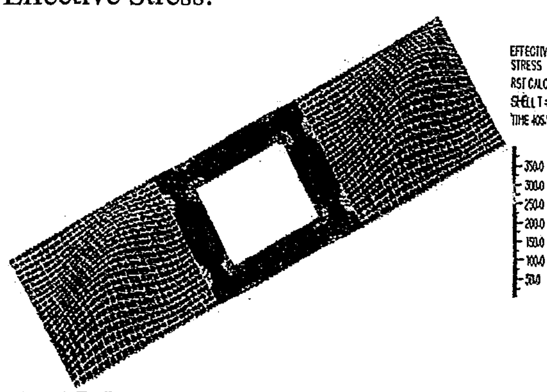	

<table>
<tr>
<td rowspan="2">Lip-Reinforcement
$t_r/t=7$,
$\frac{\tau_{ul(Reinf.)}}{\tau_{ul(Solid)}} =$
1.019</td>
<td>Deformed Shape Magnified by 10%:
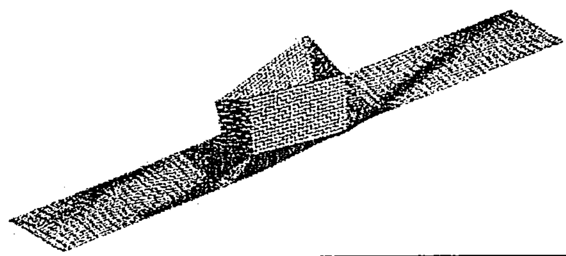</td>
<td rowspan="2">• Diagonal shear failure outside the opening region
• Plasticity occurs throughout the plate</td>
</tr>
<tr>
<td>Effective Stress:
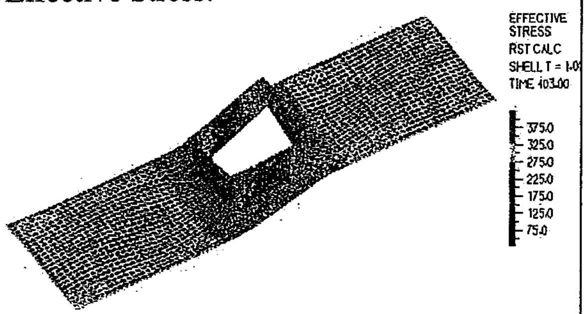
</td>
</tr>
<tr>
<td>Angle-Reinforcement
$t_r/t=7$,
$\frac{\tau_{ul(Reinf.)}}{\tau_{ul(Solid)}} =$
1.042</td>
<td>Deformed Shape Magnified by 10%:
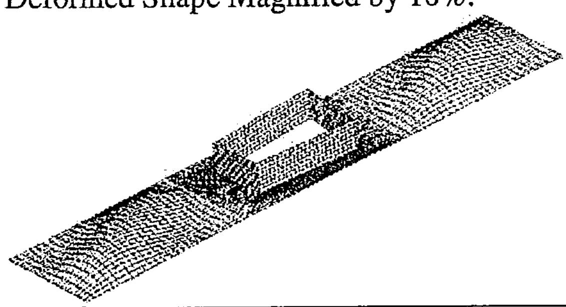</td>
<td rowspan="2">• Diagonal shear failure outside the opening region
• Plasticity occurs throughout the plate</td>
</tr>
<tr>
<td></td>
<td>Effective Stress:
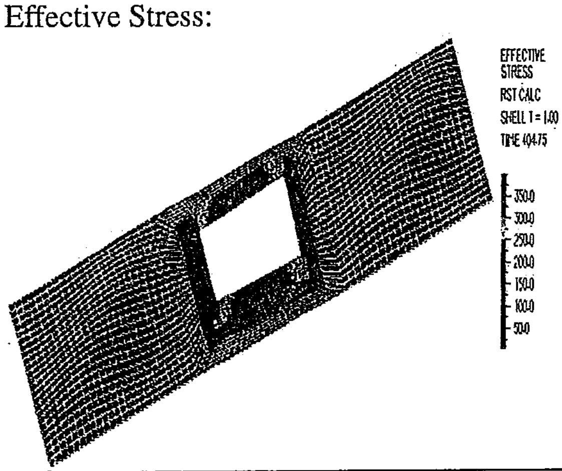
</td>
</tr>
</table>

Figure 6.12 10% magnified Deformed Shape of Plates at Failure Load for Plate with (h/t=50)

Model Description	Deformed Shape and The Effective Stress at the Failure Load Level for Thick Plates (h/t=200)	Failure Descriptions
No Reinforcement	Deformed Shape Magnified by 10%: 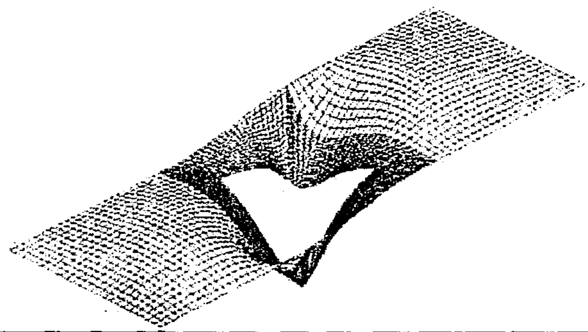 Effective Stress: 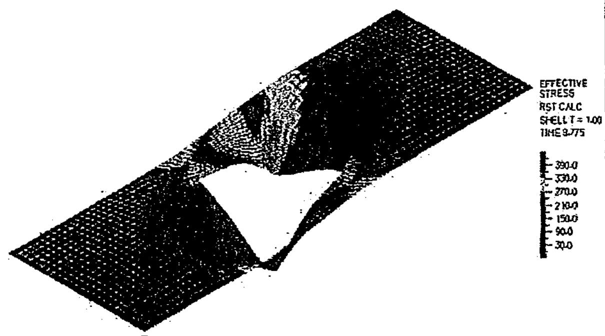 	• Diagonal shear failure at the opening region • Plasticity occurs around the four corners of the opening
Flat-Reinforcement $t_r/t=2$, $\frac{\tau_{ul(Reinf.)}}{\tau_{ul(Solid)}} = 1.426$	Deformed Shape Magnified by 10%: 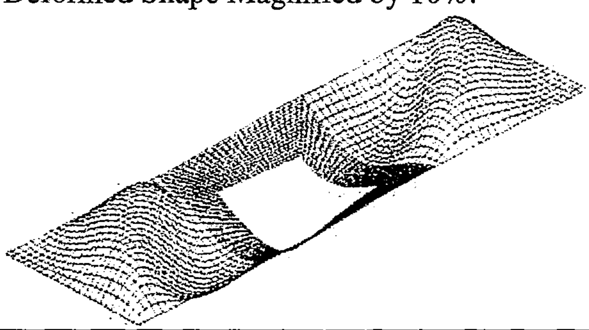 Effective Stress: 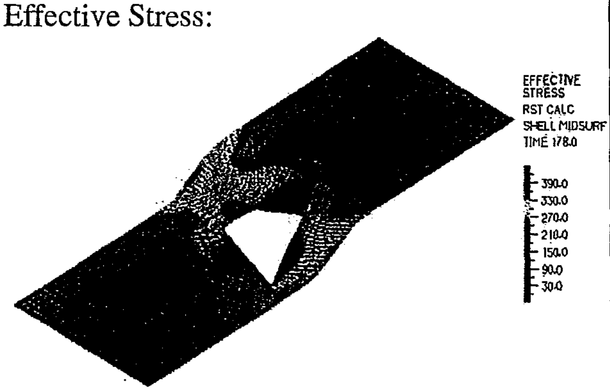 	• Diagonal shear failure occurs outside the opening region • Plasticity occurs around the opening region and outside of the opening region

<table>
<tr>
<td rowspan="2">Lip-
Reinforcement
$t_r/t=6$,
$\frac{\tau_{ul(Reinf.)}}{\tau_{ul(Solid)}} =$
1.032</td>
<td>Deformed Shape Magnified by 10%:
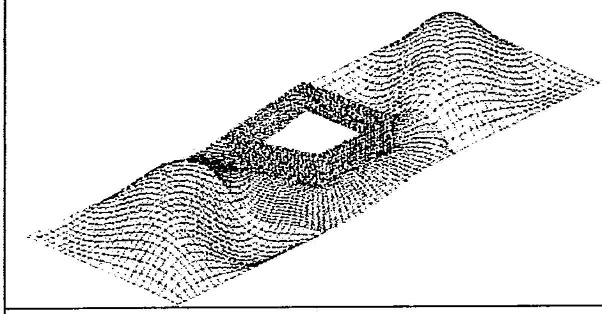</td>
<td rowspan="2">• Diagonal shear failure outside the opening region</td>
</tr>
<tr>
<td>Effective Stress:
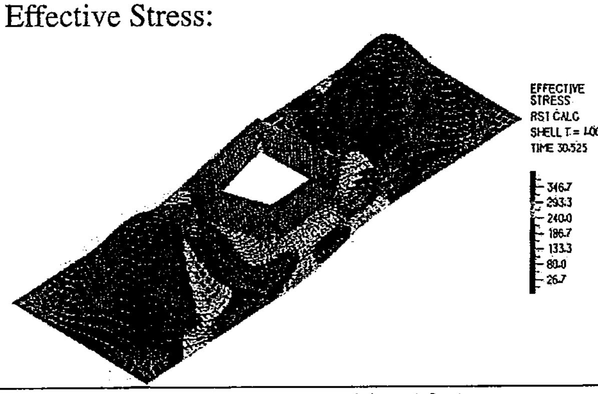
</td>
</tr>
<tr>
<td>Angle-
Reinforcement
$t_r/t=2$,
$\frac{\tau_{ul(Reinf.)}}{\tau_{ul(Solid)}} =$
1.228</td>
<td>Deformed Shape Magnified by 10%:
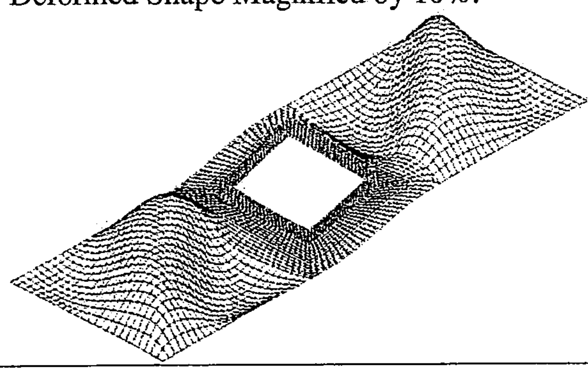</td>
<td rowspan="2">• Diagonal shear failure outside the opening region</td>
</tr>
<tr>
<td></td>
<td>Effective Stress:
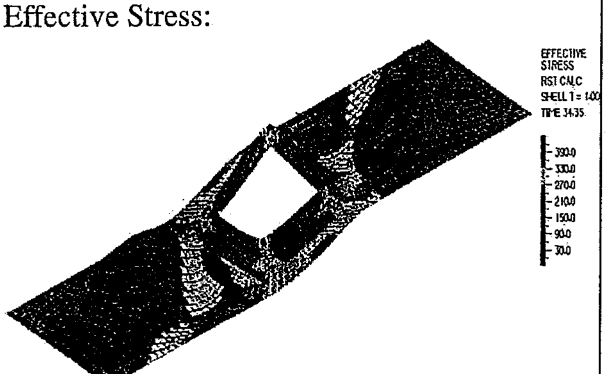
</td>
</tr>
</table>

Figure 6.13 10% magnified Deformed Shape of Plates at Failure Load for plates with h/t=200

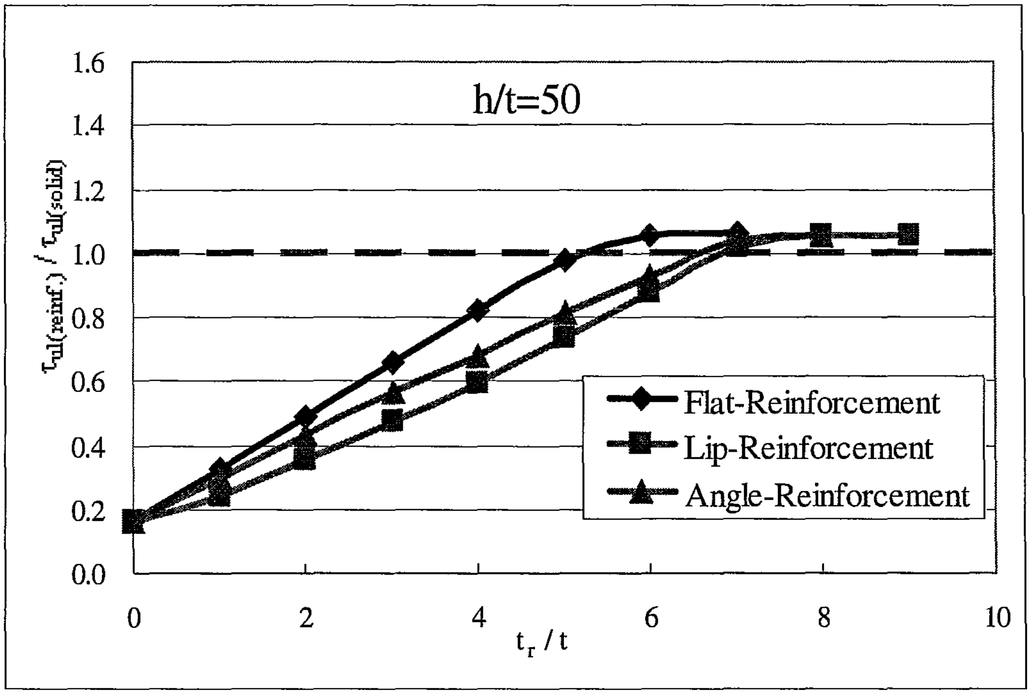

Figure 6.14 Ultimate Shear Strength of Plates with Flat- Reinforcement versus $t_{rcinf.} / t$ (h/t=50)

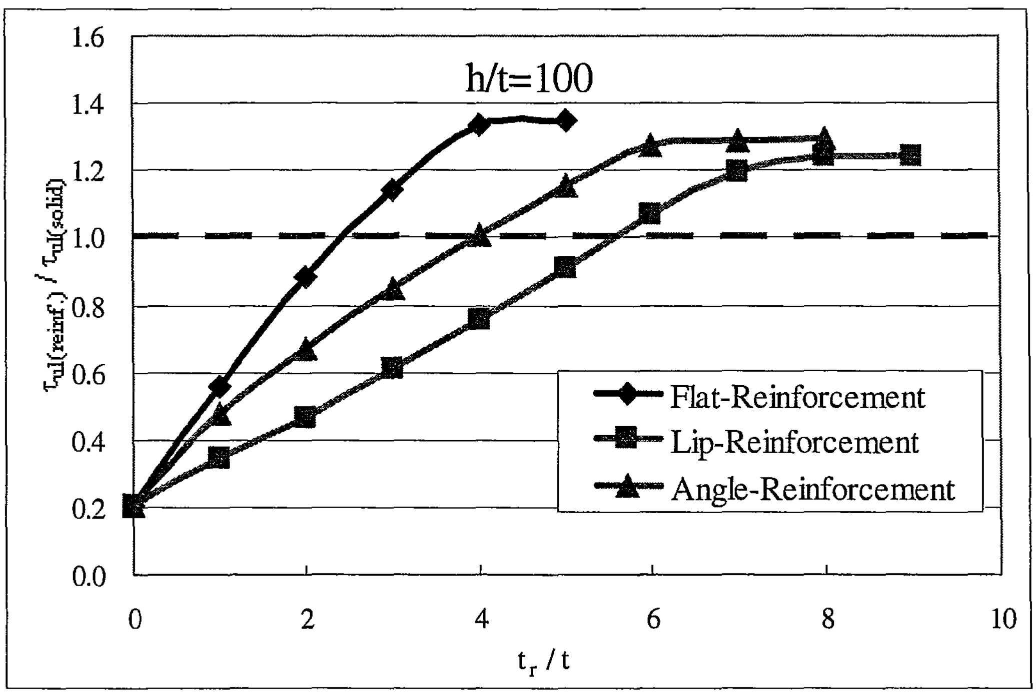

Figure 6.15 Ultimate Shear Strength of Plates with Flat- Reinforcement versus $t_{reinf.} / t$ (h/t=100)

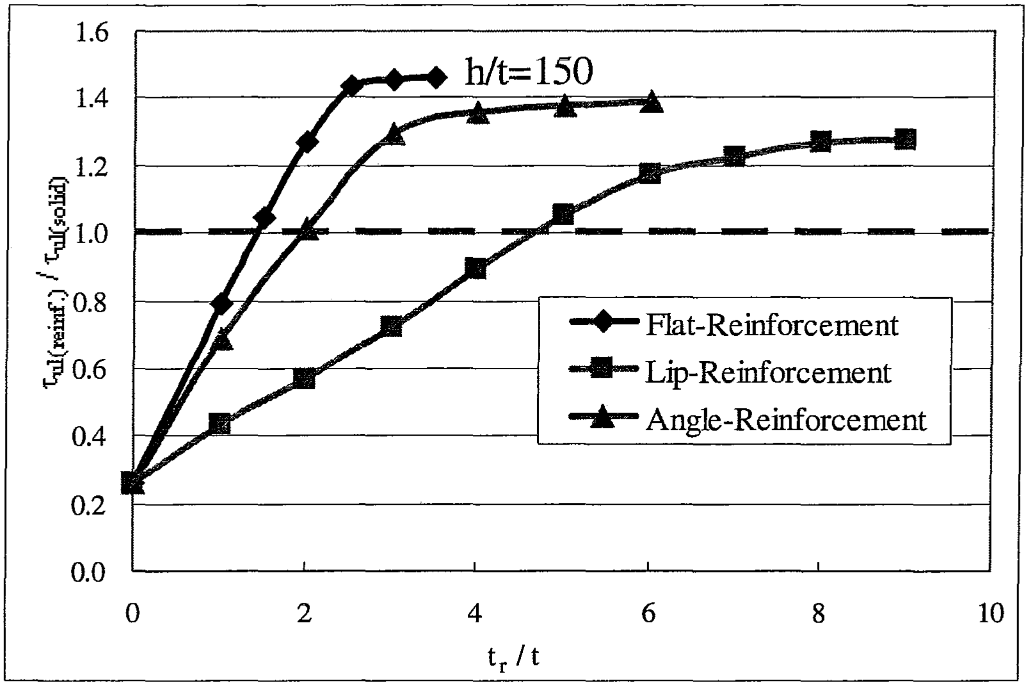

Figure 6.16 Ultimate Shear Strength of Plates with Flat- Reinforcement versus $t_{reinf.}/t$ (h/t=150)

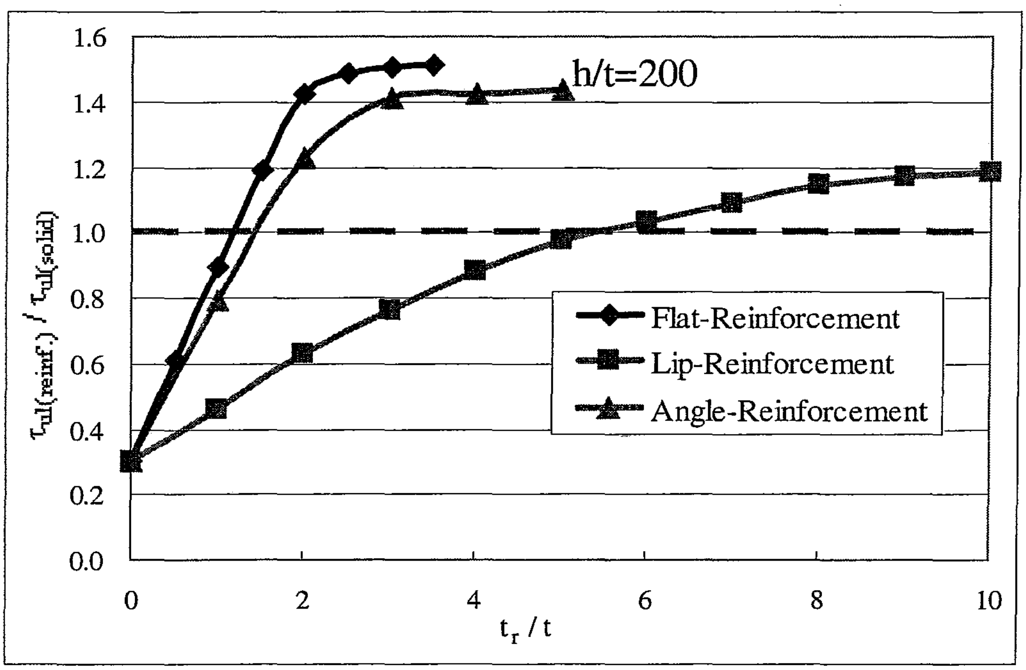

Figure 6.17 Ultimate Shear Strength of Plates with Flat- Reinforcement versus $t_{reinf.}/t$ (h/t=200)

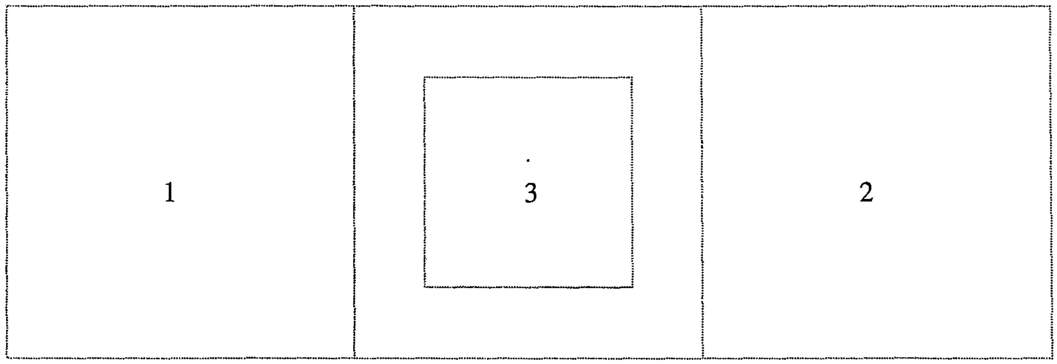

Figure 6.18 Three parts divided by the flat-reinforcement

Chapter 7

CONCLUSIONS AND RECOMMENDATIONS

7.1 Summary

As the demand for higher strength, lighter weight, and more versatile structural materials increases, steel especially cold-formed steel are utilized as structural material in more and more buildings. Structural cold-formed steel sections can be used as joists, truss members, and studs; they can be also used as frame systems, floor systems and wall systems, etc. Thus, it is common to see openings in these plated structures for all kinds of reasons, such as for water pipes, plumbing, electric wiring, etc. Relatively large openings are also required sometimes to allow access for building maintenance and inspections.

In cold-formed steel sections, openings are often introduced in the web of a beam or a column. Existence of large openings can greatly influence the behavior of sections. The structural behavior of steel members with all different kinds of web openings has been investigated for many years. Considerable progress has been made in the investigation of plated structures having openings. However, very limited studies were found on the behavior of plates with openings subjected to shear loads, especially for thin cold-formed steel plates. Therefore, this research investigated the behavior of steel plates (ranging from thick to thin plates) with centrally located square openings subjected to shear loads using the finite element models. Once the behavior of web panels with openings is established, reinforcement schemes were proposed on the web panels to compensate for the reduction of strength and stiffness caused by the openings. Three reinforcement schemes, namely the flat-reinforcement, the lip-reinforcement and the angle-reinforcement, were evaluated in this research.

7.2 Conclusions

This section presented the important findings obtained through the finite element analysis to satisfy the objectives of this research. These findings are summarized in point forms as the following:

Behavior of Square Plate under Uniaxial Compression

- The finite element model can predict the buckling load and the ultimate strength of the plate under compression with reasonable accuracy.
- The compressive ultimate strengths obtained from finite element modeling are very similar to those obtained from the AISI (2007) method for relative thicker plates; but are slightly higher than those calculated from the AISI (2007) for thinner plates.
- The maximum difference between the results obtained from the two methods is about 14%, which occurs when h/t=200 (the thinnest plate). This may be caused by the fact that thin plates tend to have more post-buckling strength and the AISI (2007) method may have under-estimated the post-buckling strength of plates under compression.

Shear Behavior of Solid Plates

- The ultimate shear strength of a plate decreases as the slenderness ratio (h/t) of the plate increases.
- The ultimate shear capacity of a plate also decreases, but to a lesser extent, as the aspect ratio (a/h) of the plate increases.
- The post-buckling strength of thin plates can be many times larger than the shear-buckling strength of them.
- By ignoring the post-buckling strength of thin plates, the AISI (2007) has underestimated the shear strength of thin plates.
- The current AISI (2007) specification has over conservatively estimated the ultimate shear strength of thin webs.
- The AISI (2007) code equations of calculating the shear strengths of webs were modified according to the data obtained from the finite element analysis to include the post-buckling strength.
- The modified AISI (2007) Code method of calculating the shear strength of webs is able to better estimate the ultimate shear strength of solid web plates.

Shear Behavior of Plates with Openings

- Centrally located square opening can significantly reduce the ultimate shear strength of the plate.
- The parametric study has shown that the opening size is the primary parameter influencing the ultimate shear strength of plate.
- The reduction in the ultimate shear strength displays an approximately linear relationship with the increase of the opening sizes.
- The ultimate shear strength decreases as the slenderness of the plate increases. However, the extent of the effect on the ultimate shear strength of plate decreases as the openings size increases.
- The ultimate shear strength of plates with square openings tends to increase as the plate aspect ratio increases. However, the increasing in the ultimate shear strength tends to decrease and eventually fades out as the aspect ratio increases.
- The aspect ratio is the least significant parameter in the sense of affecting the ultimate shear strength of plates with square opening as compared to the other two parameters.
- The AISI (2007) tends to underestimate the ultimate shear strength of thick to moderate thick plates with square openings, but overestimate the ultimate shear strength of thin plates with square openings.

- A new equation of estimating the shear reduction factor (q_s) for web plates with centrally located square opening was proposed based on the finite element analysis.
- The proposed equation is able to better estimate the ultimate shear strength of plates with centralized square openings.

Shear Behavior of Plates with Reinforced Openings

- The ultimate shear strength of the reinforced plate increases as the size of the reinforcement (t_r/t) increases.
- It tends to be easier to restore the shear capacity by all three reinforcement schemes for thin plates.
- All three reinforcement schemes are capable of restoring the ultimate shear strength of a plate with a square opening to that of a solid plate if enough reinforcements are provided.
- The flat-reinforcement is the most effective way comparing the other two reinforcement schemes.
- The lip-reinforcement is the least effective reinforcement configuration to restore the shear capacity of plates with square opening.

7.3 Recommendations for Future Study

The following studies are recommended for future studies on the reinforcement schemes for cold-formed steel sections having large web openings.

- This study only considered plates with centrally located square openings. Future studies can consider different types and locations of unreinforced/reinforced openings.
- This study only considered opening reinforcements for plates under pure shear loads. Future studies can consider different types of loads or their combination loads.
- This study only evaluated three reinforcement schemes. Future studies can investigate a variety of different types of reinforcement schemes for the openings.
- This study examined different opening reinforcement schemes for plates with the aspect ratio equal to 3 (a/h=3). A future study could apply reinforcements on plates with larger aspect ratios (i.e. longer plates).

REFERENCES

Abdel-Rahman, N. and Sivakumaran, K. S. (1997). Material Properties Models for Analysis of Cold-Formed Steel Members. Journal of Structural Engineering, 123 (9), pp. 1135-1143.

Acharya, S. R. (2009). Reinforcement Schemes for Cold-Formed Steel Joists Having Web Openings. Doctoral Dissertation, McMaster University.

Acharya, S. R., Heerema, P. and Sivakumaran, K. S. (2007). Testing of Cold-Formed Steel Members with Reinforced Web Openings in High Shear Zones. In 6th International Conference on Steel and Aluminum Structures, Oxford, UK.

Acharya, S. R. and Sivakumaran, K. S. (2006). Flexural Strength of Steel Plates with Reinforced Opening. In Proceedings of the Tenth Asia-Pacific Conference on Structural Engineering and Construction (EASEC-10), Thailand, Bangkok.

Acharya, S. R. and Sivakumaran, K. S. (2008). Bending Strength of Cold-Formed Steel Members with Reinforced Openings. In Proceeding of the 2nd Canadian Conference on Effective Design of Structures, Hamilton, Canada.

ADINA User Manual (2008). ADINA R & D, Inc., Watertown, MA USA.

AISC (1963). American Institute of Steel Construction specification for the Design, Fabrication and Erection of Structural Steel for Buildings, 6th Edition. AISC, New York, N. Y.

AISI (2001). Standard for Cold-Formed Steel Framing-Prescriptive Method for One and Two Family Dwellings. American Iron and Steel Institute, Washington DC, USA.

AISI (2007). North American Specification for the Design of Cold-Fomred Steel Structural Members. American Iron and Steel Institute, Washington DC, USA.

Alinia, M. M. and Dastfan, M. (2006). Behavior of Thin Steel Plate Shear Walls Regarding Frame Members. Journal of Constructional Research 62 (2006), pp. 730-738.

Bakker, M. C. and Pekőz, T. (2003). The Finite Element Methods for Thin-Walled Members-Basic Principles. Thin-Walled Structures (41), pp. 179-189.

Bathe, K. (1996). Finite Element Procedures. Printice Hall, New Jersey, USA.

Basler, K. (1961). New provisions for Plate Girder Design. In Proceeding of the AISC National Engineering Conference, New York, pp. 65-74.

Basler, K. (1961). Strength of Plate Girders in Shear. Journal of the Structural Division, In Proceedings of the American Society of Civil Engineers Vol. 87 (ST7), pp. 151-180.

Basler, K. (1963). Strength of Plate Girders in Shear. Trans. ASCE 128, pp. 683-719.

Basler, K. and Thurlimann, B.(1959). Plate Girder Research. American Institute of Steel Construction. New York.

Binskin, L. (1944). Strengthening of Circular Holes in Plates under Edge Forces. Journal of Applied Mechanics, pp. A-140.

Budiansky, B. and Connor, R. W. (1948). Buckling Stresses of Clamped Rectangular Flat Plates in Shear. NACA Tech. Note No. 1559.Chern, C. and Ostapenko, A. (1969).

Ultimate Strength of Plate Girder under Shear. Friz Engineering Laboratory. Report No. 328.7, Lehigh University.

Copper, P. B. and Snell, R. R. (1972). Tests on Beams with Reinforced Web Openings. Journal of Structural Division, 98 (ST3, Mar), pp. 611-632.

Cougdon, J. D. and Redwood, R. G. (1968). Plastic Behavior of Beams with Reinforced Holes. Journal of Structural Division, 93 (ST9, Sep), pp. 1933-1957.

Coughlan, J. (1970). The Buckling and Collapse Behavior of Plate Members Containing Holes. M.Sc. Thesis, University of Wales.

CSA (2002). North American Specification for the Design of Cold-Formed Steel Structural Members, Volume S136-01. Ontario, Canada.

CSA (2004). Handbook of Steel Construction. 8th Edition. Canadian Institute of Steel Construction, Toronto, Ontario.

Daniel, V., Nicolau, M., Dimache, A. and Modiga, M. (2004). Ultimate Strength of Plate Girders in Shear. University of Galati.

Davis, C.S. and Yu, W. W. (1973). Cold-Formed Steel Members with Perforated Elements. Journal of the Structural Division. ASCE, 99(10).

Davis, J. M. (2000). Recent Research Advances in Cold-Formed Steel Structures. Journal of Constructional Steel Research 55 (2000), pp. 267–288.

Dawson, R. G. and Walker, A. C. (1972). Post-buckling of Geometrically Imperfect Plates. Journal of the Structural Division. ASCE, 98(1), pp. 75–94.

Dubina, D. and Ungureanu, V. (2002). Effect of Imperfections on Numerical Simulation of Instability Behavior of Cold-Formed Steel Members. Thin-Walled Structures 40 (2002) 239-262.

Fujii, T. (1967). Minimum Weight Design of Structures Based on Buckling Strength and Plastic Collapse (3rd Report) – An Improved Theory on Post-Buckling Strength of Plate Girders in Shear. J. Soc. Naval Arch. Japan, Volume 122, pp. 119-128.

Gardner, L. and Nethercot, D. A. (2004). Numerical Modeling of Stainless Steel Structural Components- A Consistent Approach. Journal of Structural Engineering.

Hagen, N. C. (2005). On the Shear Capacity of Steel Plate Girders with Large Web Openings. Doctoral Thesis, Norwegian University of Science and Technology.

Hagen, N. C. and Larsen, P. K (2009). Shear Capacity of Steel Plate Girders with Large Web Openings, Part 1: Modeling and Simulations. Journal of Constructional Steel Research. 65 (2009) 151-158.

Hagen, N. C., Larsen, P. K. and Aalberg, A. (2009). Shear Capacity of Steel Plate Girders with Large Web Openings, Part 2: Design Guidelines. Journal of Constructional Steel Research. 65 (2009) 142-150.

Hancock, G. J., Murray, T. M. and Ellifritt, D. S. (2001). Cold-formed steel structures to the AISI Specification. Marcel Dekker, Inc., New York, NY.

Höglund, T. (1971). Strength of Thin Plate Girders with Circular and Rectangular Web Holes without Web Stiffeners. In Proceeding of the colloquium of the International Association of Bridge and Structural Engineering, London.

Höglund, T. (1997). Shear Buckling Resistance of Steel and Aluminum Plate Girders. Journal of Thin-Walled Structures, Volume 29 (14), pp. 13-30.

John, W. and Sons, New York (1979). Thin Plate Design for in-Plane Loading.

Kawai, T. and Ohtsubo, H. (1968). A Method of Solution for the Complicated Buckling Problems of Elastic Plates with Combined Use of Rayleigh-Ritz's Procedure in the Finite Element Method. In Proceedings of the 2nd Air Force Conference on Matrix Methods in Structural Mechanics.

Kroll, W. D. (1949). Instability of Simply Supported Square Plates with Reinforced and Unreinforced Holes Subjected to Shear. Journal of Research, National Bureau of Standards (43), pp. 465-478.

Kumar, M. S., Alagusundaramoorthy, P. and Sundaravadivelu, R. (2007). Ultimate Strength of Square Plate with Rectangular Opening under Axial Compression. Journal of Naval Architecture and Marine Engineering 4 (2007), pp. 15-26.

Larson, M. A. and Shah, K. N. (1976). Plastic Design of Web Openings. Journal of Structural Division, 102 (ST5, May), pp. 1031-1041.

Lee, S. C., Davidson, J. S. and Yoo, C. H. (1996). Shear Buckling Coefficients of Plate Girder Web Panels. Computer and Structures, Volume 56 (5), pp. 789-795.

Lee, S. C. and Yoo, C. H. (1999). Experimental Study on Ultimate Shear Strength of Web Panels. Journal of Structural Engineering, Volume 125 (8), pp. 838-846.

Lee, S. C. and Yoo, C. H. (1998). Strength of Plate Girder Web Panels under Pure Shear. Journal of Structural Engineering, Volume 124 (2), February, 1998, pp. 184-194.

Lee, S. C., Yoo, C. H. and Yoon, D. Y. (2002). Behavior of Intermediate Transverse Stiffeners Attached on Web Panels. Journal of Structural Engineering ASCE 2002; 128 (3), pp. 337-345.

Miller, T. H. & Pekőz, T. B. (1994). Unstiffened strip approach for perforated wall studs. Journal of Structural Engineering, ASCE, 120(2), pp. 410-421.

Narayanan, R. (1983). Plated Structures- Stability and Strength. Applied Science Publishers. New York, USA.

Narayanan, R. and Chow, F. Y. (1985), Experiments on Perforated Plates Subjected To Shear. Journal of Strain Analysis, Volume 20 (1), pp. 23-34.

Narayanan, R. and Der-Avanessian, N.G.V. (1984). Elastic Buckling of Perforated Plates under Shear. Thin-Walled Structures, Volume 2, pp. 51-73.

Narayanan, R. and Der-Avanessian, N.G.V. (1985). Design of Slender Webs Having Rectangular Holes. Journal of Structural Engineering, Volume 111 (4), pp. 777-787.

Narayanan, R. and Der-Avanessian, N.G.V. (1986). Analysis of Plate Girders with Perforated Webs. Thin-Walled Structures, 4:363-380.

Narayanan, R. and Rockey, K.C (1981), Ultimate Load Capacity of Plate Girders with Webs Containing Circular Cut-Outs. Proceedings of the Institution of Civil Engineers, 71 (2), pp.845-862.

Ng, M.Y. (2004). Effective Reinforcement Schemes for Cold-Formed Steel Flexural Members with Large Web Opening. M.Sc. Thesis, McMaster University.

Ng, M.Y., Sivakumaran, K. S., and Fox, S. R. (2005). Flexural Testing of Cold-Formed Steel Members with Reinforced Web Openings. In 33rd Annual General Conference of the Canadian Society of Civil Engineering, Ontario, Canada.

Olaru, V. D., Nocolau, M., Dimache, A. and Modiga, M. (2004). Ultimate Strength of Plate Girders in Shear. The Annals of 'Dunarea De Jos' University of Galati, pp. 59-64.

P.S. Bulson, New York (1969). The Stability of Flat Plate.

Paik, J. K. (2007). Ultimate Strength of Perforated Steel Plates under Edge Shear Loading. Thin-Walled Structures 45, pp. 301-306.

Paik, J. K. and Thayamballi, A. K. (2006). Some Recent Developments on Ultimate Limit State Design Technology for Ships and Offshore Structures. Ships Offshore Strenctures, I (2), pp. 99-116.

Pannock, R. W. (2001). Strength of Light Gauge Cold Formed Steel Joists with Web Perforation: Senior Report. University of New Brunswick, New Brunswick, Canada.

Pellegrino, C., Maiorana, E. and Modena, C. (2008). Linear and Non-Linear Behavior of Steel Plates with Circular and Rectangular Holes under Shear Loading. Thin-Walled Structures (2008), doi: 10.1016/j.tws.2008.11.001.

Porter, D. M., Rocket, K. C. and Evans, H. R. (1975). The Collapse behavior of Plate Girders Loaded in Shear. The Structural Engineer. Vol.53.

Ralph, G., Dawson and Alastair, C. and Walker (1972). Post-Buckling of Geometrically Imperfect Plates. Journal of the Structural Division, Proceedings of the American Society of Civil Engineers, pp75-95.

Redwood, R. G. and Lupien, R. (1978). Steel Beams with Web Openings Reinforced on One Side. Canadian Journal of Civil Engineering, Volume 5, No. 4, pp. 451-461.

Redwood, R. G. and Shrivastava, S. C. (1980). Design Recommendations for Steel Beams with Web Holes. Canadian Journal of Civil Engineering, Volume 7, No. 4, pp. 642-650.

Roberts, T. M. and Azizian, Z. G. (1984). Strength of Perforated Plates Subjected to In-plane Loading. Thin-Walled Structures 2 (1984), pp. 153-164.

Rockey, K. C. (1980). The Buckling and Post-Buckling Behavior of Shear Panels Which Have a Central Circular Cut-Out. Thin-Walled Structures, pp. 658-672.

Rockey, K. C, Anderson, R. G. and Cheung, Y. K., London (1967). The Behavior of Square Shear Webs Having a Circular Hole, Proceedings of Swansea Conference on Thin-Walled Structures, pp. 148-169.

Rockey, K. C and Hill, H. V., New York (1967). Thin Walled Steel Structures-Their Design and Use in Building.

Rondal J. (1987). Residual stresses in cold-rolled profiles. Construction and Building Material, 1(3):0–0.

Rondal J. (1992). Discussion of "Residual Stresses in Cold-Formed Steel Members". Journal of Structural Engineering, Volume 118, No. 5, pp. 1427-1428,

Sabir, A. B. and Chow, F. Y. (1983). Elastic Buckling of Flat Panels Containing Circular and Square Holes. Proceedings of the International Conference on Instability and Plastic Collapse of Steel Structures. pp. 311-321.

Schafer, B. W, Peköz, T. (1998). Computational Modeling of Cold-Formed Steel Characterizing Geometric Imperfections and Residual Stresses. Journal of Constructional Steel Research 47, pp. 193-210.

Segner, E. P. (1964). Reinforcement Requirements for Girder Web Openings. Journal of Structural Division, 90 (ST3, Jun), pp.147-164.

Shan, M.Y., LaBoube, R.A., and Yu, W.W. (1996), Bending and Shear Behavior of Web Elements with Openings. Journal of Structural Engineering, 122 (8), pp. 854-859.

Shanmugam, N. E. and Narayanan, R. (1982), Elastic Buckling of Perforated Square Plates for Various Loading and Edge Conditions. Proceedings of the International Conference on Finite Element Methods. Shanghai, China.

Shanmugam, N. E., Singapore (1997). Openings in Thin-Walled Steel Structures. Thin-Walled Structures Volume 28, No. 3/4, pp 355-372.

Sharp, M. L. and Clark, J. W. (1971). Thin Aluminum Shear Webs. Journal of Structure Division. ASCE 97, ST4, pp. 1021-1038.

Sherbourne, A. N. and Haydl, H. M. (1980). Carrying Capacity of Edge-Compressed Rectangular Plates. Can. J. Civ. Eng., 7, pp. 19-26.

Sivakumaran, K.S. and Abdel-Rahman, N. (1998). A Finite Element analysis Model for the Behavior of Cold-formed Steel Members. Thin-Walled Structures 31(1998) 305-324.

Stein, M. N. (1947). Buckling Stresses of Simply Supported Rectangular Flat Plates in Shear. NACA Tech. Note No. 1222.

Thangavadivel, T. (2003). Behavior of High Performance Steel W-Shape Members. M.Sc. Thesis, Mcmaster University.

Timoshenko, S. P., Gere, J. M., New York (1961). Theory of Elastic Stability. 2nd Edition. McGraw-Hill, New York.

Uenoya, M. and Redwood R. G. (1977). Elasto-Plastic Shear Buckling of Square Plates with Circular Holes. Computers and Structures, Volume 8, pp. 231-300.

Uenoya, M. and Redwood, R. G. (1979). Critical Loads for Webs with Hole. Journal of Structure Division, 105 (ST10, Oct), pp. 2053-2067.

Ugural, A. C. (1981). Stresses in plates and shell. Mcgraw Hill Companies. FL. USA. pp. 156.

Vilnay, O. and Rockey, K. C. (1981). A Generalized Effective Width Method for Plates Loaded in Compression. Journal of Constructional Steel Research, Volume 1 (3), pp. 3-11.

Wagner, H. (1931). Flat Sheet Metal Girders with Very Thin Metal Web. Washington, DC, NACA TM.

Wang, T. M., Snell, R. R. and Copper, P. B. (1975). Strength of Beams with Eccentric Reinforced Holes. Journal of Structural Division, 101 (ST9, Sep), pp. 1783-1800.

Williams, D. G. (1979). Thin plate design for in-plane loading. John Wiley & Sons. New York.

Wilson, J. M. (1886). On Specifications for Strength of Iron Bridges. Trans., ASAE, 15(I), PP 401-403 AND 489-490.

Yamaki, N. (1959). Postbuckling Behavior of Rectangular Plates with Small Initial Curvature Loaded in Edge Compression. Journal of Applied Mechanics, September 1959, pp. 407-414.

Yu, W.. Cold-Formed Steel Design, Second Edition, New York.

Yuan, B. (1997). Local Buckling of High Strength Steel W-Shaped Sections. M. Sc. Thesis. Mcmaster University.